Deepwater Horizon Release Estimate of Rate by PIV

June 21, 2010

Plume Team - FRTG

Report to

Dr. Marcia Mcnutt , USGS Director and Science Advisor to the Secretary of the Interior
Lead to the National Incident Command Flow Rate Technical Group

Prepared By

Plume Calculation Team

Aliseda, Alberto	Assistant Professor of Mechanical Engineering, University of Washington
Bommer, Paul	Senior Lecturer, Petroleum and Geosystems Engineering, University of Texas at Austin
Espina, Pedro	National Institute of Standards and Technology
Flores, Oscar	Department of Mechanical Engineering at University of Washington
Lasheras, Juan C.	Penner Distinguished Professor of Engineering and Applied Sciences, University of California at San Diego
Lehr , Bill (Lead)	Senior Scientist, National Oceanic and Atmospheric Administration Office of Response and Restoration
Leifer, Ira	Associate Researcher, Marine Science Institute and Institute for Crustal Studies, University of California, Santa Barbara.
Possolo, Antonio	National Institute of Standards and Technology
Riley, James	PACCAR Professor of Mechanical Engineering, University of Washington
Savas, Omer	Professor of Mechanical Engineering, University of California at Berkeley
Shaffer, Franklin	Department of Energy National Energy Technology Laboratory
Wereley, Steve	Professor of Mechanical Engineering, Purdue University
Yapa, Poojitha	Professor of Civil and Environmental Engineering, Clarkson University

All the calculations and conclusions is this report are preliminary, and intended for the purpose, and only for the purpose, of aiding the response team in assessing the extent of the spilled oil for ongoing response efforts. Other applications of this report are not authorized and are not considered valid. Because of time constraints and limitations of data available to the experts, many of their estimates are only approximate, subject to revision, and certainly should not be used as the federal government's final values for assessing volume of the spill or its impact to the environment or to coastal communities. Each expert that contributed to this report reserves the right to alter his conclusions based upon further analysis or additional information.

Table of Contents

EXECUTIVE SUMMARY

The plume modeling team observed video both before and after the cutting of the riser pipe. The 'before' video looked at the end of the original riser leak and from the kink in the riser and from the kink leak above the BOP. The later video examined the leakage shortly after the severing operation but before any capping operation.

The main method employed to make estimates was a common fluid dynamic technique called particle image velocimetry (PIV). While difficult in practice, it is simple in principle. A flow event, e.g. an eddy or other identifiable item, is observed at two consecutive video frames. Distance moved per time between frames gives a velocity, after adjustment for viewing angle and other factors. Repeated measurement over time and space give an estimated mean flow. Flow multiplied by cross-section area of the plume gives a volume flux.

Because of time and other constraints, only a small segment of the leakage time was examined, and assumptions were made that may through later information or analysis be shown to be invalid. For example, the Team assumes that the average flow between the start of the incident and the insertion of the RITT was relatively constant and the time frames that were included in the examined videos were representative of that average. If this were not true, then the actual spillage may differ significantly from the values stated below.

Most of the experts, using the limited data available and with a small amount of time to process that data, concluded that the best estimate for the average flow rate for the leakage prior to the insertion of the RITT was between 25 to 30 thousand bbl/day. However, it is possible that the spillage could have been as little as 20,000 bbl/day or as large 40,000 bbl/day. Further analysis of the existing data and of other videos not yet viewed may allow a refinement of these numbers.

The video of the post-cut was of higher quality than earlier video. The best estimate of the PIV experts was for a flow of 35,000 to 45,000 bbl with the possibility that the leak could be as large as 50,000 bbl/day. After consultation with groups from the Department of Energy, a joint estimated range of 35,000 to 60,000 bbl was provided to the NIC.

Deepwater Horizon, on fire after the explosion

BACKGROUND

When the Deepwater Horizon drilling unit sank in the Gulf of Mexico, initial loss estimates were given as 1000 bbl/day. By April 26, it was obvious that this estimate was too low. Based upon visual observations of oil on the surface, a working number of 5000 bbl/day was adopted. However, the large amount of surface oil, the volume recovered or burned, and a re-examination of the pipe leakage, convinced the National Incident Command (NIC) that it was necessary to re-visit the 5000 bbl/day number.

On May 19, the NIC Interagency Solutions Group established the Flow Rate Technical Group that has as one of its subgroups the Plume Team represented in this report. Experts on fluid dynamics, subsurface well blowouts, petroleum engineering and oil spill behavior were assembled as part of a larger effort to improve spill size estimation. The team consists of both government scientists and leading scholars at academic institutions throughout the United States.

On May 27, the Team issued an Interim Report that established an estimated range for the minimum possible spillage rate but did not issue an estimate for a possible maximum value because the quality and length of the video data could not support a reliable calculation. Instead, they requested, and received, more extensive videos from British Petroleum (BP). See Table 1.

Table 1: List of video segments on BP-provided hard-drive.

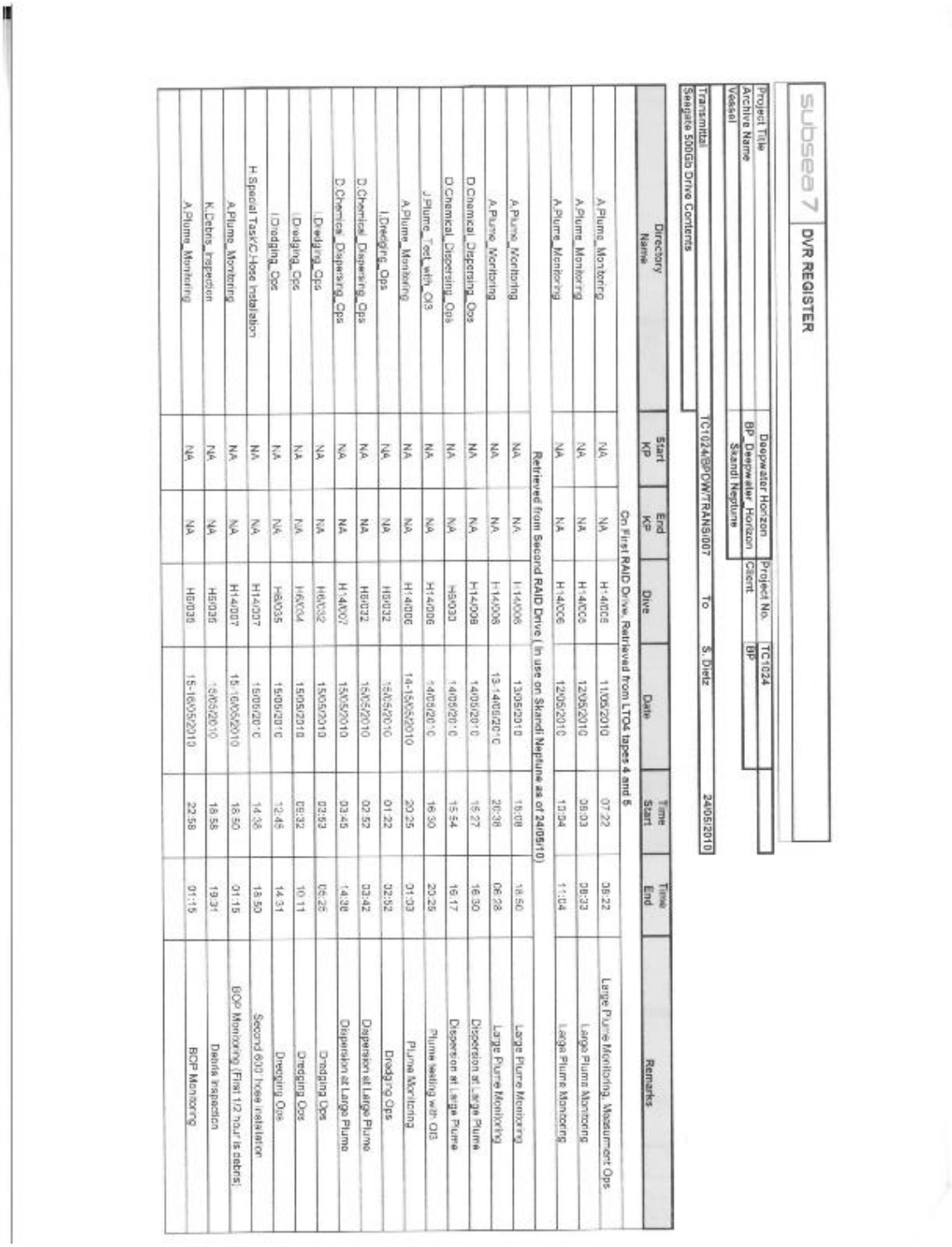

subsea 7 | DVR REGISTER

Project Title	Deepwater Horizon	Project No.	TC1024
Archive Name	BP_Deepwater_Horizon	Client	BP
Vessel	Skandi Neptune		
Transmittal	TC1024SDWTRANS1007	To	S.Dietz
Seagate 500Gb Drive Contents			

24/05/2010

Directory Name	Start KP	End KP	Drive	Date	Time Start	Time End	Remarks
On First RAID Drive, Retrieved from LTO4 tapes 4 and 5							
A.Plume_Monitoring	NA	NA	H14006	11/05/2010	07:22	08:22	Large Plume Monitoring, Measurment Ops
A.Plume_Monitoring	NA	NA	H14006	12/05/2010	08:03	08:33	Large Plume Monitoring
A.Plume_Monitoring	NA	NA	H14006	12/05/2010	10:04	11:04	Large Plume Monitoring
Retrieved from Second RAID Drive (In use on Skandi Neptune as of 24/05/10)							
A.Plume_Monitoring	NA	NA	I-14006	13/05/2010	18:08	18:50	Large Plume Monitoring
A.Plume_Monitoring	NA	NA	H14008	13-14/05/2010	20:38	06:28	Large Plume Monitoring
D.Chemical_Dispersing_Ops	NA	NA	H14008	14/05/2010	15:27	16:30	Dispersion at Large Plume
D.Chemical_Dispersing_Ops	NA	NA	H5033	14/05/2010	15:54	16:17	Dispersion at Large Plume
J.Plume_Test_with_Oil3	NA	NA	H14006	14/05/2010	16:30	20:25	Plume testing with Oil3
A.Plume_Monitoring	NA	NA	H14006	14-15/05/2010	20:25	01:03	Plume Monitoring
I.Dredging_Ops	NA	NA	H5032	15/05/2010	01:22	02:52	Dredging Ops
D.Chemical_Dispersing_Ops	NA	NA	H5032	15/05/2010	02:52	03:42	Dispersion at Large Plume
D.Chemical_Dispersing_Ops	NA	NA	H14007	15/05/2010	03:45	14:38	Dispersion at Large Plume
I.Dredging_Ops	NA	NA	H5032	15/05/2010	03:53	05:25	Dredging Ops
I.Dredging_Ops	NA	NA	H5034	15/05/2010	05:32	10:11	Dredging Ops
I.Dredging_Ops	NA	NA	H5035	15/05/2010	12:45	14:31	Dredging Ops
H.Special Task\C-hose Installation	NA	NA	H14007	15/05/2010	14:36	18:50	Second 600 hose installation
A.Plume_Monitoring	NA	NA	H14007	15-16/05/2010	18:50	01:15	BOP Monitoring (First 1/2 hour is debris)
K.Debris_Inspection	NA	NA	H5035	16/05/2010	18:56	19:31	Debris Inspection
A.Plume_Monitoring	NA	NA	H5035	15-16/05/2010	22:58	01:15	BOP Monitoring

After May 16, the Riser Insert Tube Tool (RITT) was placed into the riser at the main leak point, reducing the oil being released into the environment from this source. The recovery rate of gas and oil for the tube between the insertion and May 25 is shown below.

Table 2: Gas and oil flow rates from the RITT

Date	Oil (bo)	Gas (mmcf)	Oil + Gas (boe)	Gas Portion (%)	High Oil (bopd)	Low Oil (bopd)	High Gas (mmcf/d)	Low Gas (mmcf/d)
16-May-2010	290	0.9	440	34%				
17-May-2010	1,410	3.5	2,015	30%				
18-May-2010	1,930	10.4	3,721	48%	2,191	1,066	12.5	5.3
19-May-2010	3,014	17.5	6,025	50%	4,102	1,521	23.2	10.5
20-May-2010	2,185	15.6	4,882	55%	5,389	44	32.4	4.4
21-May-2010	2,173	4.9	3,025	28%	3,599	646	7.6	1.8
22-May-2010	1,361	7.1	2,586	47%	4,531	0	14.7	2.0
23-May-2010	1,120	2.9	1,616	31%	3,103	0	5.6	2.0
24-May-2010	6,078	9.8	7,771	22%	8,961	2,523	16.1	2.0
25-May-2010	2,596	15.8	5,316	51%	7,337	877	30.4	9.4
Total	22,158	88.4	37,397	41%	8,961	0	32.4	1.8
Average*	2,430	9.7	4,106	40%				

As can be seen from the table, the amount of oil and gas fluctuated significantly. Part of this fluctuation was due to movement of the end of the RITT in the riser due to tidal effects and the natural separation of the oil from the gas in the riser (gas tends to rise to the top). However, examination of the videos also shows significant intermittency in the gas fraction of the flow.

During the time period of the videos examined by the Team, there were two main leak points, shown in Figure 1. The figure also displays the ultimate fate of the released fluid and gas. The main leak, until the most recent severing operation, came from the broken end of the riser, some distance away from the Blowout Preventer (BOP). The leakage was only from the annulus (inside pipe diameter of nineteen and a half inches) surrounding an interior drill pipe (pipe diameter of six and five eighth inches). According to BP, the mouth of the riser was damaged in the initial incident, reducing the cross-sectional area by 30%. Figure 2 shows the damaged riser. After May 1, and perhaps earlier, a second leak source appeared in the kinked riser above the BOP. The number of holes and leakage volume in the kink has increased over time, as BP has attempted to stop oil release by such operations as the RITT and Top Kill.

Figure 1: Graphic showing leaks and oil fate

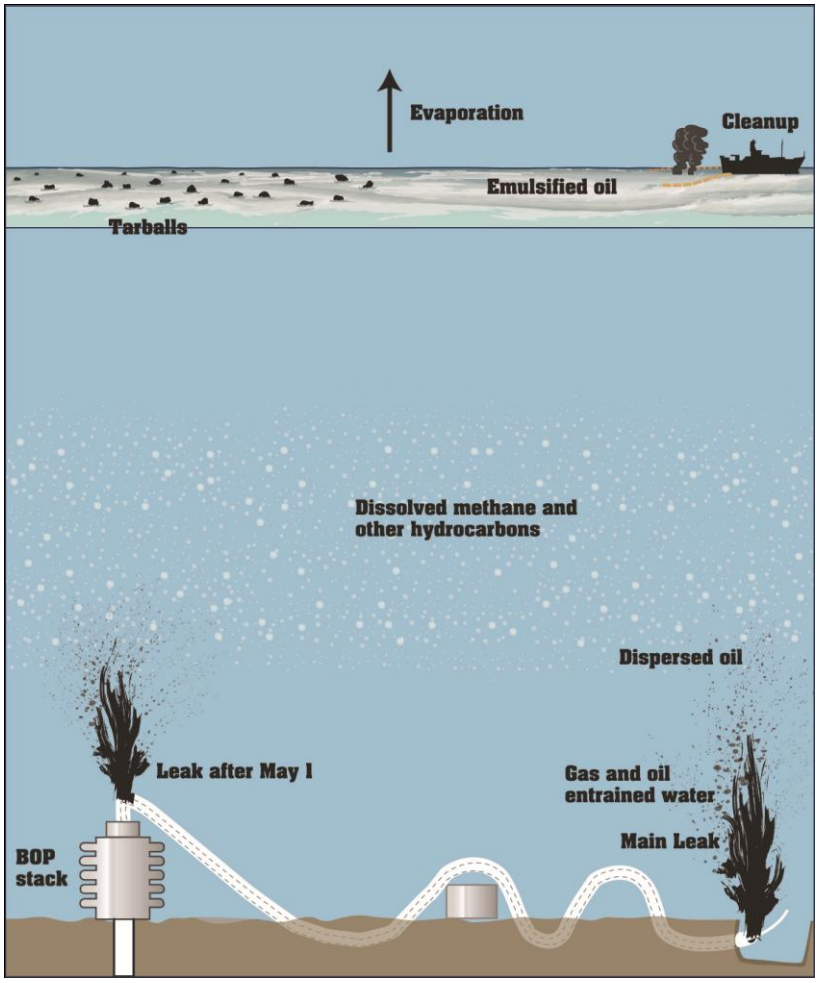

At certain times, a dispersant wand was inserted in the plume and dispersant added. These chemicals are designed to lower surface tension and reduce the average oil droplet size. Unfortunately for flow rate estimation, they add an additional component to

the flow and produce a less defined plume. Measurements were not done using video while dispersant was being applied

While particle image velocimetry (PIV), described in the next section, was the main approach to estimating the leak rate, alternative approaches were used to provide an additional credibility check on the results from the PIV method. These included looking at expected flow based upon properties of the reservoir and reservoir fluid, comparison of this release with a controlled experiment in the North Sea, using well-established similarity characteristics of turbulent jets, and calculating a possible release size, based upon surface oil and oil recovered or burned. Appendix 2 describes an estimate made using one of these alternative methods. Some of these same methods will be or are being examined by other FRTG teams.

Figure 2: Riser outlet showing its reduced cross-sectional area

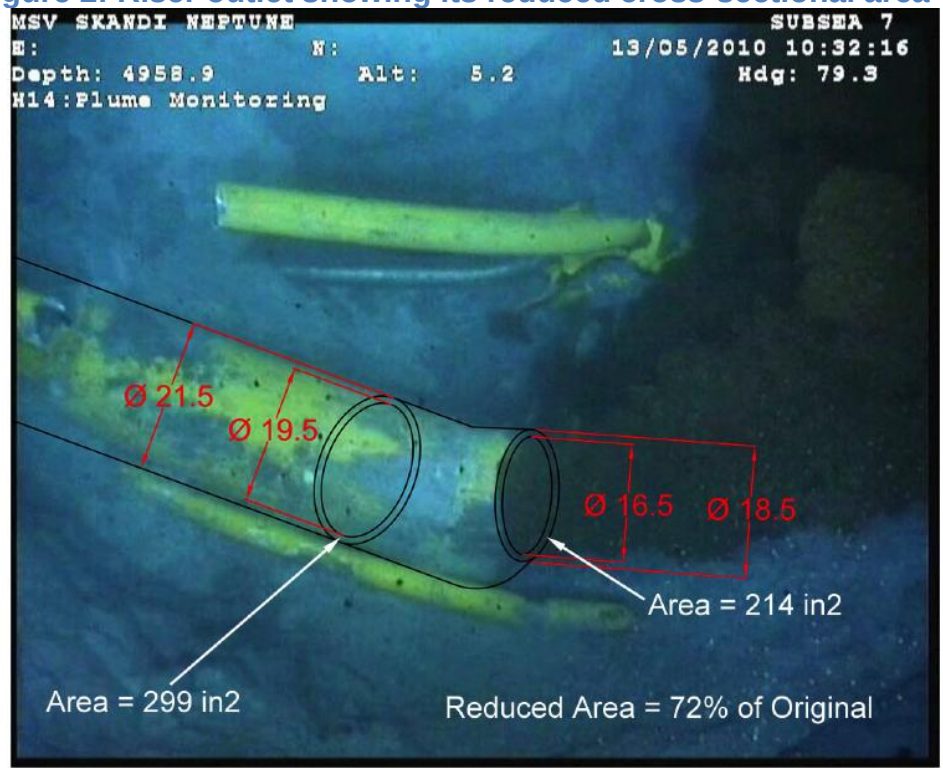

PARTICLE IMAGE VELOCIMETRY

The term particle image velocimetry was first proposed in 1984 by R. J. Adrian, a reviewer of this report. While difficult in practice, PIV is simple in principle. In this method a flow event, e.g. an eddy or other identifiable item, is observed at two consecutive video frames. Distance moved per time between frames gives a velocity, after adjustment for viewing angle and other factors. Repeated measurement over time

and space give an estimated mean flow. Flow multiplied by cross-section area of the plume gives a volume flux.

Many researchers were drawn to PIV because it provided a new way to study turbulent flow structure. Turbulence is a phenomena that is characterized by multiple length scales. To measure turbulent flow, therefore, the method must be able to operate at different scales with possible flow movement in all directions. True PIV uses small solid particles illuminated by laser light and recorded under very short time exposures. In this instance, natural markers in the flow were employed. These markers themselves changed over time, increasing the complexity of the problem.

Figure 3 illustrates the approach. Because the flow velocity is not uniform throughout the plume, multiple locations, known as interrogation spots, must be sampled to estimate and average velocity. Similarly, the cross-sectional area is time and spatially dependent as well as having diffuse boundaries so that an average cross-section, dependent upon the location of the interrogation spots, needs to be calculated. A further challenge for measuring the flow in this case is that it is not spatially or temporally uniform in mixture of gas and fluid.

Figure 3: Illustration of PIV

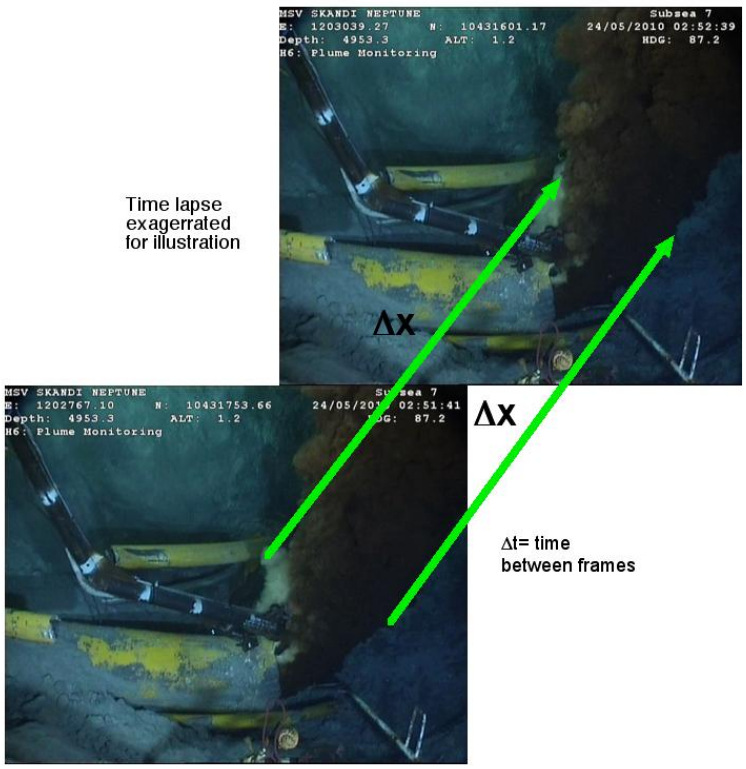

For each of the interrogation sites a vector velocity $\Delta X/\Delta t$ is computed. The vector average of these velocities provides an average velocity. Combined with an average cross-section area, this yields a net flux of both gas and oil. A key parameter was this average ratio of gas to liquid. This term seemed to vary over the time period of the spill and during the time of the video clips. Increasing gas increased the velocity of the plume but decreased the mass flow. Analysis of the available short movies of the riser flow shows the existence of periods when the flow oscillates from pure gas to seemingly pure oil. This could be an indication of Slug Flow Regime. These periods of gas-oil flow fluctuation are in the range of minutes. Longer periods may also exist but would require examination of longer clips to determine.

Another key question was the fluid velocity at the interior of the jet, something that obviously could not be directly observed. The different PIV experts approached this problem in different ways. Most assumed a correction factor for the interior velocity, usually two or two multiplied by the square root of two. One expert chose larger scale structure that he believed would feel the interior flow directly so that no correction was necessary.

KINK LEAK

The Kink leak began sometime around May 1. The Team has requested clarification of the exact date from BP. The number of holes in the riser pipe at the kink increased on or before May 15. The team believes that the amount of escaping oil from this source increased as the holes widened, increased in number, and as the RITT insertion placed more upstream pressure on the riser. Estimation of the flow from the kink was challenging because only one plume, labeled J1 below, was clearly visible and unobstructed in the video.

Figure 4: Kink leak (Annotations by Savas)

NEW LEAK AT SEVERED RISER

By June 3, BP had severed the riser just above the BOP. According to the oil company estimates, this was expected to increase the total leak rate by approximately 20%. Surprisingly, the interior of the riser pipe contained not one, but two pieces of drill pipe inside (Figure 5). One team member speculated that the drill pipe snapped during the accident into several segments that would fit side by side inside the riser. The team requested from BP videos of the leak after the cut but before the installation of a dome designed to capture part of the flow. The damage to the riser during cutting complicated the task of estimating flow cross section.

Figure 5: Cut riser showing two pipes inside

The quality of the video was much better for the severed riser flow than the video used for earlier estimates. This allowed for greater confidence in calculated flow. The PIV experts were able to use the visible flange and bolts as references although parallax adjustments were required. There was a noticeable difference in the color of the two distinct plumes emanating from the cut riser. BP attributed this to greater gas content in the lighter plume.

Figure 6: Cut riser leak

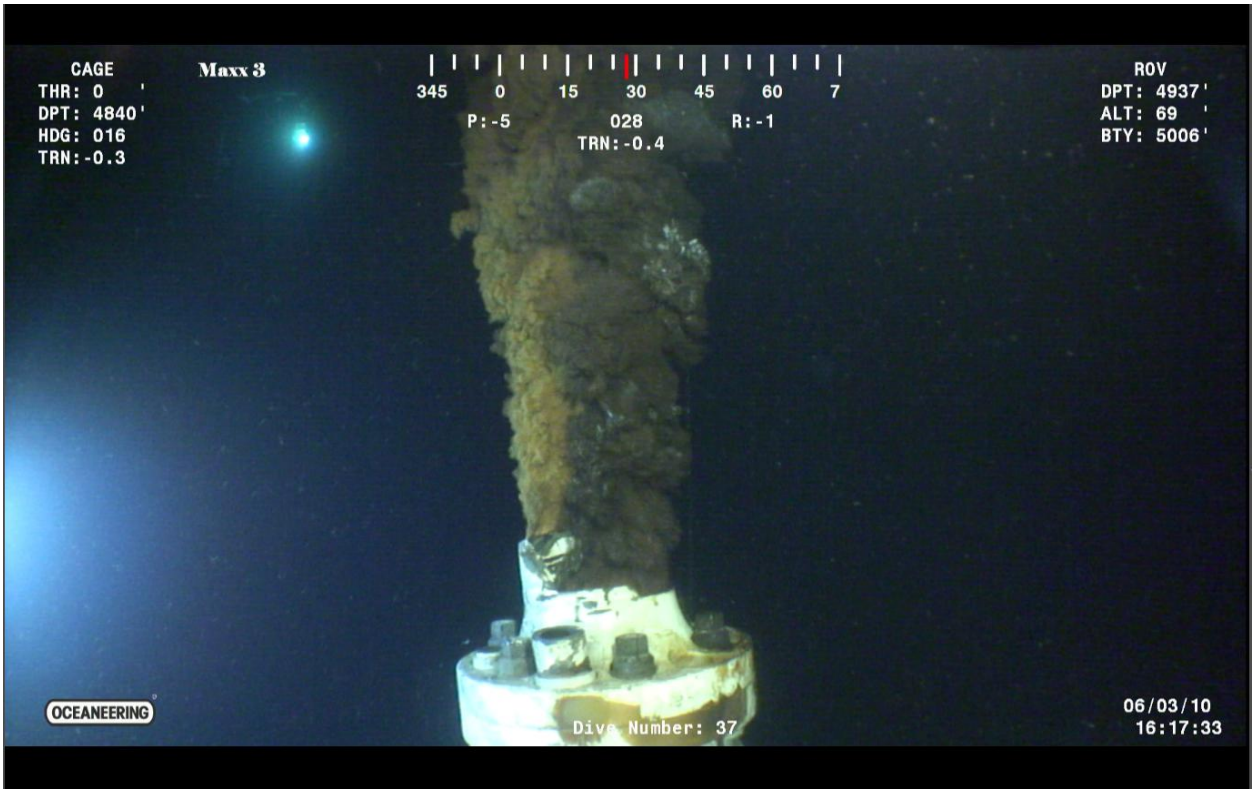

Shortly after the cut, BP placed a 'Tophat' over the riser stub, allowing the capture of some of the oil. This Tophat had vents that could be equipped with a pressure gauge, allowing an alternative method to estimate the flow. Teams affiliated with the Department of Energy, using the subsequent pressure readings to estimate flow, pooled their findings with the Plume Team results to produce a common estimate for operation purposes to the National Incident Command.

CONCLUSIONS

As with earlier estimates, the conclusions in this report are only to aid the Response, not to determine the final Federal estimate of spillage. Because of time and other constraints, only a small segment of the leakage time was examined, and assumptions were made that may through later information or analysis be shown to be invalid. For example, the Team assumes that the average flow between the start of the incident and the insertion of the RITT was relatively constant and the time frames that were included in the examined videos were representative of that average. If this were not true, then the actual spillage may differ significantly from the values stated below.

Most of the experts have concluded that, given the limited data available and the small amount of time to process that data, the best estimate for the average flow rate for the leakage prior to the insertion of the RITT is between 25 to 30 thousand bbl/day. However, it is possible that the spillage could have been as little as 20,000 bbl/day or as large 40,000 bbl/day. Further analysis of the existing data and of other videos not yet viewed may allow a refinement of these numbers.

For the time period after the riser cut, most of the experts concluded that the likely range for the flow was between 35,000 and 45,000 bbl/day but could be as high as 50,000 bbl/day.

The Plume Team then met with other experts from the Department of Energy, who employed non-PIV methods to estimate flow rate. The combined groups reached a consensus estimated flow range of 35,000 bbl/day to 60,0000 bbl/day.

APPENDICES

Appendix 1 includes some statistical conclusions on the separate PIV estimates, treating each estimate with equal weights. It does not necessarily represent the consensus of the Team, which has already been presented in the Conclusions. Team members who did not conduct PIV analysis—but instead served as experts to the Team on related subjects—provided Appendices 2 and 3. Appendices 4-8 describe the separate PIV results. Appendix 9 lists the biographies of the team members. Review comments are included in Appendix 10.

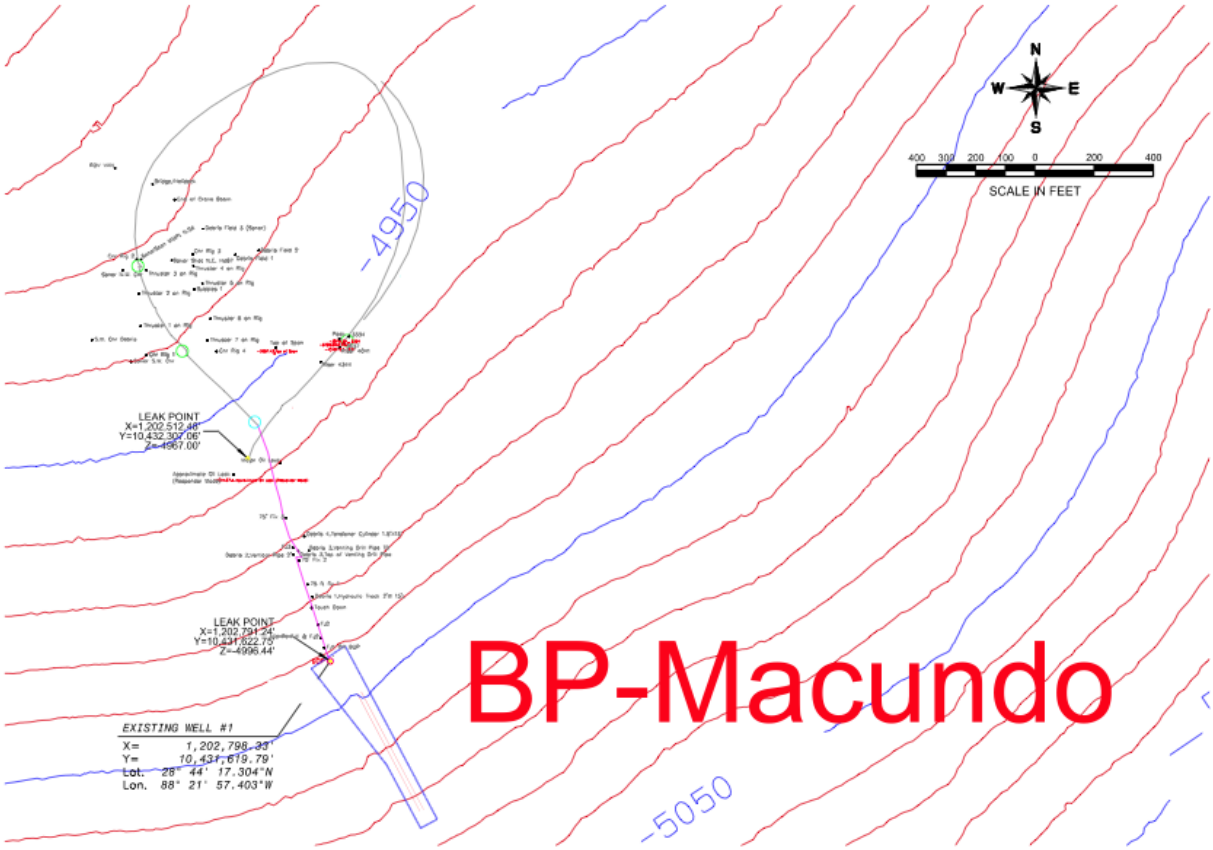

Appendix 1: NIST Statistical Analysis

Pooling Plume Team Expert Assessments

Antonio Possolo & Pedro Espina
National Institute of Standards and Technology

June 18th, 2010

1 Summary

In the course of the Plume Team meeting that took place in Seattle on June 13th, 2010, and subsequently during a teleconference co-chaired by U.S. Secretaries Chu and Salazar on June 14th, several members of the Plume Team produced or revised their independent measurements of the average daily volume of oil flowing from the stub left after the riser pipe was cut in preparation for deployment of the "Lower Marine Riser Package" (LMRP) containment system ("Top Hat").

A statistical method was used to reconcile the estimates produced by the Plume Team experts with one another and with the actual average daily volume being captured by the recovery vessels at the Deepwater Horizon incident site. The corresponding analysis yielded an interval from 23 000 bbl/day to 49 000 bbl/day[1] that, with approximately 95 % probability, includes the true value of that average daily volume of oil.

2 Assessments

The following table summarizes the intervals that five experts, A–E, a subset of the Plume Team, provided during the June 13th, 2010, Plume Team meeting in Seattle, or during the teleconference co-chaired by U.S. Secretaries Chu and Salazar on June 14th. These are estimates of the average daily volume of oil flowing from the stub left after the riser pipe was cut.

Two additional Plume Team members (F and G) produced estimates of the oil leak prior to the riser cut aforementioned, but these results are not considered here because this report only applies to the after cut situation. However, it is worth noting that Expert F expressed confidence in the method and results produced by expert D.

EXPERT	LOW (BBL/DAY)	HIGH (BBL/DAY)	CONFIDENCE
A	24 000	40 000	Medium-High
B	24 000	40 000	Medium-High

[1] Standard barrels of crude oil per day.

C	24 000	40 000	Medium-High
D	42 000	49 000	Very High
E	30 000	40 000	Medium-High

The values listed above were multiplied by the factor 1.35 × (0.30 / 0.41) = 0.988 prior to reconciliation, for the reasons discussed during the teleconference of June 14th and relating to the proper conversion to barrels of oil at sea surface thermodynamic conditions, and to the use of the same volume fraction of oil in the total leak flow as used by other FRTG teams who also estimated the oil leak.

3 Approach

We use probability distributions to model the uncertainty implied in each expert's assessment, and apply a statistical method by Stone [1961][2] to reconcile these distributions. More specifically, we use Stone's [1961] linear pool, which is equivalent to asking each expert to cast a vote in favor of his work, where his vote is a random draw from the probability distribution that encapsulates the expert's assessment and that expresses his confidence in his results. The final result is a probability distribution that represents the Plume Team's collective state of knowledge about the average volume of oil flowing from the stub left after the riser pipe was cut.

4 Details

With the exception of expert D, who during the teleconference of June 14th expressed very high confidence in his assessment, the other members of the Plume Team expressed views of their work that were consistent with medium to high confidence in their assessments. We translated this "medium to high" confidence into a 65 % probability,[3] and took "very high" confidence to mean 90 % probability. This conforms to the Guidance Notes for Lead Authors of the IPCC Fourth Assessment Report on Addressing Uncertainties that have been used by the Intergovernmental Panel on Climate Change in the preparation of their fourth assessment report [Solomon et al., 2007, Table 3, *Quantitatively calibrated levels of confidence*], where "medium" is taken to mean confidence of about 50 %, "high" is taken to mean confidence of about 80 %, and "very high" is taken to mean confidence of about 90 %.

Also assuming that the probability distributions implicit in the experts' assessments were Gaussian, and using the confidence levels just mentioned, we derived the means and standard deviations of these distributions: for example, expert A's implied mean is 31 600 bbl/day, and the implied standard deviation is 8 500 bbl/day.

[2] Stone's [1961] method was further elaborated by Bacharach [1979], Lindley [1983], and Clemen & Winkler [1999], among others.

[3] The average of 50 % and 80 % probability.

We produced a statistical sample of size 1 000 000 by repeating the following two steps: (i) select one expert uniformly at random (each one with the same probability of being selected); and (ii) draw one value from the selected expert's distribution.

The figure depicts a smooth estimate of the probability density of the results, produced using a kernel density estimator.[4] The corresponding mean (blue dot) is 36 300 bbl/day: the interval from 23 000 bbl/day to 49 000 bbl/day (horizontal blue line) should include the true average number of barrels of oil exiting the stub of the riser pipe per day, with probability approximately 95 % (shaded area under the curve). The most probable value (where the probability density achieves its maximum), is 44 600 bbl/day (red diamond).

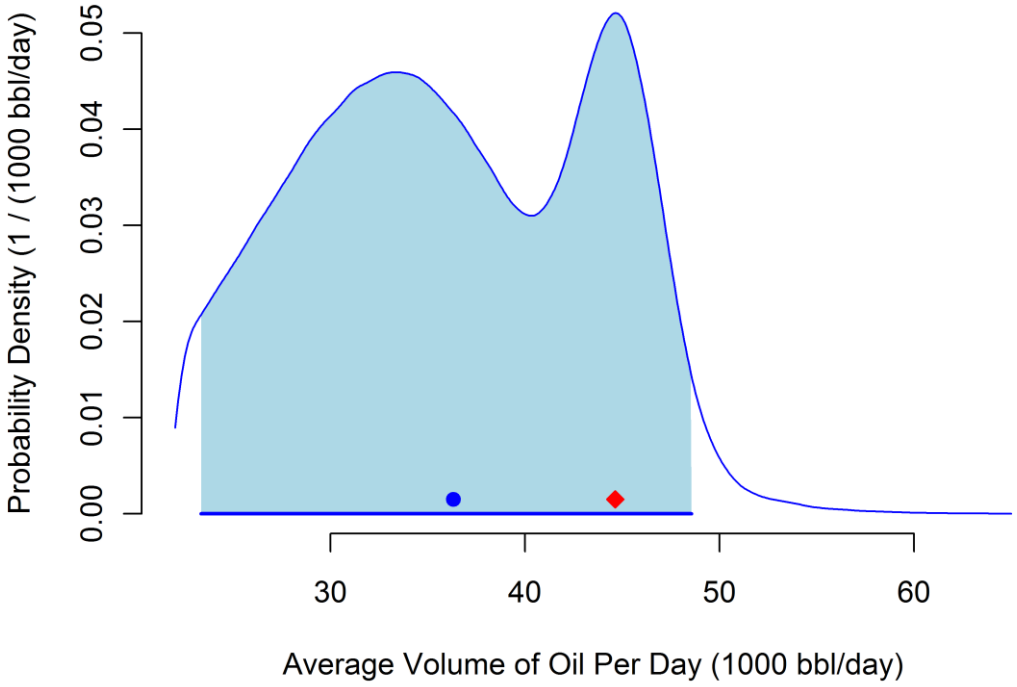

Acknowledgments

The authors are much indebted to Dr. Blaza Toman (*Mathematical Statistician*, NIST Division 898), Dr. Michael Moldover (*NIST Fellow*, NIST Division 836), and Drs. John Wright and Aaron Johnson (NIST Division 836) for their guidance and review of this work.

[4] As implemented in the function density of the R [R Development Core Team, 2009] environment for statistical programming, computation, and graphics.

References

Bacharach, M. (1979) Normal Bayesian Dialogues. *Journal of the American Statistical Association*, 74 (368): 837–846.

Clemen, R. T. and Winkler, R. L. (1999) Combining Probability Distributions from Experts in Risk Analysis. *Risk Analysis*, 19 (2), 187–203.

Lindley, D. V. (1983) Reconciliation of probability distributions. *Operations Research*, 31(5): 866–880.

R Development Core Team (2009) R: A language and environment for statistical computing. R Foundation for Statistical Computing, Vienna, Austria. ISBN 3-900051-07-0, URL http://www.R-project.org.

Solomon, S., Qin, D., Manning, M., Marquis, M., Averyt, K., Tignor, M. M. B., and Miller, H. L. (2007, editors) *Climate Change 2007 — The Physical Science Basis*. Working Group I Contribution to the Fourth Assessment Report of the Intergovernmental Panel on Climate Change (IPCC). Cambridge University Press, New York, NY, 2007.

Stone, M. (1961) The opinion pool. *Annals of Mathematical Statistics*, 32 (4): 1339–1342.

Appendix 2: Reservoir Fluid Study

Personal Work Report

To: Bill Lehr, NOAA
From: Paul Bommer, Ph.D.
Department of Petroleum and Geosystems Engineering
The University of Texas at Austin
June 2, 2010

Re: Reservoir fluid study and oil flow rate from the BP Mission Canyon 252 1-01 blow out.

Bill:

My approach to this problem, described in more detail below, is to determine what type of fluid is in the reservoir, construct a flow model in the reservoir, and construct a flow model through a conduit to the surface. In summary, I calculate the oil flow rate range at the top of the blow out preventers with the riser attached as between 9,200 and 22,000 stock tank (standard condition) barrels of oil per day. These results are based on the data currently available from BP and my selection of the most likely flow conduit.

The Reservoir Fluid: The reservoir is a gas – volatile oil reservoir. This is important because the reservoir fluid is actually a critical fluid in the reservoir at 11,856 psia and 243 deg F. A critical fluid is a fluid at the critical point in the reservoir meaning gas and liquid are indistinguishable from each other at this point. Two companies analyzed the reservoir fluid samples and came to only slightly different conclusions.

The first study was done by Core Labs (PENCOR) on April 22, 2010. In this study the fluid was characterized as a gas with a dew point. This can be seen in Appendix A, second page, where the percentage of liquid begins at zero at the dew point of 6,504 psia at 243 deg F. Below the dew point the liquid percentage increases rapidly to a maximum of 59.96% at 6,000 psia and 243 deg F. As pressure continues to be decreased the fluid shows a retrograde phenomena as some of the liquid vaporizes back into the gas phase with 49.63% liquid remaining at 1,000 psia and 243 deg F.

Once the gas leaves the reservoir and enters the flow conduit to the surface some cooling takes place due to the geothermal gradient and the Joule-Thompson effect if the gas is free to expand. To demonstrate the effect of cooling on the amount of liquid present a test was performed by PENCOR at 100 deg F. Using this data (see the first page of Appendix A) there is 67% liquid at 2,250 psia and 100 deg F. This pressure is chosen because it is the pressure at the ocean floor due to the weight of sea water.

The second study was performed by Schlumberger and reported on May 19, 2010. An excerpt from this study is shown in Appendix B. This study reported the reservoir as a

liquid with a bubble point of 6,348 psia at 243 deg F. This means that there were gas bubbles that appeared in the test cell rather than liquid droplets as in the PENCOR test. This reinforces the notion that this is a critical fluid at reservoir conditions. The Schlumberger tests are the same type run by PENCOR except that the Schlumberger tests were all done at 243 deg F (none at 100 deg F). At the ocean floor pressure of 2,250 psia and the reservoir temperature of 243 deg F the percentage of liquid from the Schlumberger test of Appendix B is 59.7%. Please note that this compares favorably with the results form PENCOR, which under identical conditions recorded 53.8% liquid in the test cell. Therefore, I believe the fluid can be adequately described using either data set.

Both studies also performed a flash calculation from reservoir conditions to standard conditions. Partial results from the flash calculation are shown in Table 1. I have made an independent flash calculation using the base data from Schlumberger and arrived at very similar results.

Multi-Stage Separator Test

PENCOR ID No. 36126-53: 18,142 ft Depth

Separator Conditions		Liquid	Gas	Gas	Solution	Solution	Liberated	Separator
Pressure (psia)	**Temperature** (°F)	**Density** (g/cm^3)	**Density** (g/cm^3)	**Gravity** (Air = 1.0)	**GOR, R_s** (scf/stb)	**GOR, R_s** (scf/sep bbl)	**GOR, R_l** (scf/stb)	**Shrinkage** (stb/bbl at P,T)
6,504	**243**	**0.528**		**N/A**	**2,554**		0	**N/A**
1,250	130	0.731	0.073	0.683	475	607	2,079	0.783
450	120	0.763	0.027	0.730	260	306	216	0.848
150	120	0.768	0.015	0.894	123	139	137	0.881
15	60	0.833	0.002	1.538	0	0	123	1.000

Summary Data

Total Solution Gas-Oil Ratio	2,554	scf/stb
Stock Tank Oil Gravity	38.2	°API at 60 °F
Formation Volume Factor	2.367	(Bbl at P_{sat} /stb)
Accumulated Gas Gravity	0.740	(Air = 1.00)
Color of Stock Tank Oil	Light Crude	

Notes:

- stb: stock tank barrel at 60 °F
- sep bbl: volume of separator liquid at P,T.
- Solution GOR is given as the gas volume per stock tank barrel (stb) and per separator barrel (sep bbl)
- Separator Volume Factor is the inverse of the Separator Shrinkage Factor
- Liberated GOR (R_l) is gas liberated from previous stage to current stage per stock tank barrel (stb)
- See following page for flash gas compositional analyses

Table 1
PENCOR Flash Calculation Results

Flash calculation results from the Schlumberger study, while not identical, are very similar to the results shown in Table 1.

The viscosity of the fluid is shown in Table 2. The average viscosity in the reservoir, between the original pressure and the flowing pressure at the bottom of the well is 0.165 cp.

Preliminary Viscosity at 243°F
PENCOR ID No. 36126-53: 18,142 ft Depth
Measured using Electro-Magnetic Viscometer
Piston used 0.2 - 2.0 cP

Pressure (psia)	Measured Viscosity Centipoise (cP)
14,500	0.190
14,000	0.186
13,000	0.178
11,856	0.168
11,000	0.161
10,000	0.154
9,000	0.146
8,000	0.139
7,000	0.139
6,900	0.140
6,800	0.134
6,504	0.162
6,430	0.172
6,300	0.182
6,000	0.205
5,000	0.266
4,000	0.330
3,000	0.405
2,000	0.475
1,000	0.595
150	0.879

Table 2
Reservoir Fluid Viscosity

The Reservoir: Data from BP shows that this reservoir is a sandstone. The average properties are shown in Table 3. The reservoir is estimated to cover 4,500 acres with one well estimated to drain 1,500 acres.

MD Interval (ft)	Net Pay (ft)	Porosity (%)	Sw (%)	ko (md)
17,804-17,806.5	2.5	22.48	24	397.28
18,067-18,089	22	20.67	17.17	86.53
18,120-18,191	64.5	22.08	9.7	275.22
18,217.5-18,238.5	6.5	21.08	21.85	110.39
Total Net Pay (ft)	95.5			
	Wtd Avg	21.7	12.6	223.7

Table 3
Average Reservoir Properties
From BP Data

A flow model for the reservoir can be constructed using the radial single phase (liquid) version of Darcy's Law shown as equation (1).

$$\frac{q}{p_e - p_{wf}} = \frac{k_o h}{141.2 B_o \mu_o \left[\ln\left(\frac{r_e}{r_w}\right) + s \right]} \quad \text{..... (1)}$$

$q =$ liquid flow rate (STB/day)

$p_e =$ reservoir boundary pressure = 11,856 (psia)

$p_{wf} =$ flowing pressure inside, but at the bottom of the well (psia)

$k_o =$ permeability to reservoir fluid (md)

$h =$ net reservoir thickness (ft)

$B_o =$ liquid formation volume factor = 2.367 $(\text{reservoir bbl/STB})$

$\mu_o =$ viscosity of reservoir fluid = 0.165 (cp)

$r_e =$ radius to the well drainage boundary = 4,560 (ft)

$r_w =$ well bore radius = 0.254 (ft)

$s =$ reservoir skin damage = 0 (dimensionless)

$$\frac{q}{p_e - p_{wf}} = \frac{223.7(95.5)}{141.2(2.367)0.165\left[\ln\left(\frac{4,560}{0.254}\right) + 0 \right]} = 39.5 \text{ STB/day/psia} \quad \text{..... (2)}$$

Equation (1) is also called the reservoir inflow performance relation (IPR) with the result shown as volume of liquid at standard conditions flowing per day per incremental drop in pressure that is necessary to induce flow into the bottom of the well. Equation (2) is the IPR for this reservoir. So long as the reservoir pressure does not fall below the bubble (dew) point, this equation will apply to the critical single phase fluid in the reservoir. Equation (2) can be rearranged to solve for the pressure remaining at the bottom of the well (p_{wf}) that is available to support a given flow rate (q) to the surface with a constant boundary pressure (p_e).

The Flow Conduit: There are several possibilities for the flow conduit from the reservoir to the ocean floor. I will discuss three possibilities.

(1) I believe the most likely conduit is the annular space between the outside of the production casing and the inside of the various liners and casing strings that sealed the balance of the well. This belief is based on the rapidity of gas reaching the surface just before the blow out, but this is another subject that has been outlined in a forum at The University of Texas Energy Institute. A webcast of the forum can be seen at www.energy.utexas.edu. The entrance to this path is the reservoir outside the 7" casing. The exit from this path is past the well head seals. This path leads to the maximum flow rate calculated as a portion of this work.

(2) As a second possibility, the annular flow path of option (1) is used, except in this case the rupture discs in the 16" casing burst (see Appendix C and D for diagrams). Once the disc ruptures the reservoir fluids can enter the annular space between the 16" casing and the 18" liner. The shoe (end) of the 18" liner is exposed to open formation that was tested to a fracture pressure of 5,385 psi. The formation would fracture when exposed to the disc rupture pressure of 7,500 psi allowing reservoir fluids to exit the well. If a permeable sand is present in the open interval, reservoir flow will begin to charge this formation with reservoir fluids. The flow of reservoir fluid into the fracture diminishes the fluid escaping at the surface. This becomes the minimum flow estimate calculated in this work.

The fracture that is created in this scenario initiates 3,900' below the mud line. The vertical stress at this point is roughly 6,150 psi. This should cause the fracture to be a vertical fracture and if it is charging a permeable sand, it is unlikely that the fracture can escape beyond the sand boundaries to any large extent. This means the fracture is confined and will not grow to the mud line and erupt outside the well.

(3) The least likely conduit is through the bottom of the 7" casing and up the inside of the 7" and 9 7/8" casing to the surface. The entrance to this path is through the guide shoe, float joints, and float collar at the bottom of the 7" casing. The exit of this path is in the annulus between the 9 7/8" casing and a segment of 5 1/2" drill pipe and 3 1/2" tubing that was being used in the well at the time of the blow out. Although not completely conclusive there was a test on the check valves in the float collar that indicated they were not leaking at the end of the cement job. If this is true this path was sealed by the floats in the collar and by the 189 feet of cement that solidified in the float joints between the collar and shoe. For reservoir flow to enter through a leaking float collar, the reservoir gas bubble would be required to migrate down, against gravity. I think the natural path for a gas bubble is to rise through the cement and mud in the annulus.

It has been speculated that the production casing collapsed due to the gas pressure in the annulus and that this created an entry point to the inside of the casing. The collapse rating of the 7" should have been at least 12,000 psi (32 ppf, HCQ-125) which is more than the

reservoir pressure. The collapse rating of the 9 7/8" is 10,695 psi (62.8 ppf, Q-125, corrected for axial load) which is more than the gas pressure should be at the depth the 9 7/8" casing was used. Therefore, the production casing should not have collapsed.

I have made flow calculations for this path, but I consider this pathway so unlikely that I do not present these results as a bound on the flow rate.

A well bore diagram from BP is shown in Appendix C. Although not shown on the well bore diagram, the well head and the blow out preventers attach at the mud line and extend above the ocean floor.

A well bore diagram showing the calculated gas bubble pressures in the annulus and the possible fracture point discussed as conduit (2) is shown in Appendix D.

Exit Pressure: The pressure exerted by the ocean water at the sea floor is roughly 2,250 psi. This pressure is exerted at every leak point where fluid can flow out of the well. BP measured flowing pressures above and below the blow out preventers. These pressures are shown in Figure 1. The flow restriction through the blow out preventers creates an 850 psi pressure loss. An additional 400 psi pressure loss is created by the various flow restrictions in the marine riser. There is also a pressure loss in the leaking well head seals, but this cannot be measured.

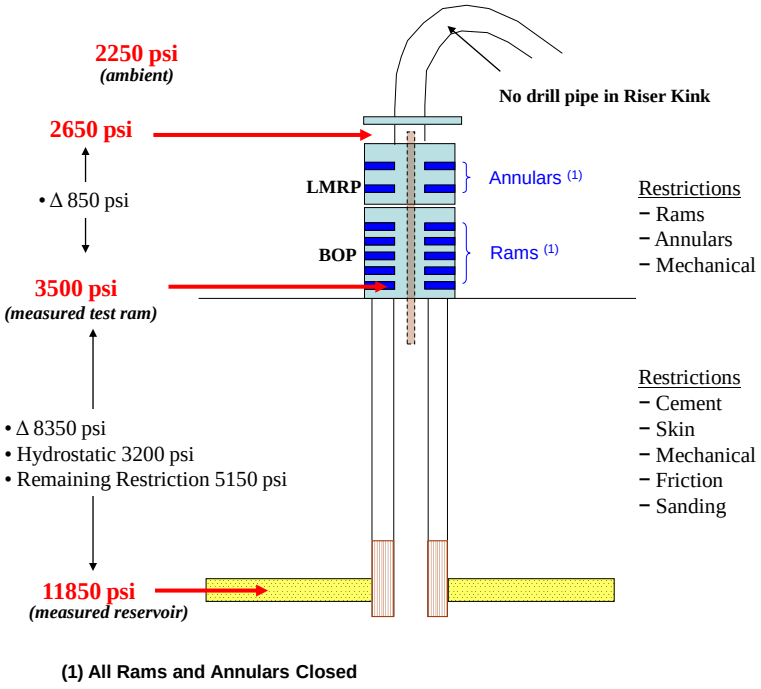

Figure 1
BP Flowing Pressure Measurements

Flow Calculation: The flow rate up a given conduit is computed using a nodal analysis approach and the modified Hagedorn and Brown two phase flow correlation. The basis for this correlation is the steady state mechanical energy balance neglecting any kinetic energy change. The method is an iterative one where the correlation predicts the flow regime and liquid hold up at any point in the flow conduit and uses this to compute the average flowing fluid density. The average flowing density is used to estimate the pressure gradient at a given point and another step is then taken along the flow path.

A number of flow rates are chosen and the correlation used to calculate the flowing pressure at the bottom of the well. This is the flowing bottom hole pressure $\left(p_{wf}\right)$ necessary to flow the fluid to the ocean floor up the flow conduit and still have the pressure required to exit the well head.

A graph of the flow rate versus bottom hole flowing pressure such as shown in the following figures is called the vertical lift performance (VLP) of the flow conduit in question. Also plotted on the figures is the inflow performance relation (IPR) that describes flow from the reservoir. Where these two lines intersect is the maximum rate the reservoir can flow into the bottom of the conduit with sufficient bottom hole flowing pressure remaining to flow up the conduit to the surface.

Flow Conduit (1) – the annulus: The annulus is simulated using a conduit diameter described as a hydraulic diameter. The hydraulic diameter is the customary turbulent flow approximation equal to four times the computed hydraulic radius of the sections being considered. The average hydraulic diameter used in the simulation of the annulus is 3.67".

In order to simulate the flow restriction inside the blow out preventers and the marine riser (Figure 1) the exit pressure from the conduit is set at 1,250 psi more than the pressure of the sea water or 3,500 psia.

To simulate the pressure loss in the leaking well head seals a two phase choke flow equation from Ross is used. This equation is shown as equation (3).

$$p_1 = \frac{q\sqrt{GLR}}{235.4D^2} \quad \text{..... (3)}$$

$q =$ STB/day

$p_1 =$ upstream pressure $\left(\text{psi}\right)$

$D =$ choke diameter $\left(\text{inch}\right)$

$GLR =$ gas/liquid ratio $\left(\text{Scf/STB}\right)$

The leak diameter inside the seals is unknown at this time. An estimate based on hydraulic diameter between the well head housing and the seal case is 1.3". A better estimate of this

restriction may be made in the future by a careful examination of the dimensions of the seals and well head. The gas-liquid ratio is as shown in Table 1.

No flow restriction other than the open annulus is assumed in the cemented area at the bottom of the well.

Figure 2 shows the results of several simulations of annular flow for various exit pressures.

The most likely flow rate occurs when the seal, well head, blow out preventer, and marine riser restrictions are considered. This flow rate is estimated to be 22,000 STB/day.

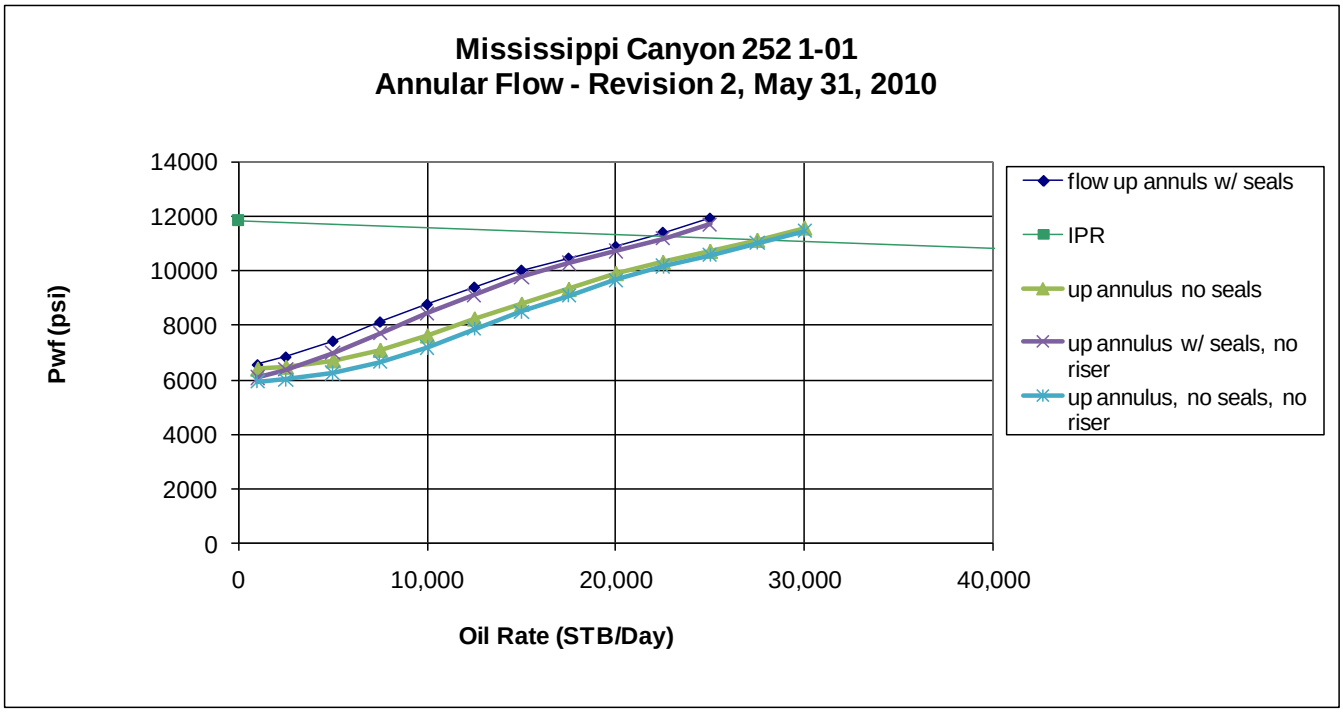

Figure 2
Annular Flow Rate
Based on Reservoir Inflow and Annular Conduit Flow Performance

As an aside, Figure 2 shows that the loss of the marine riser above the blow out preventer has very little effect on flow rate because the back pressure due to flow in the riser is only 400 psi.

Flow Conduit (2) – the annulus coupled with a fracture: The flow path is the same model described for option (1) except now a fracture has formed at 8,969' at the end of the 18" casing and the fracture is accepting part of the flow rate. The pressure necessary to hold the fracture open and inject part of the reservoir flow into the fracture is estimated to be 5,600 psi. The two phase flow model is used to predict the flow rate escaping at the ocean floor that is required to create this amount of pressure at the fracture point 3,900'

below the mud line. The annulus hydraulic diameter in this section is 4.97". The same well head and seal pressure loss boundary conditions used in option (1) are used here.

The results of this simulation indicate that 9,200 STB/day are escaping at the surface. This means that roughly 12,800 STB/day are charging the permeable sand at 8,969'. This should not be a steady state condition. Flow probably fluctuates between the fracture and the ocean floor.

Flow Conduit (3) – inside the production casing: This flow path is the inside of the 7" and 9 7/8" casing. The average diameter inside this conduit is 7.51".

The entrance to this conduit is through the float collar flapper, which must be damaged for flow to access this path. The diameter of the flapper is roughly 2.375" and the pressure loss though this short restriction is negligible.

The exit from this path is out the annulus between the 5 1/2" drill pipe and 3 1/2" tubing and the 9 7/8" casing and the inside of the 5 1/2" and 3 1/2" tubes. The 850 psi flow restriction in the blow out preventers remains the same as before as does the 400 psi flow restriction in the marine riser. Thus, the exit pressure is a constant 3,500 psi, including the pressure of the sea water.

Figure 3 shows the results of two simulations for pipe flow using exit pressures with and without the marine riser.

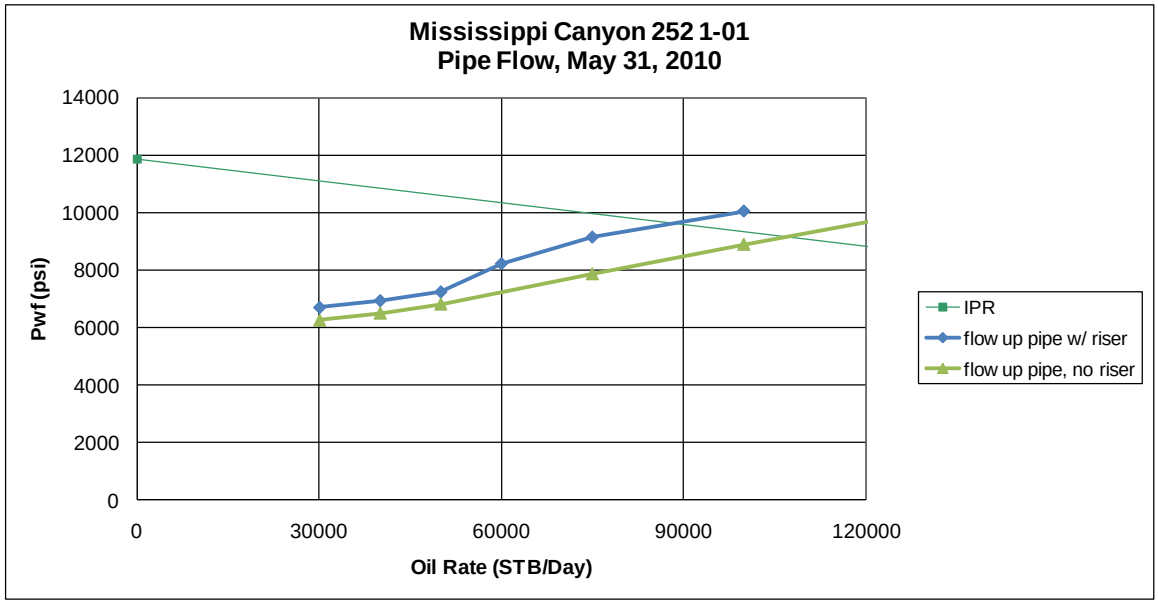

Figure 3
Pipe Flow Rate
Based on Reservoir Inflow and Pipe Flow Performance

Using the estimates shown in Figure 3, the flow rate up the pipe is 90,000 STB/day with the marine riser attached. Without the marine riser the flow increases to 105,000 STB/day.

As I do not believe this flow path is likely (see the flow conduit section for discussion), I have not included these estimates in my minimum and maximum flow rate statement.

Results: From this process I believe the flow is up the annulus. The minimum flow up this pathway is 9,200 STB/day and the maximum flow is 22,000 STB/day. Confirmation of flow rate will occur when BP severs the riser and installs the soft seal that will capture the flow to a vessel.

Constant Composition Expansion at 100°F
Pressure-Volume Relations
PENCOR ID No. 36126-53: 18,142 ft Depth

Pressure (psia)		Relative Volume (V / V_{sat})	Oil Density (g/cm^3)	Relative Liquid Volume (%)	Oil Compressibility ($\Delta V/V/\Delta psi) \times 10^6$	Y-Function ($(P_{sat}-P)/P(V/V_{sat}-1)$)
11,856	**Reservoir**	**0.939**	**0.639**			
10,000		0.956	0.628		9.60	
9,500		0.962	0.624		10.76	
9,000		0.967	0.621		11.08	
8,500		0.973	0.617		11.77	
8,000		0.979	0.613		13.21	
7,500		0.986	0.609		14.23	
7,000		0.994	0.604		14.87	
6,710		0.999	0.601		17.54	
6,636	**Saturation**	**1.000**	**0.600**	**0.00**	**18.22**	
6,616		1.001		36.20		
6,500		1.003		57.07		6.99
6,000		1.015		68.53		7.15
5,500		1.030		68.78		6.98
5,000		1.048		68.76		6.83
4,500		1.072		69.09		6.58
4,000		1.105		68.90		6.25
3,500		1.153		68.37		5.84
3,000		1.230		68.32		5.27
2,500		1.360		67.70		4.60
2,000		1.597		66.55		3.88
1,500		2.058		64.51		3.23
1,000		3.073		61.58		2.72

Appendix A
to Bommer Personal Report
PENCOR Fluid Report
at 100 deg F
April 22, 2010

Notes:
- Relative Volume (V / V_{sat}) is the fluid volume at the indicated pressure and temperature relative to the saturated fluid volume.
- Density (lb/ft^3) = Density (g/cm^3) x 62.428
- Compressibility is the average compressibility between the indicated and the next highest pressure.
- Relative Liquid Volume % is the volume of liquid relative to volume at saturation pressure

Constant Composition Expansion at 100°F
Data Presentation Figures

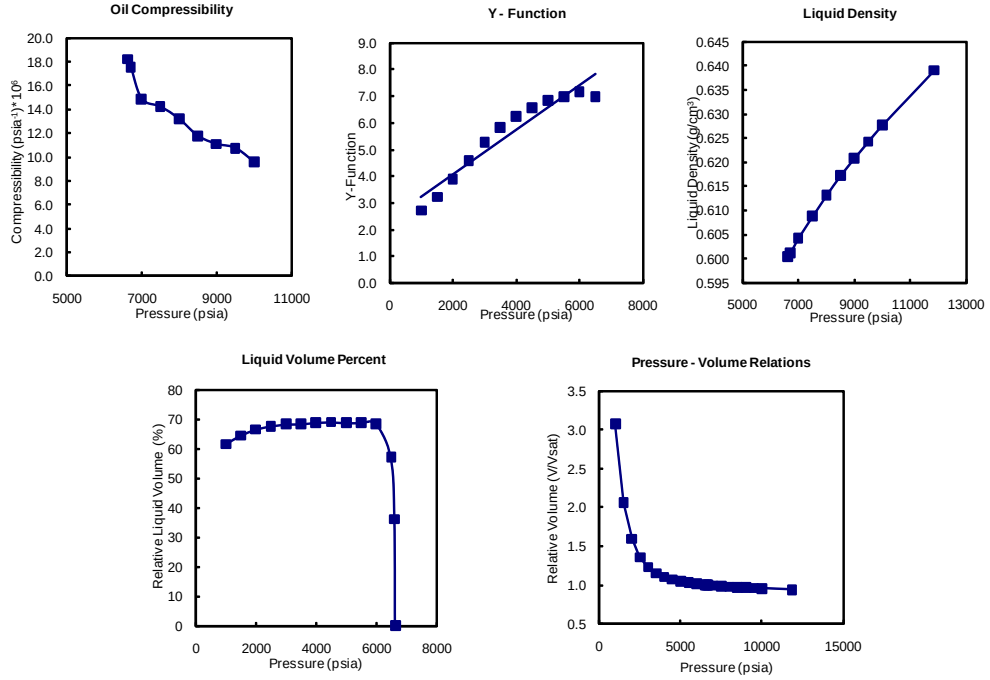

Constant Composition Expansion at 243°F
Pressure-Volume Relations
PENCOR ID No. 36126-53: 18,142 ft Depth

Pressure (psia)		Relative Volume (V/V_{sat})	Oil Density (g/cm^3)	Relative Liquid Volume (%)	Oil Compressibility ($\Delta V/V/\Delta psi \times 10^6$)	Y-Function ($(P_{sat}-P)/P(V/V_{sat}-1)$)
11,856	**Reservoir**	**0.900**	**0.587**			
10,000		0.927	0.570		15.30	
9,500		0.934	0.565		16.75	
9,000		0.943	0.560		17.66	
8,500		0.952	0.555		18.88	
8,000		0.962	0.549		21.42	
7,500		0.973	0.543		22.54	
7,000		0.986	0.536		26.60	
6,504	**Saturation**	**1.000**	**0.528**	**0.00**	**28.17**	
6,495		1.001		9.22		
6,475		1.002		31.23		
6,450		1.003		39.76		
6,400		1.005		50.10		
6,300		1.009		55.49		
6,200		1.013		56.82		3.64
6,100		1.018		57.80		3.63
6,000		1.023		59.96		3.63
5,500		1.052		59.75		3.50
5,000		1.090		59.37		3.36
4,500		1.139		58.57		3.20
4,000		1.208		57.60		3.02
3,500		1.303		57.11		2.83
3,000		1.442		55.39		2.64
2,500		1.645		54.10		2.48
2,000		1.982		53.45		2.29
1,500		2.573		50.99		2.12
1,000		3.812		49.63		1.96

Appendix A
to Bommer Personal Report
PENCOR Fluid Report
at 243 deg F
April 22, 2010

Notes:
- Relative Volume (V/V_{sat}) is the fluid volume at the indicated pressure and temperature relative to the saturated fluid volume.
- Density (lb/ft^3) = Density (g/cm^3) x 62.428
- Compressibility is the average compressibility between the indicated and the next highest pressure.
- Relative Liquid Volume % is the volume of liquid relative to volume at saturation pressure

Constant Composition Expansion at 243°F
Data Presentation Figures

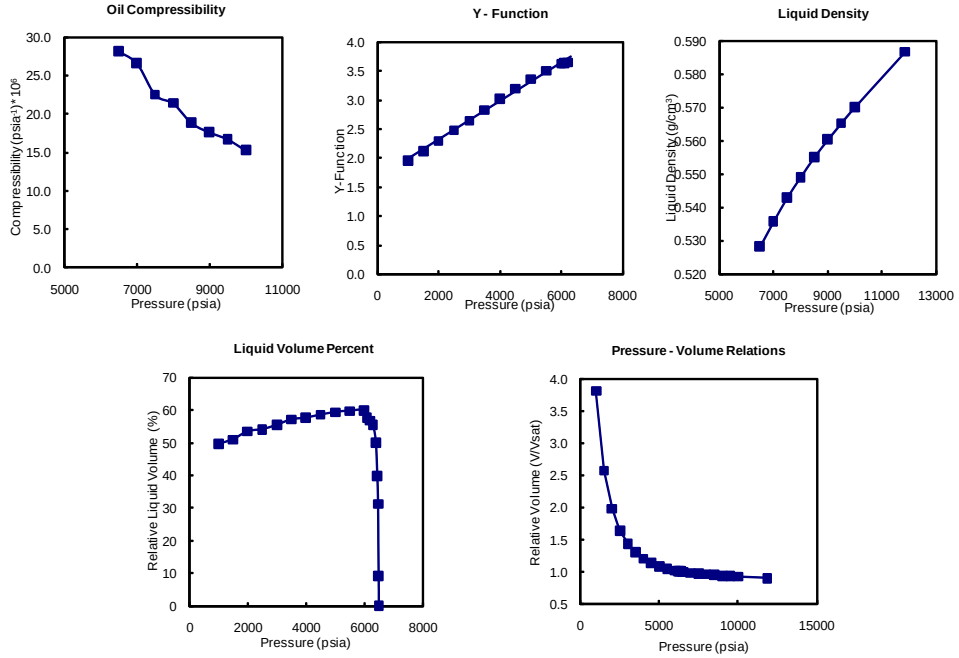

Appendix B to Bommer Personal Report
Excerpt from Schlumberger Fluid Report, May 19, 2010

Client:	BP	**Field:**	Mississippi Canyon 252
Well:	OCS-G 32306 # 1	**Sand:**	-

Schlumberger

PVT Analysis on Sample 1.18; Cylinder 20D127; Depth 18142 ft. MD

Constant Composition Expansion at Tres

The CCE study was initiated by charging a sub-sample of live reservoir fluid into the PVT cell at a reservoir temperature of 243°F and at a pressure of 15,015 psia. Sequential pressure decrease in steps and the corresponding volume changes are presented in Table 21. The pressure-volume (P-V) plots of the CCE data are presented in Figure 11. The intersection of the single-phase and two-phase lines in the P-V plot and the visual observation was used to define the bubblepoint. For the subject fluid, the bubblepoint was determined to be 6,348 psia at the reservoir temperature of 243°F. Also, calculated relative volume and oil compressibility is presented in Table 21. As seen in the table, the compressibility of this oil is 25.0 x 10e-6 1/psia at the saturation pressure.

Table 21: Constant Composition Expansion at 243°F (Sample 1.18)

Sample 1.18; Cylinder 20D127; Depth 18142 ft. MD

	Pressure (psia)	Relative Vol (Vr=V/Vsat)	% Liquid (Vl/Vsat)	% Liquid (Vl/Vtotal)	Liquid Density* Measured Pyc Flash (g/cm3)	Liquid Density* Measured Anton Parr (g/cm3)	Compressibility (10^{-6}/psia)
1	15015	0.8783					8.4
2	14015	0.8862					9.5
3	13015	0.8951			0.598	0.598	10.7
Pi	**11871**	**0.9069**			**0.590**	**0.591**	**12.2**
5	10015	0.9303					15.4
6	9015	0.9457					17.5
7	8015	0.9635			0.555	0.556	19.9
8	7015	0.9842			0.543	0.544	22.8
9	6370	0.9995			0.535	0.536	24.9
Pb	**6348**	**1.0000**			**0.535**	**0.536**	**25.0**
10	6322	1.0000	70.7	70.7			
11	6265	1.0029	70.1	69.9			
12	6215	1.0047	69.6	69.3			
13	5880	1.0184	68.0	66.8			
14	5532	1.0369	66.9	64.5			
15	5039	1.0700	65.0	60.8			
16	4537	1.1148	64.5	57.9			
17	4037	1.1759	63.6	54.1			
18	3536	1.2607	62.5	49.6			
19	3025	1.3859	61.7	44.5			
20	2530	1.5709	60.6	38.6			
21	2027	1.8762	59.1	31.5			
22	1525	2.4202	57.7	23.9			
23	1098	3.3203	54.6	16.4			

Appendix C to Bommer Personal Report
BP Well Bore Diagram

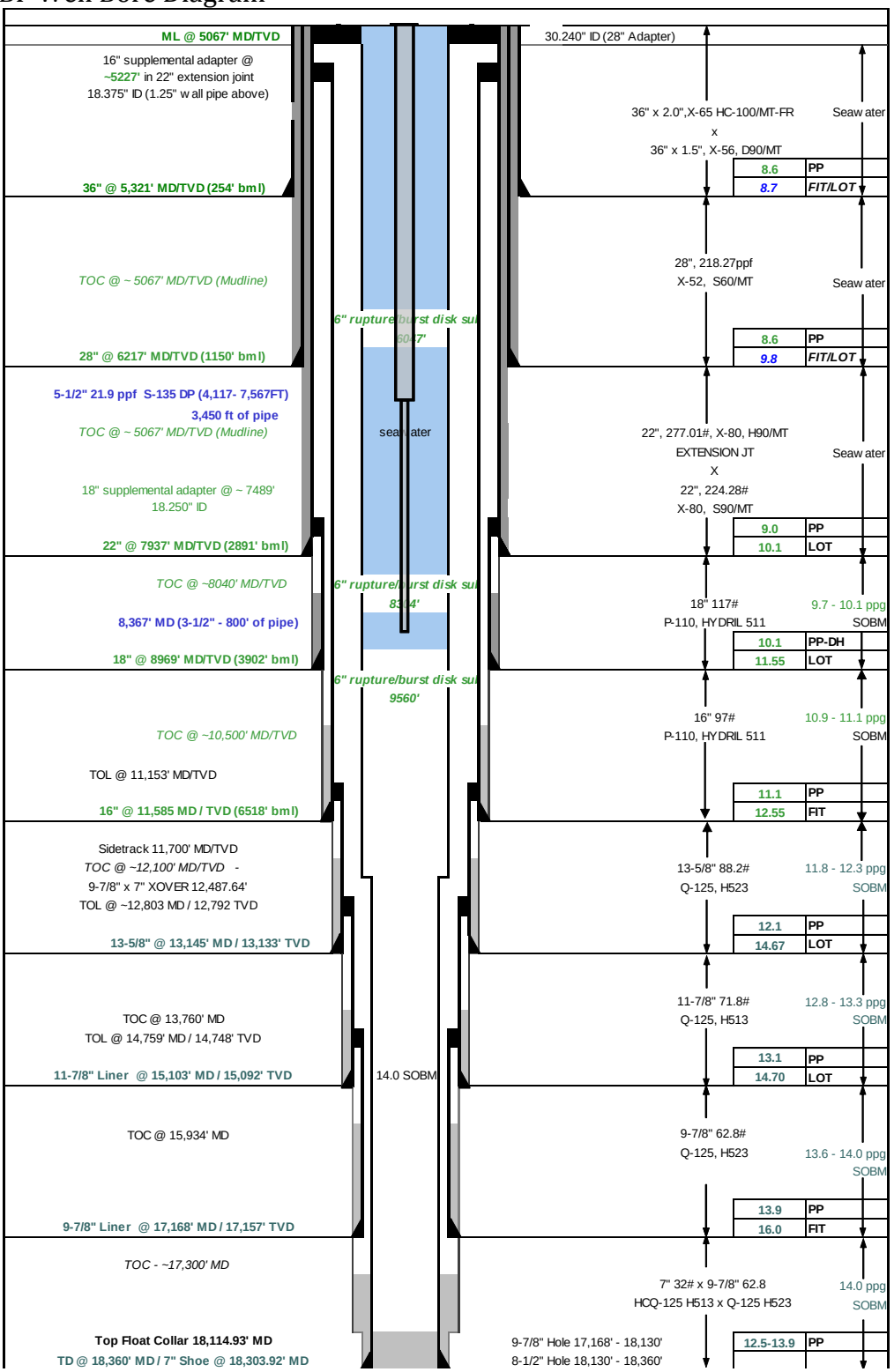

Appendix D to Bommer Personal Report
Calculated Confined Gas Bubble Pressures

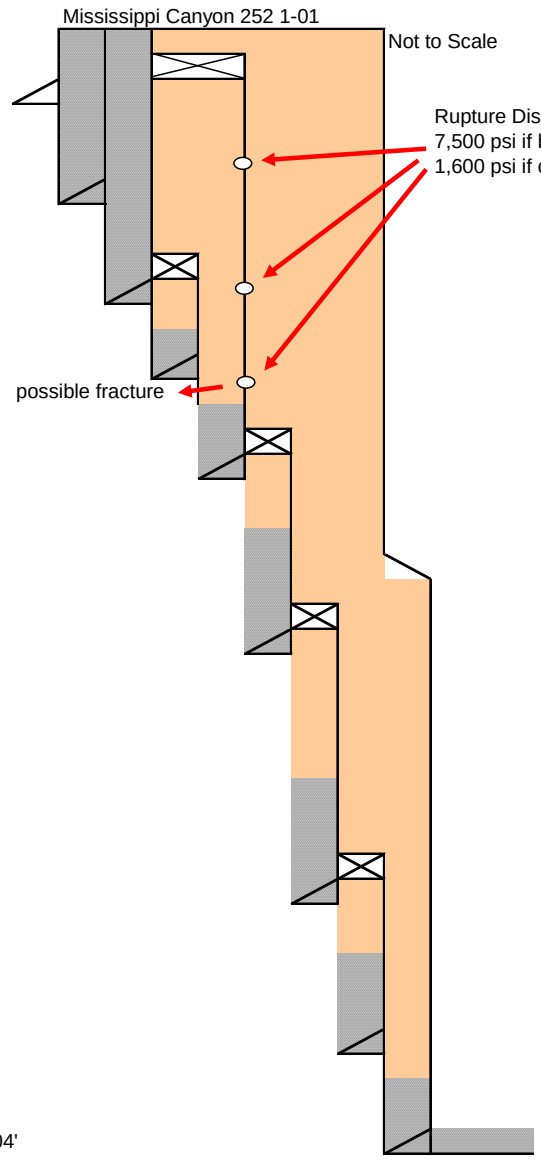

All depths from sea level.	Gas Bubble Psi	Temp deg F
5,067' mud line	7,460	100
36" conductor 5067-5321'		
28" casing 5067-6217', TOC=ML		
22" casing 5067-7937', TOC=ML	8,000	130
18" liner 7489-8969', TOC=8040'	8,215	142
16" caing from 5,227-11,585', TOC=10,500'	8,545	166
13 5/8" liner from 11,153-13,145', TOC=12,100'	9,000	184
11 7/8" liner from 12,803-15,103', TOC=13,760'	9,575	204
9 7/8" liner from 14,759-17,168', TOC=15,934'		
7" x 9 7/8" combination casing from 5,067-18,304' TOC=17,300'	11,856	243

Appendix 3: Description of Underwater Oil and Gas Release Behavior

Poojitha Yapa
Clarkson University

The report explains how oil behaves in general terms when released in deep water. This is not for a particular incident such as the recent Deepwater Horizon accident but applies to atypical subsurface well blowout. This description is based on the fundamentals of fluid mechanics, years of modeling experience, and the experience from observations of data from Deepspill - large scale field experiments conducted in Norway.

In general, when oil and gas are released from a deep water location, they are expected to breakup into bubbles or droplets of various sizes. Theses sizes can vary widely. But what was experienced in Deepspill was generally between 1 mm and 10 mm. However, they can be much smaller or much larger in different spill conditions. Let's consider oil. The larger droplets are going to move faster towards the surface, the smaller droplets are slower. Bubbles are subjected to cross currents which will move them laterally while it is moving upwards. The larger droplets will come to the water surface sooner and the smaller droplets will take a longer time. For this reason the larger droplets and the smaller droplets may not come to the surface at the same location, but quite a distance apart. If there are droplets of very fine scale, like 100 microns or 500 microns it may take weeks or even months for them to come to the surface. That is assuming that the ambient water doesn't have any downward component in the ambient velocity. If it has even a slight downward velocity, then that may negate the buoyant velocity of the smaller particles and they may stay under the water for a very long time.

Gas also has many bubble sizes. In many deepwater releases large amount gas bubbles will dissolve and may never make it to the surface. Gas bubbles move faster than oil bubbles if they are the same size. Because of this, gases can separate from the main plume and start going in a slightly different direction (Chen and Yapa, 2004). The schematic in Figure 1 depicts what has been described before. In this schematic we are using only three sizes of oil bubbles and one size of gas bubbles. In reality there will be many more sizes. Gas bubbles are in purple color and oil bubbles are in orange, pink, and green. Orange are the largest size and comes to the surface the fastest, the green are the slowest because they are the smallest bubbles. Gas bubbles, shown in purple color, in this case dissolve before they reach the surface. We are depicting here only with one size of gas bubble. A real spill may have many sizes and the bubble size distribution can be also continuous. Gases when released in deep water also have the potential to be converted into hydrates. Methane has a level of hydrate dissociation generally around 550 m of water depth as shown in Figure 2. But this is not a fixed value. It depends on parameters like water temperature and gas type. Natural gas can get converted to hydrates at a much higher level. Therefore, gases can get converted

into hydrates as they travel up. Hydrates are still buoyant. It should be noted that no hydrates were observed during the Deepspill experiments.

As hydrates travel towards the water surface they can get reconverted back into gas when they reach the lower pressure in the shallower regions. Figure 2 below, shows the thermodynamic equilibrium curve and the water temperature. This is for a location in Gulf of Mexico. Figure 3 shows schematically how the gases (shown in yellow) are converted into hydrates (shown in blue).

In summary, it is important to understand that what has been described here is the general behavior of oil and gas when it is spilled in deep water and each individual spill may have different condition depending on the environmental factors, ambient factors like water temperature, salinity and the depth at which it was released, the type of oil.

REFERENCES

Yapa, P. D. and Chen F.H., (2004). "Behavior of Oil and Gas from Deepwater Blowouts," *Journal of Hydraulic Engineering*, ASCE, June, 540-553

Chen, F.H. and Yapa, P.D. (2003). "Three-Dimensional Visualization of multi-phase (oil/gas/hydrate) plumes," *Journal of Environmental Modelling and Software*, Elsevier, the United Kingdom, 19 (2004), 751-760.

Chen, F.H. and Yapa, P.D. (2004). "Modeling Gas Separation From a Bent Deepwater Oil and Gas Jet/Plume," *Journal of Marine Systems*, Elsevier, the Netherlands, Vol 45 (3-4), 189-203

Zheng, L., Yapa, P. D., and Chen, F.H. (2003). "A Model for Simulating Deepwater Oil and Gas Blowouts - Part I: Theory and Model Formulation" *Journal of Hydraulic Research, IAHR*, August, 41(4), 339-351

Chen, F.H. and Yapa, P.D. (2003). "A Model for Simulating Deepwater Oil and Gas Blowouts - Part II : Comparison of Numerical Simulations with "Deepspill" Field Experiments", *Journal of Hydraulic Research, IAHR*, August, 41(4), 353-365

Zheng, L. and Yapa, P.D. (2002). "Modeling Gas Dissolution in Deepwater Oil/Gas Spills," *Journal of Marine Systems*, Elsevier, the Netherlands, March, 299-309

Chen, F.H. and Yapa, P.D. (2001). "Estimating Hydrate Formation and Decomposition of Gases Released in a Deepwater Ocean Plume," *Journal of Marine Systems*, Elsevier, the Netherlands, Vol 30/1-2, 21-32

Zheng, L. and Yapa, P.D. (2000). "Buoyant Velocity of Spherical and Non-Spherical Bubbles/ Droplets," *Journal of Hydraulic Engineering, ASCE,* November, 852-855

Zheng, L., and Yapa, P.D., (1998). "Simulation of Oil Spills from Underwater Accidents II: Model Verification," *Journal of Hydraulic Research, IAHR*, February, 117-134.

Yapa, P.D., and Zheng, L., (1997). "Simulation of Oil Spills from Underwater Accidents I: Model Development," *Journal of Hydraulic Research, IAHR*, October, 673-688

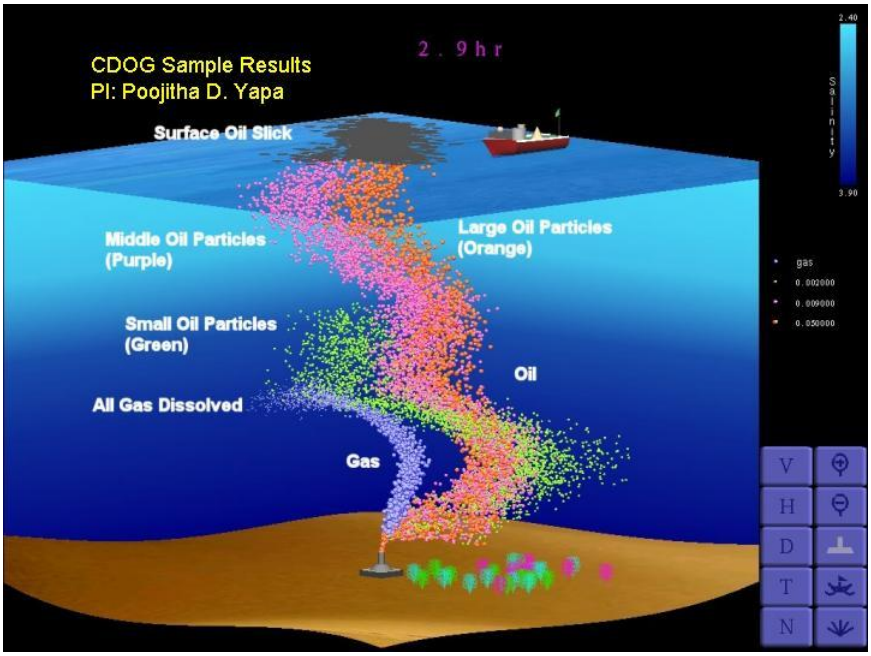

Figure 1: A Schematic representation of how oil and gas behave when released underwater (from various projects under PI: Yapa)

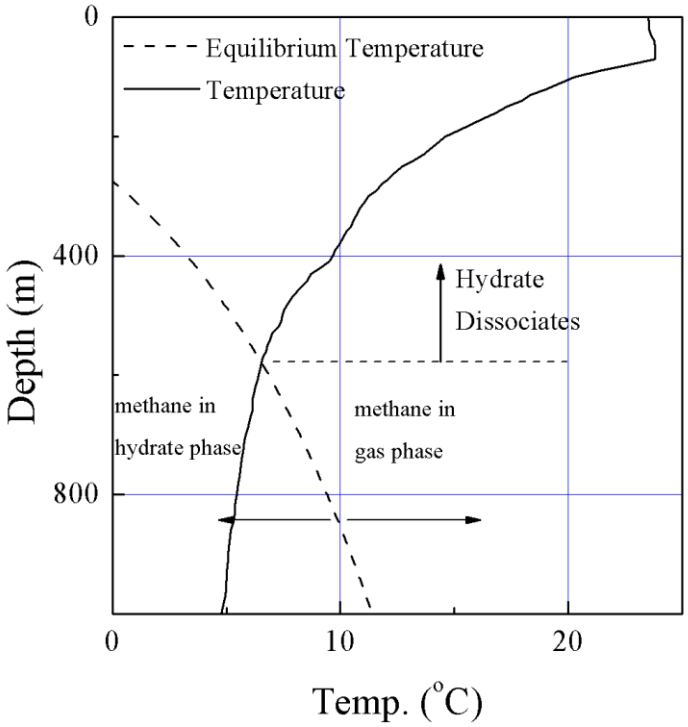

Figure 2: A typical ambient temperature and thermodynamic equilibrium curve for Methane (Yapa and Chen 2004)

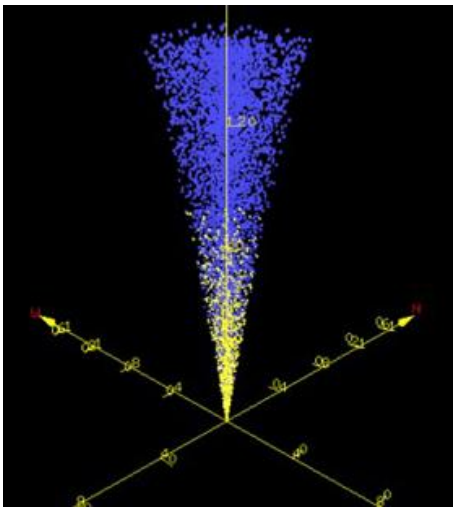

Figure 3 Schematic representation of gas (yellow) converting to hydrates (blue) as they travel upwards. Ambient current = 0.

Appendix 4: 2010 of Mexico Oil Spill Estimate

Ömer Savaş
Department of Mechanical Engineering
University of California Berkeley
Berkeley, CA, 94720-1740
savas@me.berkeley.edu
June 7, 2010

1 Observations

This report discusses the flow rate at the collapsed well head of the Deepwater Horizon drilling unit
oil spill site in the Gulf of Mexico, which sank on April 22, 2010. The basis of the discussion is the four videos among the many downloaded from a secure **ftp** site set up by the USGS,

- Video 1: **H14 BOP Plume May 15 1915-1920.asx (04:59),**
- Video 2: **H14 BOP Plume May 15 1920-1945.asx (25:14),**
- Video 3: **BOP.wmv (05:05),** wide view of discharge at BOP , and
- Video 4: **20100514224719234@H14 Ch1-H264h.mov (09:40),** RITT close up.

The first two seem to be a continuous stream of images divided into two parts. The flow in view is the discharge at the kink (collapsed pipes) immediately downstream of the blowout preventer (BOP). Only a limited discussion of the discharge at the broken end of the riser (for the discussion here, named riser insertion tube tool (RITT)) is presented. I tried numerous video players. In particular, the variable play speed play feature of openly available VLC Media Player was quite helpful ($0.03\times - 4\times$ on my computer). I found that playing the videos at $4\times$ speed gave a better understanding of the flow patterns. I went over the files numerous times. I captured a random image and annotated it to describe my observations below.

Figure 1 summarizes my observations of the discharge flow pattern at the kink. The flow field has in the foreground one very clear, classic, turbulent jet J_1. There is a weak stream of discharge on the right side coming from the underneath of the buckled pipe and wrapping around it, labeled J_0, the origin of which is evidently under the bend. On the left side of the picture, I marked as J what I consider to be the main discharge jet which is pointing away from the camera. In fact, this jet is the dominant feature in the wide view Video 3 taken down stream of the jet at distance. The jet, judging from that view, seems to be discharging $30 - 45^o$ from the horizontal. There seems to be a fourth jet J_2, obscured by J, which seems to be discharging somewhat toward J, but slightly to its left.

The jets J_1 and J_0 are clearly in the view and are the most amenable to direct analysis. J_1 shows all the characteristics of a classical turbulent jet e.g. linear growth, sharp intermittent interface. Fortuitously, the weaker jet J_0 acts as an exquisite marker of the entrainment field of J_1, marked as E_{01}. PIV may be used to estimate the entrainment velocity at the *edge* of J_1. J_0, however,

oscillates back and forth, and at times its plume is entrained by J, behind J_1. This entrainment field into J is marked as E_0.

There is a strong inflow at the left edge of J, marked by E_2. This is especially clear when the video is played at high speeds. It is likely that the fluid in E_2 is the plume of a jet hidden from the view, marked as J_2. Velocities in E_2 seem to be much higher than in E_{01}. Lastly, the plume of J_1 itself is being entrained by J, which may be observed at the upper regions of the flow field. This entrainment field is labeled as E_1.

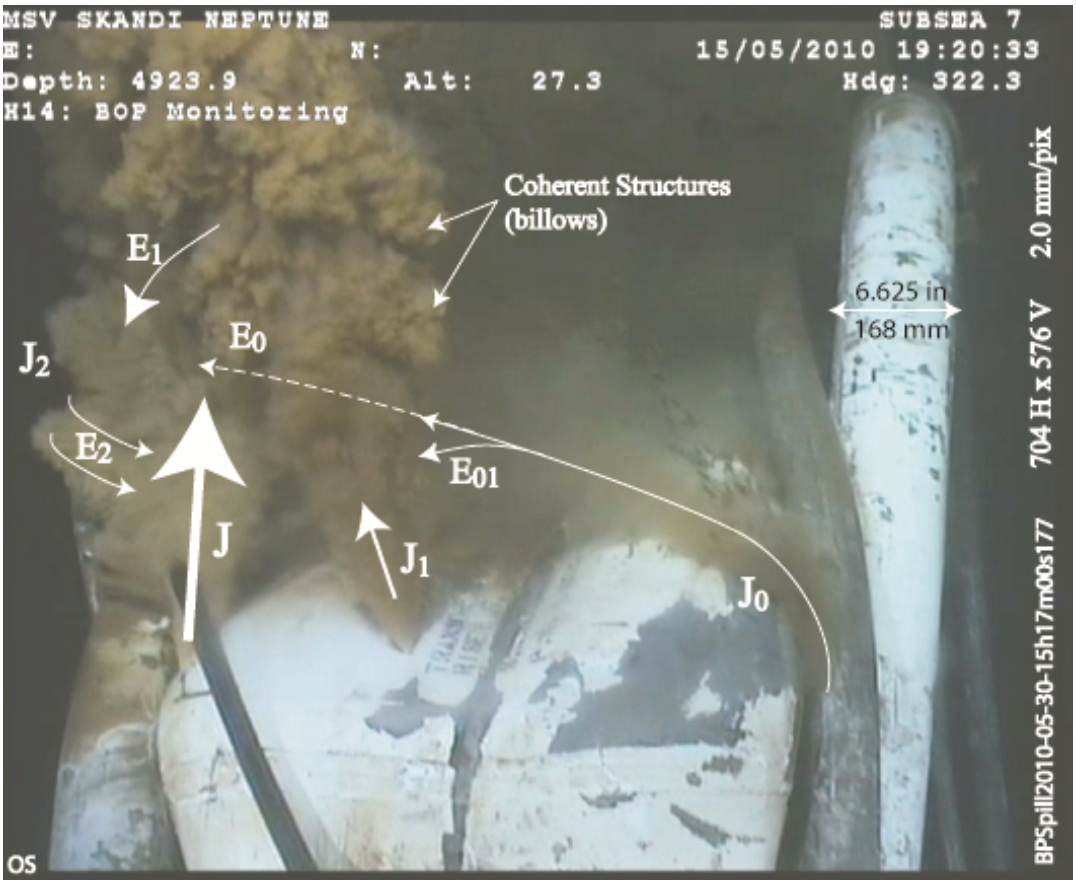

Figure 1: Summary of observations of the discharge flow field at the kink. J-jet, E-entrainment. The picture is 704 pixels wide and 576 pixels high; the length scale: 1 pixel = 2.0 mm.

2 Analysis

I have used numerous tools in my analysis of the flow field in Fig. 1. These include the self similar behavior of turbulent jets, our in-house Particle Image Velocimetry/Lagrangian Parcel

Tracking software (PIV/LPT), Adobe Photoshop©, and numerous tools developed on the IDL© platform.

2.1 Turbulent Jet Self-Similarity

The discharge jet J_1 in Fig. 1 looks like a classical turbulent jet of a high Reynolds number. This is evident in the presence of sharp interfaces (intermittency), a multitude of cascading length scales (from the large coherent structures, billows, to the fine scales cut-off at the camera resolution), a linear spread except for a slight tilt (~ 13^o) to the left. The ratio of the largest and smallest lengths scales is a clear indicator of the jet Reynolds number

$$Re = \quad , \tag{1}$$

where J is the momentum flux, ρ the fluid density in the jet, and v the kinematic viscosity of the fluid. In this case, since the camera resolution is low, and it is too far away, there is no way of capturing the smallest scales of the flow. In fact, it is even a big challenge to capture them in a controlled laboratory experiment.

To estimate the volumetric discharge rate of the jet Q_j, we first write the momentum of the jet

$$J = (\rho_j U_j)\,(U_j A_j) = \rho_j Q^2_j / A_j \tag{2}$$

where ρ_j is the density of the discharging fluid, U_j the velocity of the jet at its orifice, A_j the jet orifice area, and $Q_j = U_j A_j$. Combining Eqs. 1 and 2, the jet discharge flow rate is written as

$$Q_j = v\,Re \ , \tag{3}$$

where I did not attempt to distinguish ρ from ρ_j. Since the jet is developed in the ambient water, the kinematic viscosity $v \sim 2cs$ is that of the ambient sea water. From Fig. 1, I estimate the jet discharge orifice diameter as $D_1 = 12\pm1$ pixels, hence its area as $A_j \sim 4.5cm^2$, using the length conversion factor of 2mm/pixel shown in the figure. Based on my experience with turbulent flows, I am guessing that

$$Re_{J1} \sim 10^6. \tag{4}$$

For comparison, the Reynolds number for candle light is ~100. The flow rate estimate from Eq. 3 is

$$Q_{J1} \approx 0.02 \times 10^6 \times \ \sim 4.2 \cdot 10^4 \ \mathrm{cm^3/s} \rightarrow 3{,}700 \ \mathrm{m^3/day} \tag{5}$$

This estimate is for the darker jet J_1 only. A higher value for v may be used since the jet is a mixture of water and more viscous oil (v ~ 5 cs for oil). The Reynolds number remains uncertain, could be as low as half a million, or could be many millions. I present below an independent estimate for *Re* based on the velocity of the coherent structures shown in Fig.1.

Figure 2: Two successive images from a video sequence (24 fps), showing the advection of large structures downstream of J_1. Circles mark a group of *dark patches* that can be tracked individually.
Individual frames are 880 pixels wide and 720 pixels high; the length scale: 1 pixel = 1.6 mm.

2.2 Image Analysis

2.2.1 Direct Image Analysis

The most straight forward technique is to analyze a few sample pictures visually, using Adobe Photoshop and ticker.pro. An indirect check of the guess in Eq. 4 can be done by estimating the speed of the coherent structures at the downstream of the jet in Fig. 2. By overlaying two successive images in Photoshop, and, independently using ticker.pro, I estimate the displacement of the coherent structures at about 70 cm downstream of the discharge to be about 40±10 pixels/step, or 150±40 cm/s at 24 frames/second video rate. (The images in Fig. 2 are converted to 880 × 720 resolution during extraction from the video stream, hence 1 pixel=1.6 mm.) This is about half of the centerline velocity in a uniform density, non-buoyant turbulent jet. This implies a centerline velocity of about U_o = 3.0 m/s at 70cm downstream of the discharge. Using the inverse decay law of centerline velocity for a turbulent jet, I estimate the velocity at the jet discharge to be about

$$U_{J1} = (70cm / 2.4cm) \times 3.0m/s \approx 85 \text{ m/s} \qquad (6)$$

(projecting a virtual origin at one diameter behind the wall). Along with $A_j = 4.5cm^2$, this suggests
a discharge flow rate of

$$Q_{J1} = \times Uo \times Aj = \times 300cm/s \times 4.5\text{cm}^2 \approx 39,600 \text{ cm}^3/\text{s} \rightarrow 3,400 \text{ m}^3/\text{day}, \qquad (7)$$

which is somewhat lower than the above estimate in Eq. 5, yet well within the uncertainties. The Reynolds number is, from Eq. 3,

$$ReJ1 = \approx = 0.9\times10^{6}. \quad (8)$$

Again, somewhat lower than the guess in Eq. 4, yet comparable.

As a reference point, if the flow were lossless, it would take a pressure differential of about 36 atmospheres to accelerate water to 85 m/s, *a la* Bernoulli. If there were no leakage at the kink, the static pressure differential between the BOP and the sea floor would be about 340 atmospheres, assuming no restriction inside the well head.

2.2.2 PIV

PIV techniques may be employed in this case with *due* caution. These techniques are able to capture the phase velocity of large scale structures, and only at downstream when the jet is sufficiently slowed down. As the estimate above indicates, there are phase displacements as large as 40 pixels between successive video frames. Hence, one needs interrogation windows up to 128 pixels on the side to capture them. As the window size or time step is increased inordinately, the PIV approach degrades at turbulent interfaces, since the turbulence, by its very nature, will continually *re-granulate* the interface, hence *stressing* any PIV algorithm. In particular, it will underestimate displacements. Turbulence has by its nature has a cascades of time and lengths scales. If the time step is too large, the intermediate time and lengths scales will change completely between the successive PIV images, rendering any correlation algorithm helpless. This will result in only a handful of independent velocity vectors. Our PIV technique is no exception.

In our PIV/ALPT implementation, the largest displacement output was around 16 pixels per time step for the coherent structures tracked in Fig. 2, compared to 40 pixels that I deduced by examining it visually using Photoshop, and ticker.pro. I was able to get this value only after using tall interrogation window, 8 × 64 (64 pixels along the jet direction). Square windows of 32×32, 64×64, and even 128×128 yielded even lower values. In contrast, I was able to track few individual patches of *dark* material in the weak jet J_0 encircled in Fig. 2 using Photoshop in conjunction with ticker.pro. Their displacements are in the range 9-13 pixels/step (35-50 cm/s), comparable to what my PIV algorithm was giving for the obviously much stronger jet J_1. Therefore, I decided to use PIV results qualitatively only. Perhaps, we should develop a flow rate estimation scheme based on edge detection.

PIV promises the most for J_1 in Fig. 1, but only in an intermediate distance from the discharge point. The velocities are too fast closer to the discharge point, and the interface is too turbulently granulated farther downstream. For the high speed jet *J*, it provides no direct information. In the case of the faint jet J_0, we expect more vectors, since the flow is slow. Unfortunately that is the weakest of the leaks, and is of low interest.

Figure 3 shows a sample filtered result from our PIV/ALPT algorithm. The images in Fig. 2 are processed. The velocity vector field and some *selected* streamline segments are overlaid on one of the images in regions where I have some confidence in the results, either in the direction or the magnitude of the velocity vector, or both. It *qualitatively* captures some features of the flow: J_1, J_0, E_{01}, to some degree E_1, and a hint of E_2. With caution in mind, the results suggest that the velocities in E_2 are comparable to E_1, but certainly higher than in E_{01}.

Figure 3: Sample PIV/LPT results for J_1. The images in Fig. 2 are processed.

3 Discussion

3.1 Jet Strengths

It is now time to order the four jets; J, J_0, J_1, & J_2; identified in Fig. 1. First, we note here that the entrainment velocity v at the edge of a turbulent jet is indicative of its centerline velocity U_o,

$$v = 0.08U_o. \tag{9}$$

Therefore, based on our observations and the implications of the PIV results just discussed, we can use the relative entrainment strengths to put the four jets in an order. Clearly, J_0 is the weakest. Since part of J_1 is entrained into J, I conclude that J is stronger than J_1. The PIV results in the entrainment zones suggest that the phantom jet J_2 is stronger than J_1. However, to stay on the side of caution, I will assume that J_1 is comparable or stronger than J_2. The final ordering is

$$J > J_1 > J_2 >> J_0. \tag{10}$$

3.2 Oil/Gas Ratio

This brings up a whole new question about the variability of the conditions between the kink at BOP and the opening at the RITT. The RITT discharge is evidently binary/intermittent: almost unmixed (a better term is 'separated') light colored (gas) and dark colored (oil) fluids. The discharge at the kink is nearly uniform in color. I will go even further and say that the faint stream of J_0 warping around the collapsed tube on the right side at the BOP is all oil.

3.3 RITT

Flow at the RITT is an unrestrained discharge, that is, the pressure drop in the pipe is only that required to maintain the flow rate at an unobstructed (?) opening. The view of the discharge at the RITT oscillates between an almost white, apparently gaseous methane and dark liquid, presumably oil. The views with the details are essentially the shear layers at the discharge. What one sees at the edge of these shear layers primarily depend on the velocity profile of the discharge and the ratio of the density of the discharging fluid to that of the ambient fluid. For the same upstream pressure ignoring losses), to the first order, gas moves faster than liquid, since the pressure, potential energy, is converted to kinetic energy. For the same upstream pressure, gas being low in density, moves faster. This is evident in the video so the RTT discharge (Video 4). The lighter colored jet, presumably gas, shoots farther that the darker color fluid, presumably oil. The second important effect is the density ratio. Since the flow is at high Reynolds numbers, it is inertia dominated. The behavior of the visible interface is determined by the inertial effects (except when there is significant surface tension). In particular, the apparent velocity of the interface is determined by the pressure balance at the stagnation points of the large scale coherent structures in the reference frame moving with them, assuming quasi steady behavior. By accounting for this balance on streamlines extending to either side of the interface, one can deduce the apparent velocity (celerity) at the interface. Hence the density ratio becomes a factor. Intuitively, a light stream has to slow down considerably when pushing along a heavy fluid, as the case is here when the gas is trying to drag along the sea water. Consequently, our estimates base on the observed velocities of the interface must be corrected for the density ratio. This raises to points:

1. The speed estimates from the motion of the interface does not give the speed of the discharge. It has to be corrected for the density ratio. In the case of oil, whose density is close to that of the water, this correction is well within the uncertainty. For the gas phase, however, it is significant. If the velocity discharge profile at the exit of the broken pipe were uniform or close to it, we would expect to see the classical rolled up eddies at the interface. It, however, more that likely that the velocity profile there is a developed one akin to that of axial flow between to concentric cylinders.
2. The oil/gas ratio cannot be determined by simply relying on intermittency of the discharge. The result has to be corrected for differences in the discharge speeds of the gas and oil phase streams.

3.3.1 Entrainment

A fully developed turbulent jet entrains ambient fluid at a uniform rate with downstream distance. Even though (Eq. 9) for entrainment velocity at the edge of the jet is written for a fully developed turbulent jet, I will use it to estimate the jet velocity at the RITT.

Around 00:12 time mark in Video 4, an eel drifts into the view from above. It drifts toward the jet for 35 frames almost like a rigid vertical rod, evidently being entrained by the jet. It only starts swimming away from the jet after 36-37 frames in the view. During drifting, the eel moves $(\Delta x, \Delta y) \approx$ (24cm, 39cm) which translates to an entrainment velocity vector of $(u, v) \approx$ (16 cm/s, 27 cm/s), at 30 cm/s nearly normal to the discharge direction of the jet. Since the discharge jet is confined over the sea floor, the entrainment velocity will be higher that a free jet. Therefore, using Eq. 9 will yield high values for the jet velocity (in this case about 4 m/s). Nevertheless, we can conclude from the drifting eel that the discharge velocity is on the order of a meter per second at the broken end of the riser.

3.4 Comparison of BOP and RITT

Given the forensic evidence after the riser was cut off on June 3, 2010, showing two tubes instead of one at the kink, it is very uncertain, even impossible to even guess the pressure profile between the BOP and the RITT. The view of the discharge at the RITT oscillates between an almost white, apparently gaseous methane and dark liquid, presumably oil. At this depth (150 atm), the temperature of the discharge must be higher than the ambient temperature of 2^oC. Since the pipe between the BOP and the RITT is mostly horizontal, there is no hydrostatic pressure differential, between the BP and the RITT. The pressure drop is almost exclusively due to flow losses. Further, fluid had some time for heat exchange with ambient (cooling).

The situation at the BOP is quite different. The discharge is evidently homogeneous; the intermittency of the white/dark fluid of the RITT is absent. Methane has not separated into billows. It may well be in fine bubble form. Evidently, the pressure at the kink is so *high* that, even after the discharge, the methane stays in homogeneous distribution with oil within the camera view. This argument, although speculative, corroborates the high discharge velocity estimated in Eq. 6.

3.5 Uncertainty

- length scale in Fig. 1: 2.0 ± 0.02 mm/pixel
- length scale in Fig. 2: 1.6 ± 0.02 mm/pixel
- discharge diameter of J_1: D_1 = 12 ± 1 pixel = 2.4±0.2 cm
- speed of coherent structures at cm downstream of J_1 discharge: 40 ± 10 pixels/step = 150 ± 40 cm/s
- range of discharge in Eq. 7: $Q_{J1} \in$ [2300, 4800] m^3 / day

3.6 Summary

Table 1 summarizes the result of this report. To obtain limits for the total discharge rate, I summed the lowest and highest estimates in the table. The oil/gas ratio is another source of uncertainty in estimating the oil discharge ratio. The estimates range from 25% to 67% oil. The latest figure form the field is 41% oil. I have, therefore listed in the table *oil* discharge rates based on 25, 40, and 50% oil content.

The jets *J* and J_1 are clearly contributing the most discharge. Therefore, as a conservative estimate, I assumed equal discharges from J_1 and *J* to arrive at my estimate of volumetric discharge rate in the last row of the table. Given the images in Video 3, this assumption is indeed very conservative.

An estimate of the discharge at RITT remains elusive for me. The estimate in Section 3.2.1, along 25% oil content stated in the preliminary report, suggest an oil discharge rate of on the order of ~10^3 m^3/day. My confidence level on this figure, however, is low, and I will not consider it further until I have better tools to study the flow.

Flow (Fig.1)	Fluid	Discharge Q (m^3 / day)	Remarks
J	Oil/Gas	2,000 - 5,000	The dominant discharge, gas/liquid ratio uncertain

Supplemental Report
After the Cut-off at the BOP
2010 Gulf of Mexico Oil Spill Estimate

Ömer Savaş
Department of Mechanical Engineering
University of California Berkeley
Berkeley, CA, 94720-1740
savas@me.berkeley.edu
June 15, 2010

Introduction

The pipe immediately downstream of the BOP was cut off on June 3, 2010. The FRTG was asked to estimate the flow rate from the cut end. Numerous high quality HD videos (1920W×1080H pixels) were made available to the group. I have gone through 15 of them. I am writing this supplement based on the video clip

TOPHAT_06-03-10_14-29-22.avi (03:59)

which is composed of 7188 frames, that were extracted using **QuickTime Pro©**. During the teleconference on June 10, 2010, it was clear that I must provide details for my concerns and bases for my opinions. I first discuss my view of the applicability of conventional PIV techniques to the discharge problem at hand. Then, I present my approach and my final opinion. As was agreed by the members, I have looked at a 220 frame section of the video, in the frame number range of 2200-2420. The corresponding time stamps on the video are **06/03/10, 14:30:35 - 14:30:42.**

Limitations of Conventional PIV

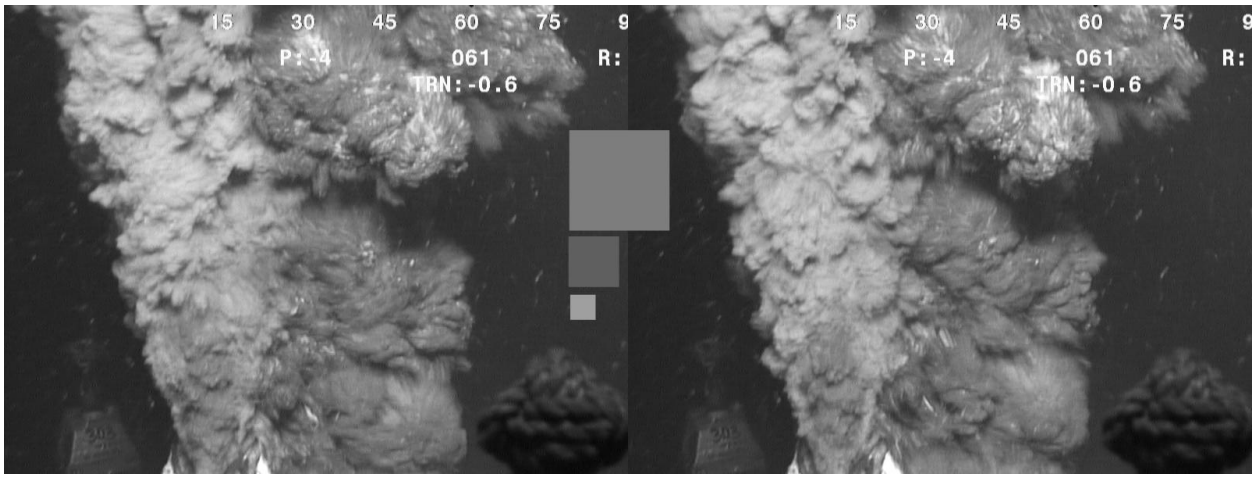

Figure 4: Cropped regions from **TOPHAT_06-03-10_14-29-22**, consecutive frames #2356 & #2357. The **Green** channel of the original **TIFF** image is shown. Images are 800W×600H and 1/30 second apart. The three squares at the center are 32, 64, and 128 pixels on the side.

I see two problems with the application of conventional PIV techniques to the discharge rate estimate. The first one is mild and perhaps can be worked around. Figure 4 shows segments of two consecutive frames from a video clip that are recorded at 30 frames per second. The images are the green channel of the TIFF files. Evidently the flow is of high Reynolds number; the length scales vary from very large scale eddies, commensurate with the width of the jet, down to the resolution of the camera and image compression technique that may have been utilized. The features at the largest scales can be visually tracked between the frames. The smaller features are, however, independent between the frames. Closer visual examination employing various methods show that scales below about 10-30 pixels in size are independent. For reference, three square interrogation windows are shown; 32, 64, and 128 pixels on the side. A classical PIV technique using common correlation algorithms with 32×32 interrogation windows will not capture the motion of the larger scales. Windows of size 64×64 are also dubious. Perhaps, windows of 128 or larger can yield information, but only on the motion of the largest features. Small windows may be sufficient very close to the exit of the pipe, but will fall short in about a diameter downstream, as seen in the figure.
The second limitation of PIV is more serious. The fluid that we are trying to measure is opaque. Optically we have access to the outermost *shell* of the discharge. As can be seen in almost all of the videos, the flow rolls into large eddies soon after leaving the pipe. Figure 5 shows an idealized cartoon of an eddy; it is rolled up, with interleaving layers of jet fluid and ambient sea water. In the figure the approximate light and camera directions are shown (see Figure 4). Overlaid are sketches of the mean velocity profile of the jet, and the velocity field of the eddy from its reference frame. Depending on the location of the eddy, one can even have a fluid element moving toward the exit of the jet (backward). The regions of the flow recorded by the camera are the outermost layers of the jet fluid. This layer, as explained above is constantly re-granulated by turbulence. Since the time between the images is too long to capture the same texture in both images, the camera records uncorrelated fine details on the jet fluid interface. In particular, if an interrogation window falls entirely on the surface of the structure (no large eddy shadow), then the correlation algorithm will yield not the velocity of the fluid parcel, but the length scale of the eddies. Any match with the local flow velocity is coincidental.

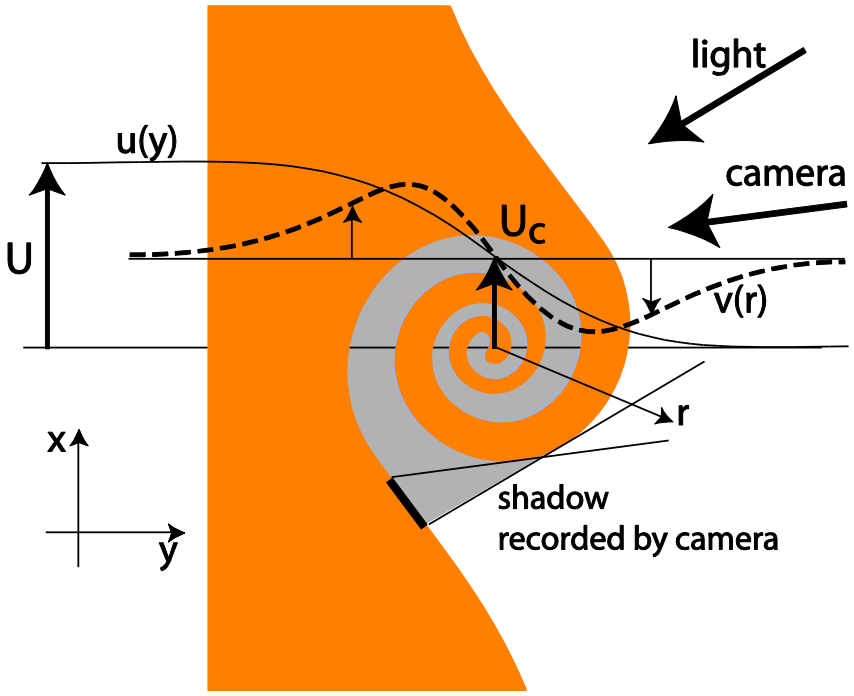

Figure 5: Flow field of a coherent eddy in the near filed of jet discharge. The jet fluid is discharging at velocity U, and is opaque. The eddy is translating at U_c. The mean profile of the jet is u(y) [solid line]. v(r) [dashed line] is the azimuthal velocity profile of the eddy in a reference frame moving with velocity U_c. Camera can only see the outer shell of the rolled up structure.

The shadows of the large eddies can be followed by the PIV if using commensurately large correlation windows (128 or larger, Fig. 6). Smaller windows will capture only smaller regions of shadow motion *and* the turbulence scales, biasing the PIV result toward the turbulence length scale. Therefore, a conventional PIV correlation algorithm will yield lower velocities for the motion the large eddies.

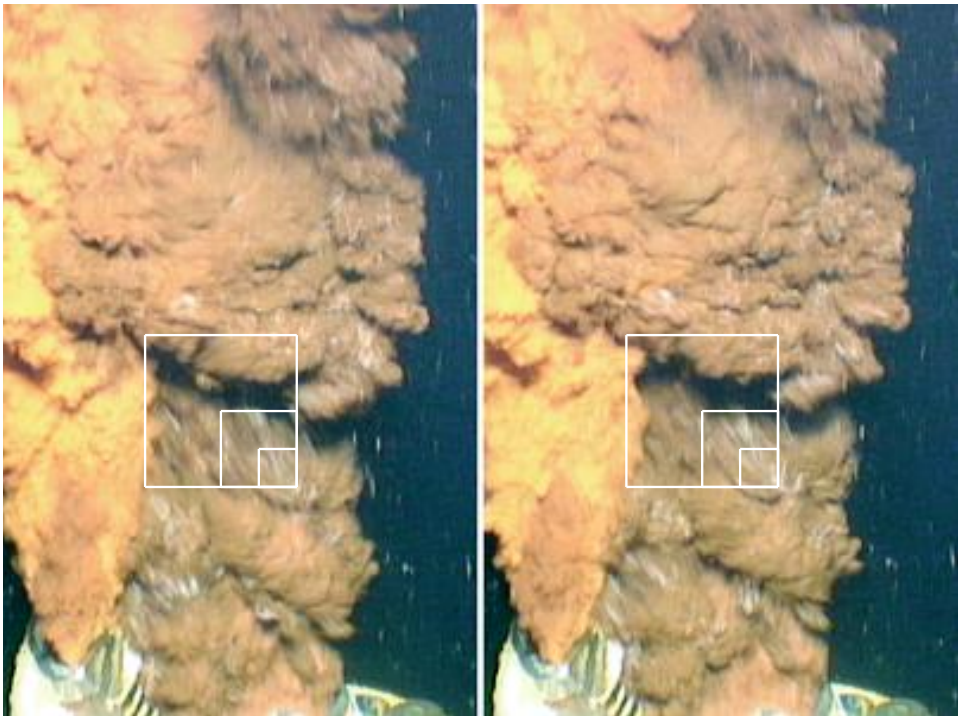

Figure 6: Cropped regions from **`TOPHAT_06-03-10_14-29-22`**, consecutive frames #2224 & #2225. Images are 400W×600H and 1/30 second apart. The three nested squares are 32, 64, and 128 pixels on each side.

Methods

I have used three independent approaches;

1. Direct visual tracking of large eddies,
2. Direct visual tracking of instability waves at the exit of the tube, and
3. Conventional PIV correlation on the **`green`** channel of the TIFF images.

Large eddy tracking

I have visually tracked large eddies using **`Photoshop`**. I used the central region of an eddy to mark its location and tracked it frame by frame for 10 steps (11 images). Figure 7 shows the beginning and the end of the first series of image frames where I marked the locations of the eddy with respect to a convenient reference on the edge of the pipe. The collective results for five series are plotted in the *xt*-diagram in Fig. 8 and tabulated in Table 2. The displacement results in the 4th column of Table 2, Δx, are the average displacements per step and are determined using the linear regression feature of **`MS Excel`**. The image calibration is done for each series separately, since the camera was moving. All measurements were done within 1.5 jet diameters.

The average large eddy velocity is 1.06 m/s, with a range of 0.47-1.61m/s. Part of this is due to the uncertainty in measurements, part is due to the uncertain conditions in the pipe. And some

part is due to the dynamics of large eddies in the field of a jet; merging and leapfrogging of vortices cause variations in their trajectories.

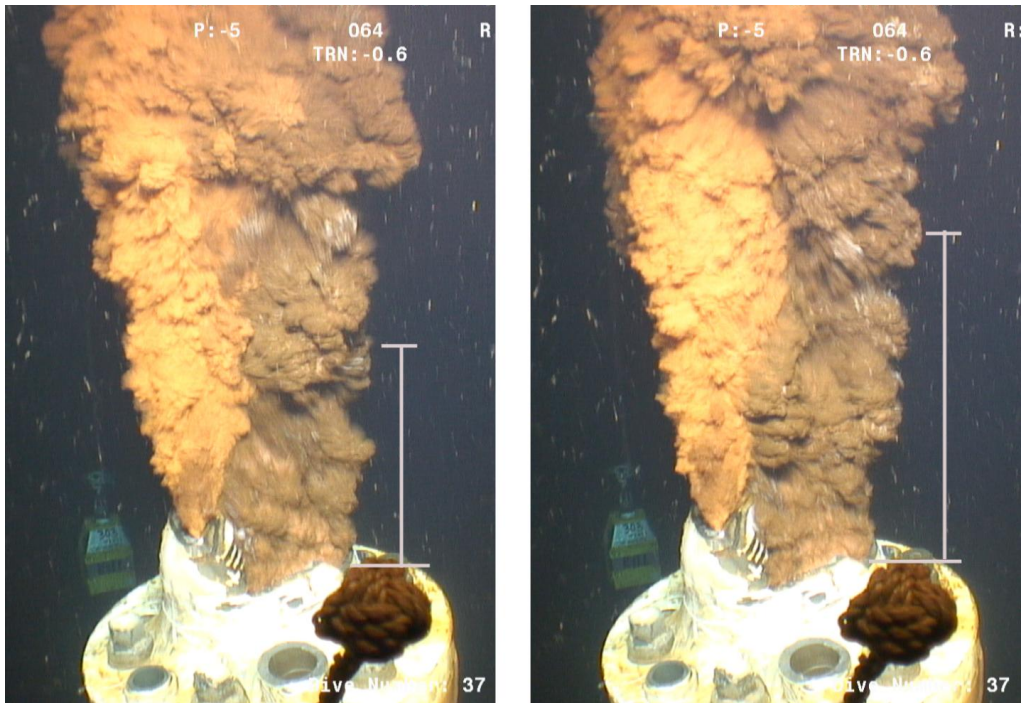

Figure 7:Visually following large eddies (coherent structures) in the flow field. Cropped images are from the first (2207) and the last (2217) images of Series 1 in Table 4. The vertical lines show the downstream position a tracked eddy with respect to a reference point on the edge of the pipe. Image segments are 700W×1000H.

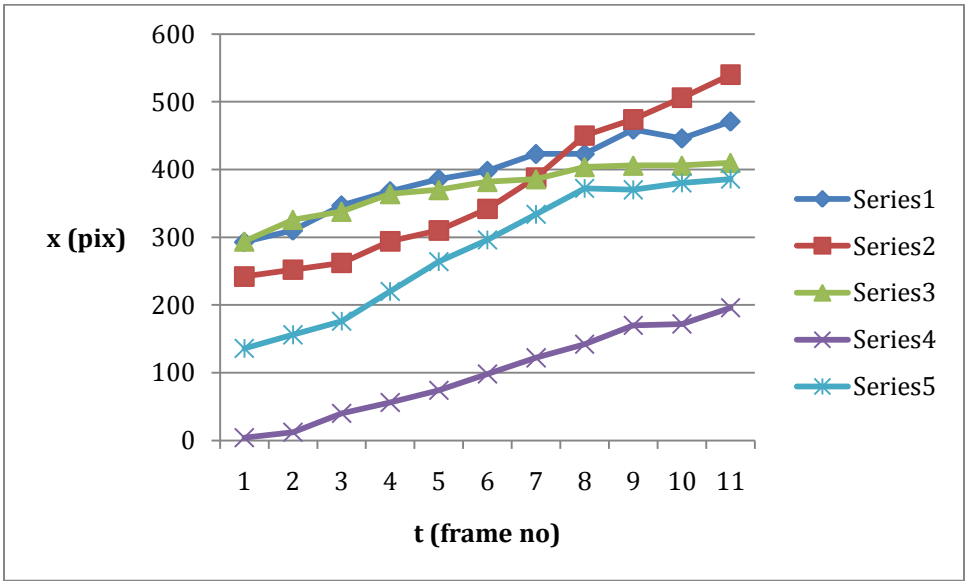

Figure 8: Trajectories of tracked large eddies in the discharge flow field.

Series	Image sequence	Time steps (1/30 sec)	Δx/step (pix)	Scale (mm/pix)	U (m/s)	Oil discharge rate (m^3/day)
1	2207-2217	10	17.4	2.04	1.06	7,100
2	2259-2269	10	32.1	1.67	1.61	10,800
3	2300-2310	10	10.9	1.46	0.47	3,200
4	2350-2360	10	20.1	1.49	0.90	6,100
5	2400-2410	10	28.2	1.51	1.28	8,600
	average				**1.06 ± 0.55**	**7,100± 3,700**

Table 2. Manual large eddy tracking in the near field of the discharge.

The discharge flow rate based on the large eddy tracking results are listed in the last column of Table 2. In these flow rate results, I assumed a cross sectional area of 0.19 m^2, ignoring probable distortions during cutting. I also have foregone extrapolating the large eddy velocity back to the exit plane of the discharge jet. The oil fraction is taken as 0.41. The discharge rate ranges from 3,200 to 10,800 m^3/day, with an average of 7,100 m^3/day. Sources of the variability were already noted above. Since no extrapolation to the exit plane nor any corrections for the density differences between the ambient sea water and discharge fluid were done, the discharge rates in the last column of Table 2 are conservative. They are likely to be higher.

Instability wave tracking

Right at exit of the cut pipe, I tracked the first signs of instabilities in successive image pairs I was able to detect. Figure 8 shows such a pair where I marked the location of the instability that was visually tracked using **`Photoshop`**. Since these are developing in the boundary layer of the exit flow, their phase speed is going to be slower than what the inviscid instability theory predicts. Furthermore, since the waves are just downstream of a solid wall where the no-slip condition is present (actually a stagnation point at lip), their speed will be further reduced. Nevertheless, that is much less than ½ of the bulk velocity inside the tube. Furthermore, buoyancy effects are negligible since the fluid has barely left the pipe.

The results are shown in Table 2. A close examination of the table shows that, when the waves are spotted near the exit, their velocity is slower, supporting the argument that the effect of the no-slip condition is present. It is assuring to see that the plot in the table suggests zero speed at the exit location where the there is a stagnation point. The average speed is 35 cm/s. Extrapolating these results to the bulk flow is a far stretch. It can, however, be used to established an exceedingly conservative lower limit for the discharge rate.

Figure 8: Visually following instability waves at their genesis. Sections from consecutive frames #2300 and #2301. The dashed line marks, where the wave was tracked (see Table 3). Image segments are 450W×250H. The tracked displacement was 6 pixels.

Image pair	**Δx (pix) x_2-x_1=Δx**	**Scale (mm/pix)**	**U (cm/s)**
2207-2208	39-32 = 7	2.06	43.3
2259-2260	22-18 = 4	1.90	22.8
2300-2301	39-30 = 9	1.45	39.2
2350-2351	23-17 = 6	1.49	26.9
2400-2401	47-35 =12	1.51	54.3
5 samples			**35±10**

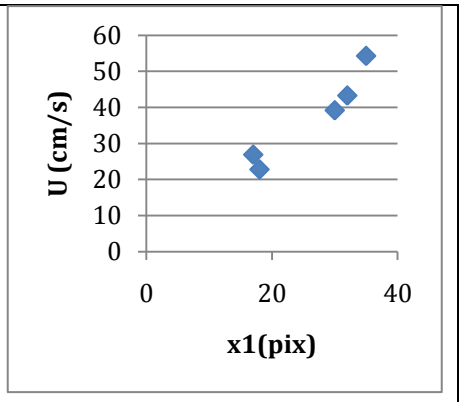

Table 3. Manual wave tracking at the exit of the pipe.

Taking the average value of 35 cm/s and multiplying by a factor of 2 to approximate the interior velocity (assuming iso-density), we obtain a volume flow rate of 0.133 m^3/s, or 11500 m^3/day. At 41% oil content, this gives an oil discharge rate of 4700 m^3/day. I have assumed here that the cross sectional area of the cut pipe is still 0.19 m^2. I consider this to be an exceedingly conservative lower limit for the oil discharge rate for two reasons: (1) density ratio will increase the velocity deduced at the center, and (2) the measured velocity of the waves is a lower fraction of the centerline velocity than the assumed value ½. Since the flow profile at exit is not known, (in fact it is known not to be uniform or top-hat), relating wave speed to the core speed is not obvious.

PIV processing

After examining the **RGB** channels of the **TIFF** images extracted from the video, I have concluded that the **Green** channel had the best signal. The **Red** channel was saturated and the **Blue** channel was dim. After cropping the images to 1000H×1000V, I processed the five series listed in Table 2 at 32×32, 64×64 and 128×128 window sizes with no dynamic adjustment. The results for Series 1 is shown in Fig. 9. For the reasons stated above, only the results near the exit plane of the jet are deemed reliable, therefore the results presented in the table are averages over a one diameter across the jet and 1/3 diameter along the jet at the exit region. The results are summarized in Table 4. For each flow series, both the average flow speed (cm/s) and an average discharge rate (m^3/s) are shown. The speeds are comparable to the values of the instability wave speeds shown in Table 3 and the figure therein. This is expected, since, at their infancy, the instability waves are moving slowly, without changing their shapes radically. They are captured in successive images, unlike the flow feature further downstream. Therefore, it is obvious that any discharge rate calculation based on these PIV results near the exit will give values comparable to that obtained from wave tracking analysis above.

The discharge rates in the table are calculated based on an exit area of 0.19 m^2 and an oil fraction of 0.41. Most important, the average speeds were multiplied by a factor of 2.9 (including density correction) to extrapolate for the *bulk* speed at the interior of the jet. This is necessary since what PIV is measuring are the speeds of the instability waves. The relation of these to centerline speed is a big source of uncertainty.

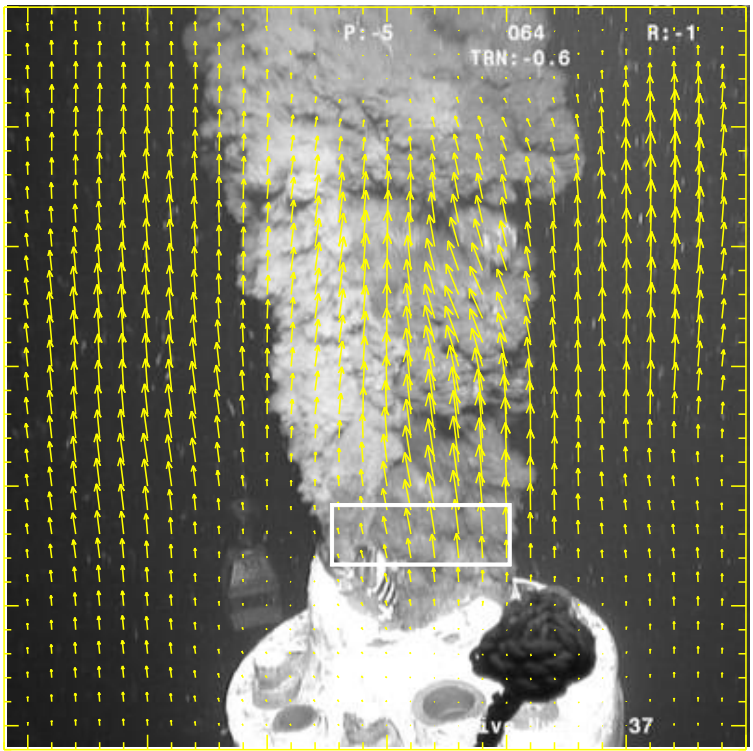

Figure 9: Sample PIV result. Average vector field of Series 1 is overlaid on frame #2207. Image processing is done at 64x64 windows. The vector field is filtered. The rectangular box over the pipe exit roughly marks the region where average velocity is determined.

Series	Image sequence	PIV @ 32×32	PIV @ 64×64	PIV @ 128×128	remarks
1	2207-2217	30 cm/s	29 cm/s	32 cm/s	
		5,900 m^3/day	5,800 m^3/day	6,400 m^3/day	
2	2259-2269	25 cm/s	30 cm/s	29 cm/s	Excessive camera motion
		5,000 m^3/day	5,900 m^3/day	5700 m^3/day	
3	2300-2310	20 cm/s	22 cm/s	8 cm/s	
		4,000 m^3/day	4,400 m^3/day	1,600 m^3/day	
4	2350-2360	25 cm/s	29 cm/s	12 cm/s	
		4,900 m^3/day	5,700 m^3/day	2,500 m^3/day	
5	2400-2410	14cm/s	14 cm/s	3 cm/s	
		2,800 m^3/day	2,700 m^3/day	600 m^3/day	

Table 4: Summary of PIV processing: Average wave speed (cm/s) at the pipe exit.

Conclusion

Table 5 summarizes the findings of this supplemental report. All results are based on an oil fraction of 0.41 and a discharge area of 0.19 m^2. The results from eddy and wave tracking analysis are the basis of the conclusion of this supplement. The results from the PIV analysis are the highest discharge rates deduced subject to the assumptions stated and are presented to provide a perspective.

Method	Oil discharge rate (m^3/day)	Remarks
Large Eddy tracking	**7,100**	**Most likely**
Instability wave tracking	4,600	Conservative minimum
Image velocimetry @ 32×32	6,400	Maximum from Table 4
Image velocimetry @ 64×64	5,900	Maximum from Table 4
Image velocimetry @ 128×128	5,900	Maximum from Table 4

Table 5: Supplemental report summary.

I consider the oil discharge rate of 7,100 m^3/day as the most likely value. It is doubtful that it is significantly lower that this value. However, it can easily be 10%, even 20% higher, since the assumptions made in calculating the flow rate from eddy tracking were on the conservative side.

Respectfully presented,

Ömer Savaş
June 15, 2010
Berkeley, CA

Appendix 5: Gulf Oil Spill PIV Analysis

Professor Steve Wereley
Mechanical Engineering and
Birck Nanotechnology Center
Purdue University

Abstract

The Flow Rate Technical Group (FRTG) was tasked with arriving at several estimates of the oil release into the Gulf of Mexico (GoM) subsequent to the April 20, 2010, blow out of the British Petroleum Deepwater Horizons well. We were initially instructed to arrive at a scientifically defensible estimate of the oil flow rate out of the end of the broken riser pipe during the period before the RITT was installed. We were to consider both the flow from end of the riser as well as the flow from multiple jets at point where the riser was kinked on top of the Blow Out Preventer (BOP). Using several different videos, I calculated flow rates ranging from 15,000 to 35,000 barrels per day. On June 3 BP cut the kinked riser pipe just above the BOP and installed a cap called the Lower Marine Riser Package (LMRP) cap to capture some fraction of the flow. There was a considerable time (on the order of hours) between the cutting and capping of the riser during which time videos were acquired showing the oil flowing vertically upwards out of the riser stub. The cutting operation accomplished two things in addition to making the LMRP cap operation possible. First, it changed the flow from several independent flows emerging from multiple locations to a single large flow emerging from one location. Second, it increased the flow rate. Simple consideration of the physics dictates that the flow must increase to some undetermined degree when the flow resistance from the kink and a considerable length of riser pipe is removed. The FRTG was also tasked with determining the oil flow rate during this period. I calculated a flow in the range of 30,000 to 40,000 barrels per day.

Introduction

The jet issuing from the broken riser pipe lying on the ocean floor could be classified as a buoyant, immiscible jet with different physical properties from fluid it is issuing into. Most notably, the density is lower and the viscosity of the oil is higher than the sea water. The reader is referred Panton (2005) for a general discussion of jet behavior. The analysis of the jet is difficult because it is opaque. It is not possible to see the interior motion of the jet as with conventional Particle Image Velocimetry. In fact, this approach would be more properly classified as correlation-based feature tracking. Basing my analysis on the features that I see—and track—at the oil/water interface introduces some complexity into the analysis and requires assumptions about how the motion of the visible structures relates to the average velocity of the jet. These issues are well-described in other reports from the FRTG so I will not repeat them here.

Pre-riser cut flow rate

Initial individual measurements (a bit of history)

On May 12, 2010, British Petroleum released the video *Crater_plume_gassing_11_may_2010_2333.wmv* that shows oil and gas emerging from the broken riser pipe lying on the ocean floor subsequent to the Deepwater Horizon accident

on April 20, 2010. Frames from the video were extracted and analyzed using the particle image velocimetry code EDPIV (custom written by Lichuan Gui and available at edpiv.com) as well as manual feature tracking. This was the first video released to the public and was of very poor quality. It had a number of compression artifacts in it. It seemed to be a screen capture at 30 Hz of a video originally recorded at 25 Hz. Nonetheless, it was possible to make a preliminary determination of the oil flow rate. I selected two images from around 23 seconds into the video (Fig 1) to analyze because they seemed representative of oil flow and I could see many flow features with my eye that I expected my custom-written PIV code, **EDPIV,** to be able to track.
These two images were analyzed by **EDPIV** using the following settings:

- initial displacement (10,-6) pixels
- window size 128x128 pixels
- grid size 32x32 pixels
- regional renormalization with 37 pixel kernel
- 5 iterations

A very small vector field measuring only 3 vectors horizontally by 2 vectors vertically was chosen. Quite large interrogation windows were needed (128x128 pixels) in order to have sufficient signal to noise ratio for **EDPIV** to successfully compute velocity vectors. These large interrogation regions span the horizontal extent of the jet and so fully sample the velocity of the flow features. The average displacement for these 6 vectors has a magnitude of 10.2 pixels. Since the vectors are calculated slightly downstream of the elliptical volume of fluid used in the manual feature tracking approach, the displacement has decreased slightly. It is also apparent that the plume has broadened at this location. The velocity field calculated is plotted on top of the first image of the pair used to calculate it and shown in Fig. 2.
Turning this displacement calculation into a volume measurement requires two additional parameters: a length scale and the time between images. The length scale was provided by British Petroleum. The outer diameter of the pipe visible in the pictures is 21 inches. Measurements in the images shows that the pipe is 124 pixels across. The time between frames is given by the time index of the images. For these two images that works out to: 22.957 - 22.890 = 0.067 sec. However, the properties information for the video says it was recorded at 25 Hz, i.e. an interframe time of 0.04 sec. I will use the 0.067 sec interframe time to come up with a *more conservative* estimate of velocity. With these parameters the velocity can be calculated from the displacement according to

$$10.2\,\frac{pixels}{frame}\times\frac{1\,frame}{0.067\,sec}\times\frac{21in}{124pixels}=25.8\,\frac{in}{sec}$$

To turn this into a volume flow rate measurement, one must multiply by the cross-sectional area of the pipe. British Petroleum has informed me that the inner diameter of the pipe is 20 inches. The volume flow rate is calculated according to

$$25.8\,\frac{in}{sec}\times\frac{\pi}{4}\times(20in)^2=8105\,\frac{in^3}{sec}$$

Units conversion to barrels per day:

$$8105\frac{in^3}{sec}\times\frac{60\times60\times24sec}{day}\times\frac{1gal}{231in^3}\times\frac{1bbl}{42gal}=72179\frac{bbl}{day}$$

On the flow analysis side, this estimate is doubly conservative because after the jet of oil issues out of the pipe, it slows and expands. By using a PIV velocity measurement from the plume area (where the speed is slower than in the pipe) and the cross-sectional area of the pipe (which is smaller than the diameter of the plume), we get a *conservative estimate* of the velocity.

I calculated an oil flow rate of 72,179 barrels per day (0.129 m^3/s) and estimated the uncertainty to be +/- 20%, meaning that the likely flow rate is in the range of 56,000 to 84,000 barrels per day. BP had released very little information to the public at the time these calculations were made. In particular, the Gas to Oil ratio or GOR was not released. After these initial measurements were made, a GOR of 3000 scf of gas per barrel of oil was announced by BP. This translates to a volume fraction of oil at the sea floor conditions of 0.29. Another factor to take into account is the variation in oil density as the temperature and pressure change from the area where the videos were recorded to sea surface conditions. The density change is estimated to increase by 35% as the oil cools and floats to the surface (Sec Chu). My original measurements above can then be adjusted by these two factors to give:

$$\left(72{,}179\frac{bbl}{day}\right)_{sea\ floor}\times0.29\times1.35=\left(28{,}258\ \frac{bbl}{day}\right)_{std\ conds}$$

BP also announced that the end of the riser was deformed to a considerable extent resulting in the exit area of the riser pipe being reduced by approximately 30%. Further, a drill pipe protruding from the end of the riser further reduced the cross-sectional area. Since the measurements were made approximately one diameter downstream of the riser exit, it is expected that these effects will not influence the flow rate calculation.

A few days later BP released four more videos. One of these was *H14 BOP Plume May 15 1920-1945*. From this video it was possible to calculate the flow out of one of the two apparent leaks at the riser kink location immediately on top of the BOP. Based on visual inspection and feature tracking, an initial flow rate calculation of 25,000 bbl/day was calculated. Making the same adjustments as above, the actual flow rate in stock barrels per day at standard conditions is

$$\left(25{,}000\frac{bbl}{day}\right)_{sea\ floor}\times0.29\times1.35=\left(9{,}788\ \frac{bbl}{day}\right)_{std\ conds}$$

A total initial estimation of the flow rate based on the poor quality videos available at the time would be 38,046 bbl/day.

Phase 1 FRTG Measurements

After the formation of the Flow Rate Technical Group, we began to analyze the pre-riser cut videos made available to us by BP. Initially these were very poor quality videos that appeared to be a screen capture at 30 Hz of a 25 Hz video. Compression artifacts, most notably pixelization, was clearly observable as were temporally non-uniform frames. After a couple of iterations with BP, full resolution videos were finally made available. These videos were shot with a variety of lighting conditions and magnifications. Several of the

videos were suitable for correlation analysis. The video *20100514221717125@H14_Ch1-H264h.mov* was suitable for correlation analysis. The ROV was stationary during this video. In order to increase the accuracy of the PIV measurements, an ensemble of 1000 images was used to calculate the jet displacement. The time index (as seen by the clock in the video) of the beginning of this ensemble was 17:30:05 and the end was at 17:30:48. This video segment was chosen because it showed mostly liquid oil flow and not gas. Using procedures similar to those described above as well as correlation averaging (Raffel, 2007), an average velocity of 7.52 in/sec and a plume diameter of 24.53 in is calculated along the yellow line (Fig 3). These numbers can be used to calculate the daily flow rate. Assuming oil to gas ratios from 0.29 to 0.5 and jet outer velocity to jet average velocity ratio of 1.5 to 2.0, a range for the oil flow rate is found to be 13,771 to 31,658 barrels per day. The combinations of these values is shown in Table 1.

Of the multiple leaks in at the kink point of the riser, only one was suitable for image analysis. The video *H14 BOP Plume May 15 1920-1945* shows these leaks. Because the ROV was hovering during the acquisition of these images, an ensemble of only 25 images could be found where the ROV was relatively stationary. The average velocity at the location indicated by the arrow in Fig 4 was 6.95 in/s while the jet diameter at that location was 7.61 in. Combining these measurements into a flow rate calculation, the flow rate was found to range from 1225 to 2815 bbl/day. These values are shown in Table 2. Because of the presence of two jets in the kink location, only one of which was measurable, the total flow rate from the two leaks was taken as twice the flow rate from the measurable jet. The total flow rate from the two locations, the kink point and the riser end, range from 14,996 to 34,473 bbl/day.

Post riser cut operation

Phase 2 FRTG Measurements

The kinked riser was cut on June 3 and a tophat was clamped on top of the riser stub. The tophat featured a riser to a surface collection ship, ethanol injection points, and several vents. During the time frame between cutting and removing the riser and installing the tophat, a ROV was tasked to acquire images of the oil flowing out of the riser stub. All of the videos have the same problem as kink jet measurements above—the ROV was afloat and hence the field of view is continuously moving. The video most suitable for correlation analysis is *TOPHAT_06-03-10_14-29-22.avi*. This video shows several well-lit views of the jet. The cross section of the riser contains two sections of drill pipe within it. At least one of these drill pipes is flowing oil as well. The color of the oil coming out of the drill pipe is lighter than that coming out of the riser. Because correlation averaging is such a versatile method for increasing the signal-to-noise ratio, a time period during which the ROV motion is minimal was found. The time index (as seen on screen) was 14:30:35. At this time frame, an ensemble of 51 images could be used because the motion of the ROV was very small compared to the size of the jet. A jet outer feature velocity of 20.24 in/sec calculated using a framing rate of 30 Hz and a scale factor based on the flange of 43 in = 527 pix (Fig 5). Instead of using the actual jet cross-sectional area which is difficult to use because the significant entrainment of the sea water, the riser cross-sectional area was used instead. Of course, there was a slight reduction in riser cross-sectional because of the shears used to

cut the riser as well as the presence of two drill pipes in the riser pipe but we also know that at the area where the velocity was calculated, the actual jet diameter would have increased from its exit diameter. These two factors offset each other and the cross-sectional area of the riser is a good approximation for the cross-sectional area of the jet. That area is 298.6 in^2. Using a oil to gas ratio of 29% and an expansion of the oil from sea floor conditions to atmospheric conditions of 135%, the oil flow can be calculated as 30,000 to 40,000 bbl/day with an expected value of 35,000 bbl/day.

References

M. Stanislas, K. Okamoto, C. J. Kähler, J. Westerweel and F. Scarano, "Main results of the third international PIV Challenge," Exp Fluids, Vol. 45, pp 27-71 (2008).

M. Raffel, C. Willert, S. Wereley, J. Kompenhans, Particle Image Velocimetry: A Practical Guide, Springer, New York (2007). (ISBN: 978-3-540-72307-3)

Gui L (1998) Methodische Untersuchungen zur Auswertung von Aufnahmen der digitalen Particle Image Velocimetry, ISBN 3-8265-3484-0, Shaker Verlag, Aachen, Germany.

Table 1. Phase 1 riser exit flow calculations.

jet disp	2.155	2.155	2.155	pix
jet ratio	1.50	1.75	2.00	
jet vel	7.52	7.52	7.52	in/sec
jet flow	5332	6221	7110	in^3/sec
GOR	0.29	0.40	0.50	
	13771	**22161**	**31658**	bbl/day

Table 2. Phase 1 velocity of the kink point jet and location of flow rate calculation.

jet vel	6.95	6.95	6.95	in/sec
jet dia	7.61	7.61	7.61	in/sec
jet ratio	1.5	1.75	2	
num jets	2	2	2	
jet flow	474	553	632	in^3/sec
GOR	0.29	0.4	0.5	
	1225	**1971**	**2815**	bbl/day

Fig. 1a. Filename and time index: 22890000 (22.89 secs). The pipe is seen running horizontally in this image with the flow issuing out of the break at approximately the horizontal center of the image. The darker colored material is crude oil. The arrow indicates the location of the lower right edge of the elliptical volume of fluid used in the manual tracking approach.

Fig 1.b. Filename and time index: 22957000 (22.957 secs).

Fig 2. PIV calculated vector field (average displacement 10.2 pixels).

Fig 3. Displacement (or velocity) field and plume diameter measurement area. The average velocity is 7.52 in/sec and the plume diameter is 24.53 in along the yellow line.

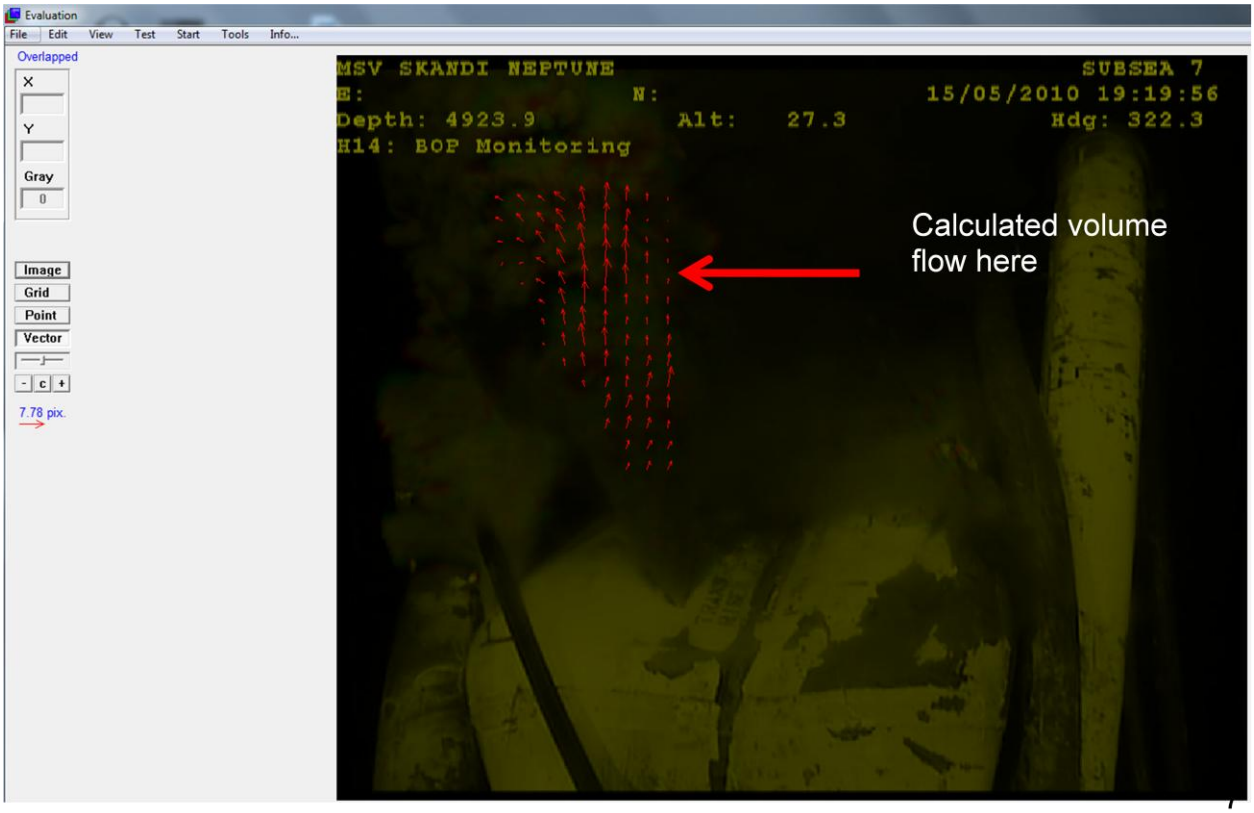

Fig 4. Velocity field for one of the jets at the location of the kinked riser and location where volume flow rate is calculated.

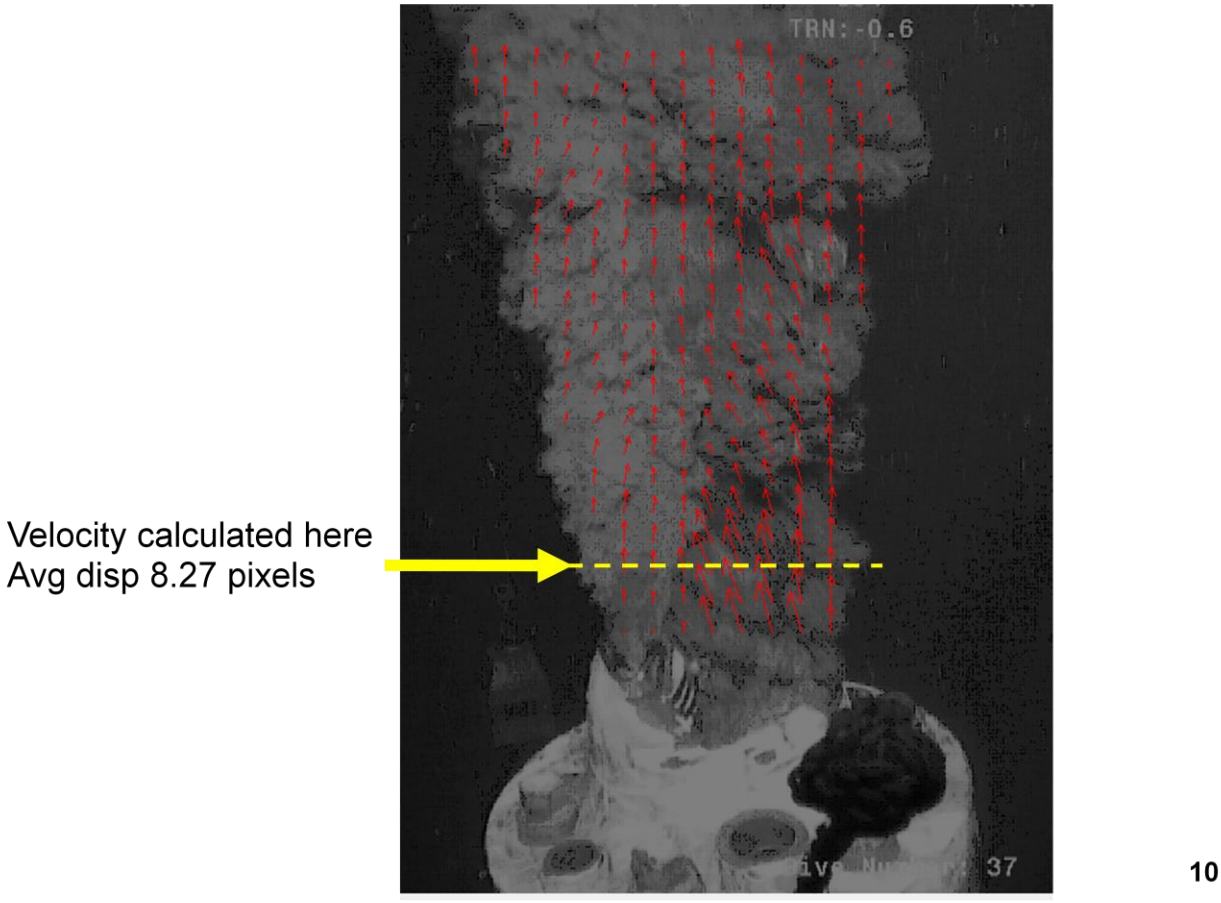

Fig 5. Phase 2 measurements made during the cut and cap operation June 3.

Appendix 6: Riser Pipe Flow Estimate

Dr. Ira Leifer
University of California, Santa Barbara

Overview

Our goal was to estimate the amount of oil issuing forth from the pipeline leaks of the Macondo incident based on BP provided (and BP selected) data for use in coming up with representative flow rates for spill response issues, not damage assessment. As a result, we were tasked to use the data at hand to provide our best possible guidance under the understanding that the results were unlikely to be accurate due both to the large number of uncertainties for a high volume, oil-gas-hydrate-tar bubble flow at these depths, and because of the demonstrated variability on a range of time scales even with the data provided, as well as our understanding of natural hydrocarbon migration systems which exhibit significant variability. As a result, the approach used did not seek to quantify oil flows with a second digit, and all values herein must be considered as probably with large uncertainty as to whether they are representative for the data herein, much less for extension to other times when no data was available or was analyzed, and far less to other times, particularly times extending to periods prior to or after various BP operations to mitigate the oil leak.

Temporal variability of emissions, pre – top kill

The oil-gas-water flow from the riser pipe exhibits clear temporal trends. Specifically, the flow shifts from a largely, buoyancy-driven gassy flow (primarily methane bubbles) to a flow that is predominantly oil – a conclusion based on the greatly reduced buoyancy of the flow. There also was a transition flow between these two cases, which is very abrupt in the case of shifting towards oily, and far slower for the shift to gassy (Fig. 1). This behavior is common in multiphase pipe flow, where the flow is no longer a well-mixed flow to what is best characterized as “slug flow.” The flows are discrete indicating significant phase separation during flow through the pipe. Specifically, the oily phase can be seen “riding” under the gassy phase. During transitions, the flow color shifts towards brown rather than the white and black observed in the two extremes indicating that the fluid most likely is an emulsion (mixture of oil/gas/water in microscopic droplets) formed by turbulence at the “boundary” between the driving gassy flow and advected oily flow layer. Of course this is a significant oversimplification of the actual multiphase flow, which clearly includes hydrate flakes (most clearly visualized during the oily phase), likely oil globules, and a varying emulsion factor for all but the clear “white” gassy phase, where the buoyancy flow is best characterized as oily bubbles.

To characterize the variability in the flow, I created an intensity interrogation window (Fig. 1) and analyzed the time variability of the oil-gas ratio through the variations in the image intensity.

Fig. 1 - Plume of oil and gas escaping the riser pipe sowing the three flow types, gassy, transition, and slightly oily. Also shown is the location of interrogation window.

The interrogation window intensity variations (Fig. 2) clearly characterize greater variability during gassy flow, a rapid switch to oily flow and a slower return to gassy flow.

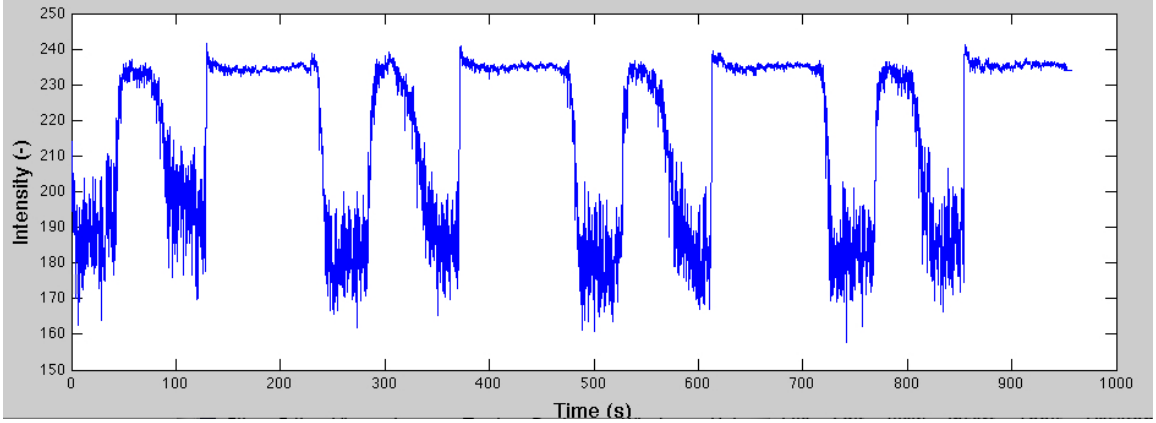

Fig. 2 - Interrogation window intensity trends. Higher value is darker.

Intensity variation of the riser pipe emissions (Fig. 2) then were evaluated by using a moving Hanning window and a spectral approximation approach (pburg, 128 pole). This analysis showed different spectral characteristics for the oily and gassy phases (Fig. 3). Thus, extrapolation of variability in the gassy and oily phases to longer time scales need to be considered separately.

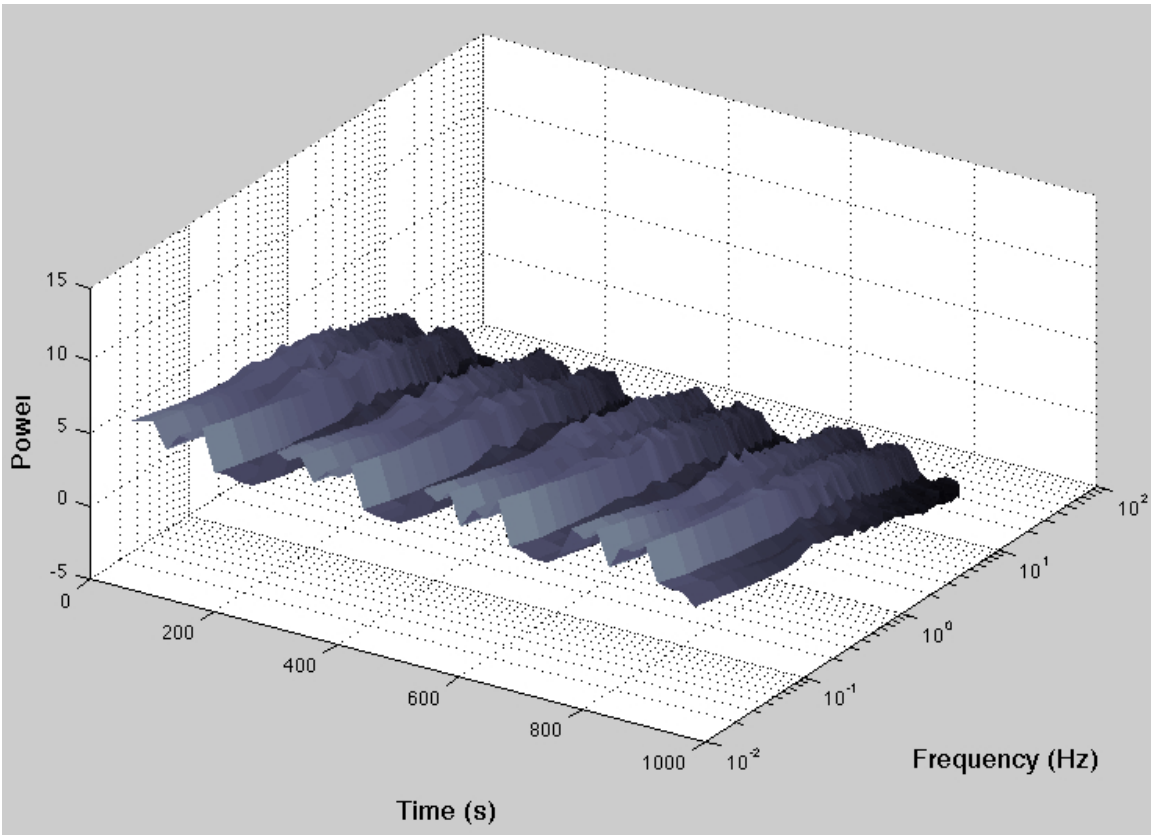

Fig. 3 - Spectragram of time varying spectra of the intensity variations, representative of oil-gas flow dynamics.

Spectragram of gassy-oily phase

Because of the difference in spectra from the oily and gassy flow regimes, it is inappropriate to analyze a spectra for the entire data set (Fig. 4) and interpret quantitatively, thus the following qualitative interpretation is presented. Of significance, the spectra for the low frequency components is highly distinct from higher frequency components. These two behaviors likely relate to turbulence in the pipe (0.2 Hz to 1 Hz), and variability in the flow associated with slug flow behavior (>1 Hz). Because the interrogation window is close to the pipe mouth, turbulence structure development in open ocean flow has a relatively smaller effect on the intensity particularly for the oily phase – a conclusion that clearly is not valid further from the pipe entryway. Extrapolating variability to longer time scales, which could represent migration processes to the well within the reservoir rock layer, and the effect of possible breaches in the well pipe structure thereby allowing fluid migration into the surrounding rock formations above the reservoir formation cannot be done from the analysis of this data set.

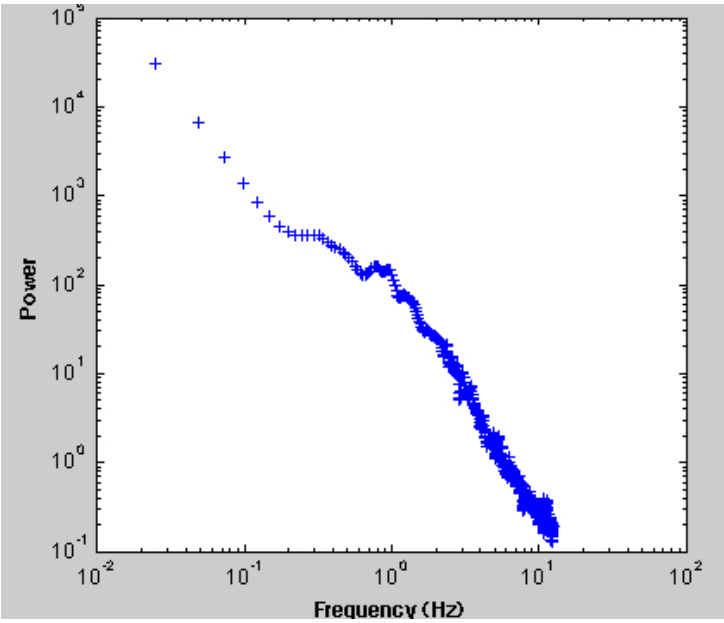

Fig. 4. Entire data set spectrum of intensity in the interrogation window (from pburg spectral approximation approach).

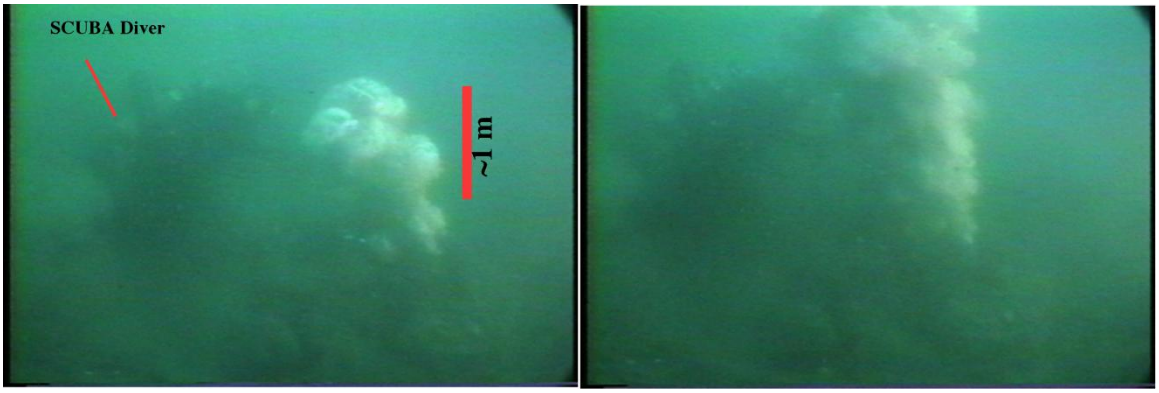

Fig. 5. Images showing initial blowout in the Coal Oil Point seep field (20 m depth), and bubble plume one second later. Size scale based on an assumed standard spherical SCUBA diver head (25 cm diameter).

Flow estimate by similarity

Based on simple velocity and size scaling estimates, a rough buoyancy flow of 400 L/s was estimated for the plume during the gassy phase. This value was, coincidentally, similar to a blowout observed in the Coal Oil Point seep field [*Leifer et al* 2006] at 20-m depth. In the Coal Oil Point seep field plume (Fig. 5), a gas flow rate of 0.4 m^3/s STP (buoyancy flux 0.13 m^3/s or 11,000 m^3/day buoyancy flux, or 34,000,000 L/day gas). Note, this natural blowout lasted only ~5 minutes. The emission flow was determined from back trajectory calculation using a Gaussian plume flux model of an atmospheric plume, thanks to the fact that the methane plume (fortuitously) drifted over an air pollution monitoring station a few minutes later.

Velocities of vertical features for the Coal Oil Point blowout plume (Fig. 5) were similar to feature velocities for the gassy phase of the Gulf Spill plume. Specifically, velocities were ~1.5 m s^{-1} versus 1.2 m s^{-1} for the Coal Oil Point blowout and Gulf spill plumes, respectively. It is important to note, though, that a dye injection in the Coal Oil Point blowout plume, a few seconds later, showed the centerline upwelling flow actually was 3-5 m/s in this depth range, with a water column average (based on time for the dye to arrive at the boat) of 3 m/s – the lower rise velocity arises from the effect of stratification [*Leifer et al* 2009]. This demonstrates that in intense, large-scale bubble jets in the acceleration phase, centerline velocities can be elevated by significantly more than a factor of two compared to edge feature velocities.

Based on assuming these two flows are comparable, and that the gassy phase represents the dominant gas transport phase, an uncorrected flux of 33,500 barrels of oil per day for a 50:50 oil to gas ratio (gassy phase), or 19400 barrels of oil per day for a 29:71 oil to gas ratio can be calculated. Here, the difference between the plume surface feature velocities, ~20% higher for SB Channel, approximately balances the fact that the buoyancy flux is ~26% lower at the Macondo depth due to the effect of methane compressibility [*Rehder et al* 2009].

This approach makes several assumptions, one of which is that the effect of hydrate skins on the bubbles is negligible. This assumption may be reasonable because most of the bubbles appear to be very small (r<150 µm) based on their behavior, thus, their surfaces area immobile whether due to oil or hydrates or ocean surfactants.

Assigning an uncertainty to this approach is difficult; around 20-40% seems likely. However, for the purposes of this report, this flux is used as a guide for comparison with the imaging velocimetry measurements.

- - - - - - - - - - - - - -

There are two dominant flow regimes, or phases observed with radically different oil to gas ratios. For this portion of the analysis I consider the oil to gas ratio to be based on what is clearly visible. Thus, while the gassy phase suggests minimal oil, the oily phase is clearly a mixture. Specifically, different portions of the plume have more vertical trajectories (Fig. 6) suggesting greater buoyancy flux and thus lower oil to gas ratios. Consistent with this interpretation are white objects interpreted as hydrate flakes, and thus associated with higher gas to oil ratios, are in the portions of the plume whose trajectory is more vertical. Also affecting the flow is the trench seabed, which forces a vertical component into the flow. Interaction with the seabed causes a blow back of oil in the background. This oil does rise buoyantly, indicating a non-negligible buoyancy contribution from gas phase, creating a vertical motion, which is independent of pipe inertia and wall effects. These plumes are illustrated in Hierarchical Digital Imaging Velocimetry (HDIV) analysis shown in Fig. 6. This analysis uses custom written HDIV software in Matlab, with two passes, and an initial, 96-pixel interrogation window, the second window being 48 pixels, and 75% overlap. Because of the low contrast in this plume, the HDIV software has significant problems, and so the results are only considered indicative.

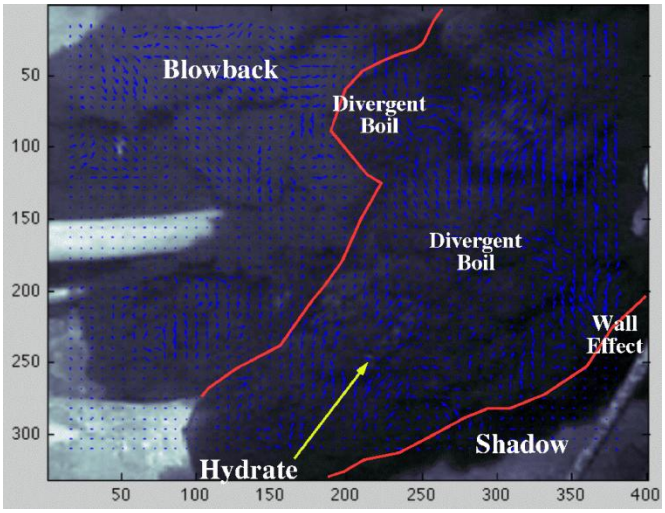

Fig. 6. Hierarchical Digital Imaging Velocimetry-derived velocity vectors and flow image illustrating oily flow characteristics.

Based on manually tracking the hydrate tinged boils, ~ 17 cm s^{-1} and assuming a 1.4 momentum – centerline velocity (top hat velocity profile within), the flow is 92 L s^{-1}. Assuming 0% produced water, and 80% oil to 20% gas ratio, a 25% fluid entrainment growth rate, and a mean plume diameter of 70 cm, the oil flow is 44 L/s, or 3800 m^3 day (23000 bbl/day) for the oily phase. The entrainment factor is less than a pure geometric factor because, based on the observations of Leifer et al (2006), it is assumed that the gas phase is above equilibrium for the first few seconds of rise and the bubbles are expanding. This process requires several seconds for these kind of flows, studies of individual bubble formation show this arises due to the added mass force which is significant (the growing bubbles must push the water aside), e.g., [*Vazquez et al* 2010].

Key is the estimate of 17 cm/s from surface feature motions to internal fluid motions. In this case, a 1.4 factor likely is highly conservative. Observations of the entrainment and advection of an eel by the flow (Fig. 7) suggests the fluid motion is 45 cm s^{-1}, or a factor of 2.6. This too likely is somewhat conservative due to the acceleration time of the oil flow on the eel's body. The eel shows no sign of attempting to swim into or out of the plume.

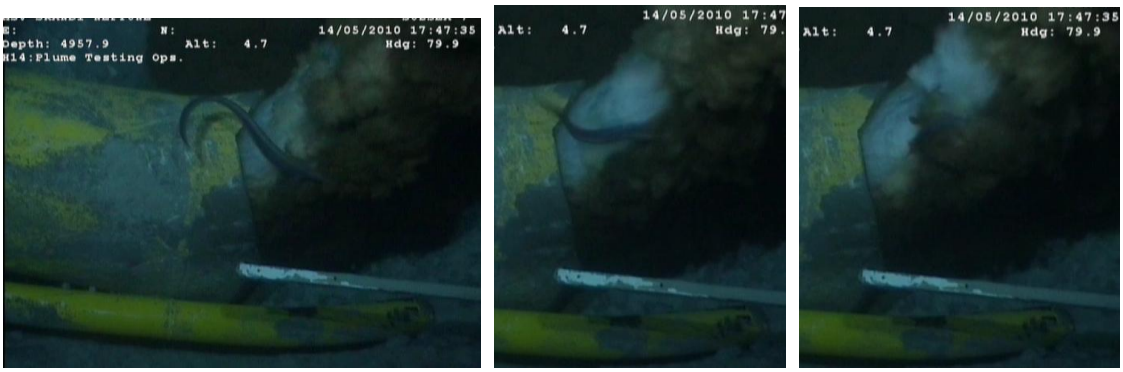

Fig. 7. Fluid velocity estimate by eel advection. Ideally, a dye injection study would have allow a proper scientific value to be determined.

This value is increased by a geometric correction factor due to the wall effect, illustrated in Fig. 8. Unfortunately, this correction factor is not known, video from overhead is at an unknown but highly oblique angle with an unknown zoom setting, and at a different time (the geometric correction factor

depends on the flow and the oil to gas ratio – where the flow is gassy, its rapid conversion from momentum driven to buoyancy driven allows the plume to remain distant from the wall such that wall effects on the plume proper (not the momentum plume) are minimal for the gassy phase. The likely correction factor could be 2 – 3 for the geometry shown in the image in Fig. 7b. Applying the momentum correction factors 2.6 and geometric correction factor of 2 suggest 89000 bbl/day for the oily phase. If one was to further assume no oil transport during the gassy phase, a best guess, conservative estimate based on a 50% duty cycle is ~45000 bbl/day for this plume. The precise duty cycle, while known for this data period, is not known for longer time periods, on the order of a day.

2*2.6*17* pi*35* 35/1000 (*0.8*1.0*0.75*3600*24) / (159)

GeoCorr * MomCorr * velocity * pi * radius* radius / (cm3/liter) * (oil ratio * produced water ratio * entrainment efficiency) * (sec/hr*hrs/day)/(liters/bbl)

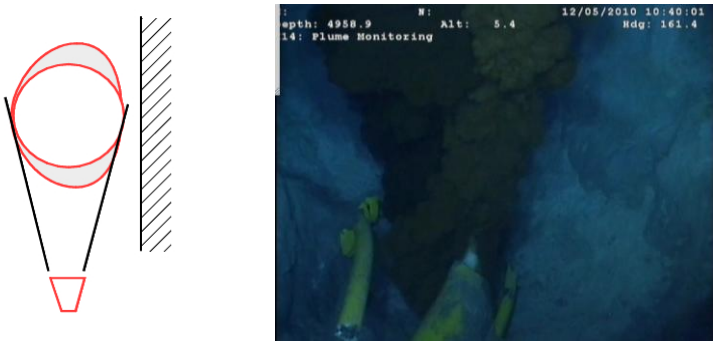

Fig. 8. Top view schematic illustrating geometric correction due to wall effects.

In addition, the overview video (Fig. 8) shows that there was a second plume some of the time, which is not the blowback plume. The two plumes in the overview image could represent the same flux divided into two plumes, or because the darker plume would be obscured by the browner plume from the view used in the flow analysis, could be in addition. It is also important to note that the darker (oilier) plume is deeper than the browner (emulsion) plume suggesting the same phase separation observed in the analyzed video. To some extent, this secondary plume is accounted for in the geometric correction factor. What is not corrected for in the geometric correction factor is that the brown plume at this point clearly has a source behind the end of the riser, which is also observed in some of the videos. The amount this secondary emission mechanism could contribute is unknowable from this video, it could be 10 to 30 percent more or 10 to 30 percent less.

The estimate however, only accounts for what is observed. However, the video data provides strong evidence that the flow is not purely oil and gas. Firstly, there clearly are flakes of hydrate, which appear in the more turbulent vortices. Here, vortical (centrifugal) forces likely are pushing these flakes to the edge where they become visible (against the dark contrast of the oily plume). These particles are too large to have formed in the distance since exiting the pipe, and thus clearly indicate the pipe has internal hydrate formation. These hydrate flakes could have formed in the flow; however, particle formation in a flow generally happens on wall surfaces suggesting portions of the pipe were partially blocked by hydrates (see below) with the highly turbulent flow periodically removing chunks and flakes. In addition, it is very common in natural seeps and also production wells for paraffins and tar and also liquid oil globules to be transported within the flow.

At one point in the video, an expulsion of oil droplets occurs during a transition from the gassy to oily phases (Fig. 9). It is impossible to determine how much oil was expelled in this event, but several liters to tens of liters seems likely. Thus, I add a 10% factor for hidden oil globules, most of which likely are

obscured. Thus the infrequency of the globule ejection event likely reflects the fact that an exceptionally large globule was in the plume at that moment. Because globule transport can occur at any time, it would be true for both gassy and oily plumes, pushing the steady state best guess estimate of ~50,000 bbl/day. Emissions from the kink would still need to be added. If the oil to gas ratio is 0.3 instead of 0.5, then ~30,000 barrels is a best estimate. However, given the other uncertainties, each of these numbers has a significant uncertainty. Best guess probably lies between these two oil to gas ratios, likely towards the 50,000 bbl/day***.

Although this estimate sought to quantify what is known, water column data, which was requested, has not been provided to eliminate the possibility of other leaks outside the area of inspection by the ROVs.

Fig. 9 Oil globule expulsion

***Deriving uncertainty limits on this number are challenging and to some extent largely misses the bigger picture. For example, reasonable uncertainties in the many assumptions could be +/-50% (25k – 75k) or larger. These uncertainties then would represent the flow at the time of the video. However, given the "geyser-like" nature of hydrocarbon migration through reservoir formations, it is impossible to state whether the flow one minute before and one minute afterwards are similar, significantly higher, or significantly lower. Thus, extrapolating from the 46 minutes of data to a daily rate is highly problematic. Natural hydrocarbon migration systems show variability of factor of two and larger on time scales from seconds to months with large eruptions where emission increase by factors of tens or hundreds commonly observed. In fact, the blowout was one such example. Also, I observed a similar occurrence on streaming internet video after the pipe was cut and before the cap was put on, which appeared to push the ROV away, and appeared to represent a short term (minutes) very significant increase.

This level of uncertainty has led me to use the more qualitative approaches outlined herein to estimate flows. An example of HDIV analysis is provided below. The more detailed HDIV analysis is very useful for better understanding better the fluid dynamics of this complex, multiphase flow, however, the additional accuracy in the HDIV techniques is far less than the many other uncertainties.

Current Velocimetry by Eel Advection

Interpretation of the buoyancy drive on the oil plume (which relates to the oil to gas ratio) depends on interpreting the plume motions as due to momentum flux from the pipe, and this requires knowledge of the currents. ADCP data was (requested) but not provided, thus it was initially assumed that because this is the deep sea, currents were small. However, because this is a trench, current amplification cannot be neglected.

Eel analysis (the eel was advected towards the blow back plume, video on 5/14/2010), allowed a very rough estimate of currents of ~20 cm/s in the trench in the direction the oil plume is advected. This velocity is not due to plume entrainment, shortly afterwards, the eel is accelerated towards the camera and towards the main plume within which it then was entrained. This implies that 1 – buoyancy fluxes need to be calculated along a vector direction that considers the current, i.e., are likely greater, and 2, the oil to gas ratio likely is slightly lower.

Fig. 10. Eel advection in 1 second was ~20 cm, suggesting significant currents played a role in plume trajectories.

Hierarchical digital imaging velocimetry applied to gassy plume

Mean velocities of 50 seconds of data all for during the gassy plume phase were calculated and show the plume core rises close to vertically. Some bubbles detrain rather rapidly, being segregated downcurrent due to lower buoyancy (oiliness most likely). However, these bubbles generally experience a tendency towards re-entrainment into the main plume. This is a process that in an area plume is termed necking and is due to acceleration of the main plume. Re-entrainment of the blowback plume also is visible. Although immediately out of the pipe, the plume is primarily in an acceleration phase, by the top of the image, the outer-edge of the plume has begun to slow down as entrainment and pressure equilibration increase the plume dimensions. Horizontal velocities from turbulence are completely averaged away. Analysis of the remaining horizontal component for the upper reaches of the plume suggest currents of ~10 cm/s; however, deriving currents from bubble plume velocities is inaccurate due to processes such as flow separation, and entrainment.

Looking at the normalized mean velocities (normalized because the point of these figures is to illustrate what we can learn from HDIV of bubble plumes not mass estimates. The figure shows a rapid acceleration of the flow (at the edge of the plume), which largely reached equilibrium after ~20 cm, decreasing thereafter as the plume broadens. There also is a standing wave feature in the velocity structure with a node at ~175 cm. Above 250 cm, velocities decrease faster as the plume broadens further. Note the shadow shows up as having small velocities due to the scene illumination angle.

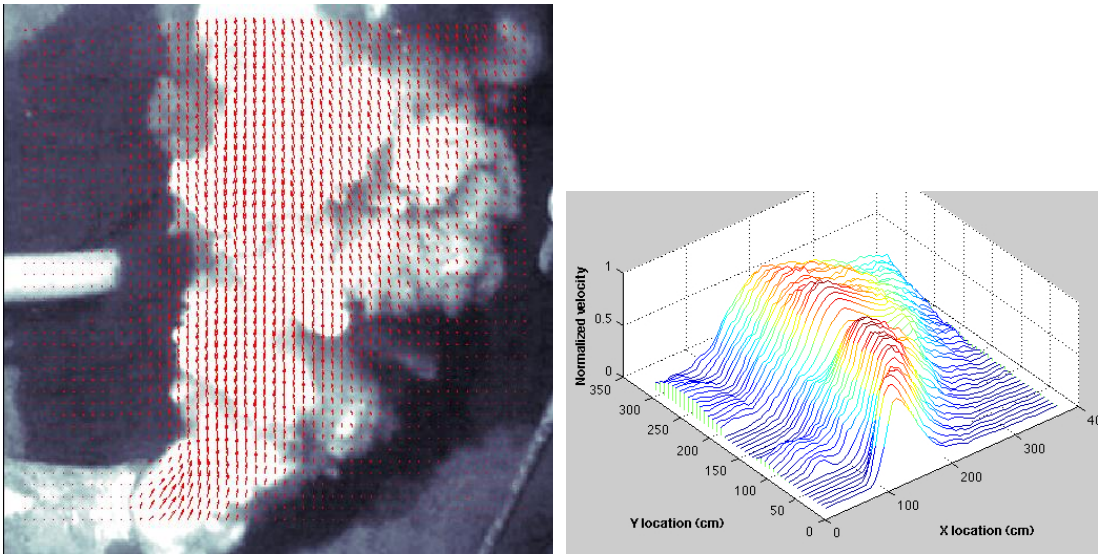

Fig. 11. HDIV velocity analysis showing 90 second averaged velocities and illustrating the trajectory of the plume.

Post kop kill, post riser cut

Top kill sand-blasted clean the inside of the well pipes, almost certainly leading to increased flow by reducing resistance in the pipes, as well likely clearing away fragments of pipe annular material, and potentially creating new migration pathways external to the shattered and fragmented casing.

Key to imaging velocimetry is the size scale. Because volume (or volume flux) varies cubically, a scale variation of 10% leads to a 30% volume flux error. The flange diameter is 109 cm, while the bolt diameter is 10.5 cm. Comparison of bolt sizes around the flange shows a 20% increase from the front of the flange to the middle. The size scale at the center of the flange, likely is about 10% less than that of the bolt and flange, or about 1.85 pixels per cm; however, at the front of the plume, the scale is about 10% larger. Where the plume grows to a diameter comparable to the size of the flange, the size scale at the plume center is ~20% larger than at its edge – i.e., representative of a flow that is 73% larger. For frame 2115, the best guess scale is 1.8, for frame 2260, it is 2.0.

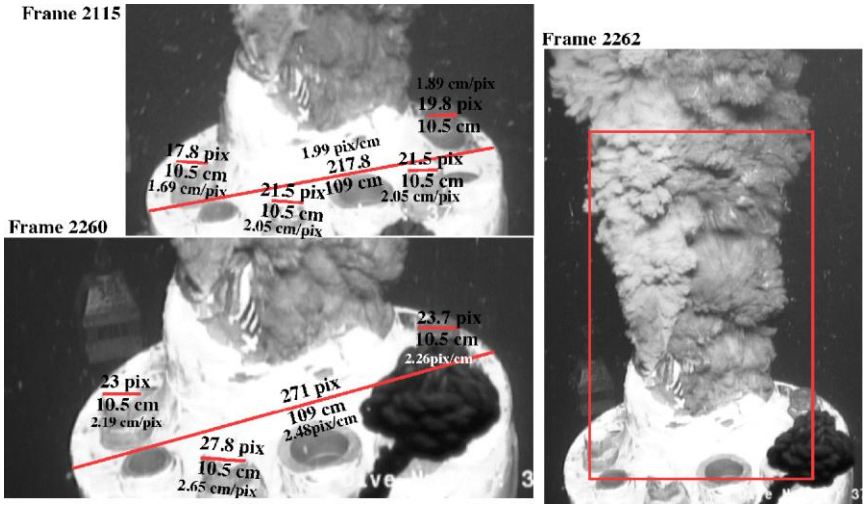

Fig. 12. Two images from 14:30:32 to 14:30:36, file TOPHAT_06-03-10_14-29-22.

The flow is extremely rapid, with very strong eddies, whose velocities are large enough to cause the outer surface flow motion to be downwards, even though the overall flow continues to move upwards. Flows are rapidly pulsed, with strong turbulence jets that visibly penetrate through other turbulence structures. As a result, HDIV analysis of techniques can be significantly challenged.

Thus, a preliminary investigation used a hand tracking approach of clearly visible structures (Fig. 13). The size scale here was estimated from the position on the plume (center or edge) and the time, and has an uncertainty of ~5%. Note, this assumes that the plumes are radially symmetric, which seems approximately accurate from video where a ROV viewed the plume from a variety of angles. The mean velocity of the darker plume from the hand analysis is 130±20 cm/s, and of the lighter plume is 190±20 cm/s, i.e., the lighter plume, which likely has a greater of emulsion as might be expected of a more turbulent, higher flow plume. In contrast, the darker, lower flow plume exhibits hydrate flakes, suggesting a higher gas composition.

This translates into a flow of 50000 bbl oil day if the full plume was all made of the dark flow,

1.2*1*pi* mean([57 97]).^2*135 * 0.41 * 1 * 0.75 * (3600 * 24) /(159/1000)

Mom Corr* GeomCorr * pi * radius* radius * velocity * oil ratio * produced water ratio * entrainment efficiency) * (sec/hr*hrs/day)/(liters/bbl) (cm3/liters)

And 87500 bbl/day if the full plume was all made of the lighter plume.

1.2*1*pi* mean([57 114]).^2*190 * 0.41 * 1 * 0.75 * (3600 * 24) /(159/1000)

Here, the features being tracked are assumed to movie at close to the plume velocity, and thus the calculation uses a low value of 1.2 for the plume centerline/momentum velocity ratio. Assuming the faster plume is one third the total plume, the mean plume flow for these three seconds of data, based on the hand analysis is 62500 bbl/day. Moreover, as with the horizontal riser plume, it seems likely that the flow contains a similar quantity of tar and large oil droplets. This could possibly account for an additional 5 - 10%, or a total of 68000 bbl/day.

Uncertainty on this number is significant and includes the oil to gas ratio (±25%), the tar globule fraction (±5%), the size scale (±5%), the effect of the ratio between the two plumes 80:20 to 66:33 (±2%), the momentum correction (±10%), uncertainty in the velocity (±15%- ±10%), which also implies a change in the plume area of ±15%, and uncertainty in the entrainment rate (±10%).

A significant unknown is whether the momentum correction used of 1.2, which in a plume in the acceleration phase can be in the range 2.8 – 5, is correct for this manner of manual tracking. Evidence that it may be correct is provided by [*Leifer et al* 2009] who measured upwelling flows for a range of engineered bubble plumes at a range of depths. Interpretation of the upwelling flow suggested that upwelling data for the blowout in [*Leifer et al* 2006] implied an unreasonably large flux ~ 10^{15} L/min! As a result, the upwelling flow was interpreted as acting as a super bubble equivalent to 25-cm diameter with mass transport primarily by wake advection. In the case, here, such a super bubble would be as 8 to 10 cm with 0.7-0.8 eccentricity, which is approximately comparable to dimensions of the turbulence eddy boils.

Although this interpretation appears appropriate for the darker plume, it is unclear whether it is appropriate for the lighter plume.

However, the largest uncertainty is the extrapolation from 3 seconds of data to a daily rate. Natural seep systems can vary by orders of magnitude on short time scales from minutes to days to weeks [*Bradley et*

al 2009] – and this is a well pipe tapping into a natural hydrocarbon migration system. As a result, it is unknown whether these values are representative at all.

S1 – 0.33 sec 40.47 cm =122.63 cm/s

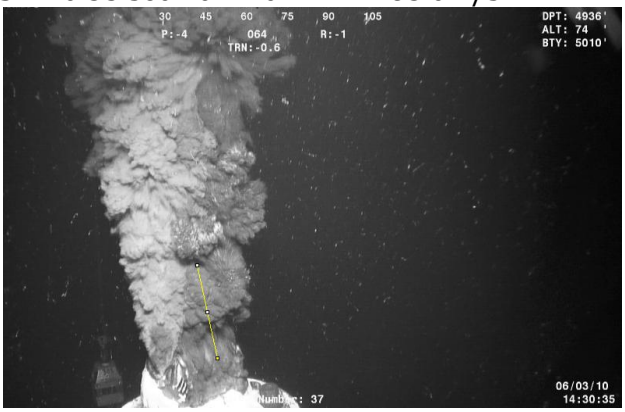

S2 – 0.66 sec, 74.53 cm = 112.9 cm/s

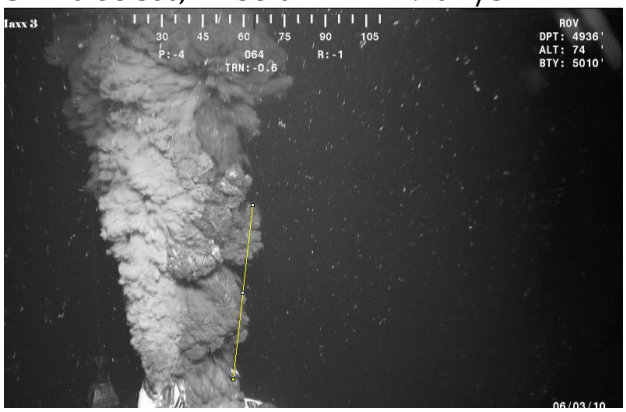

S3 – 0.1333 s, 22.3 cm, 167 cm/s

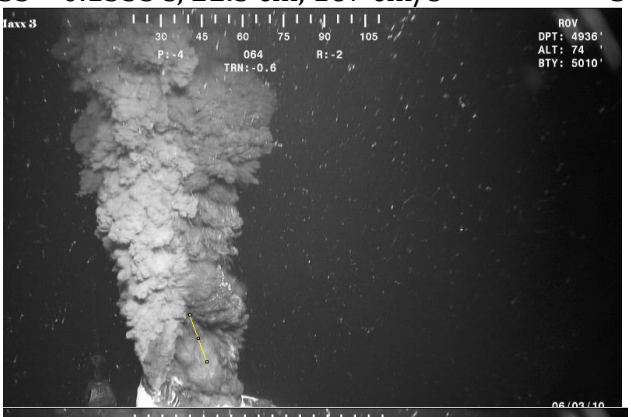

S4- 0.2 s, 31.5 cm, 157.5 cm/s

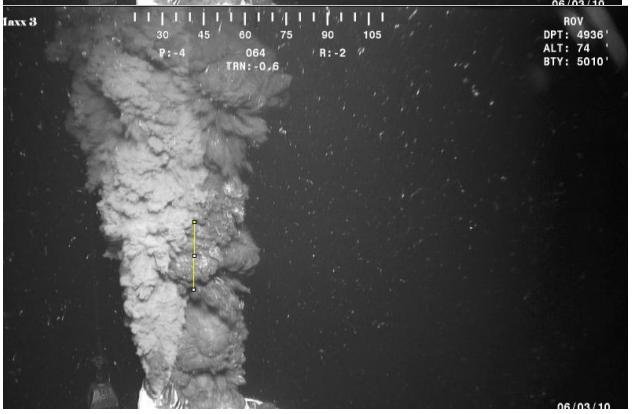

S5 – 0.267 s, 45.4 cm, 170 cm/s

S6-0.1 s, 21.7 cm, 217 cm/s

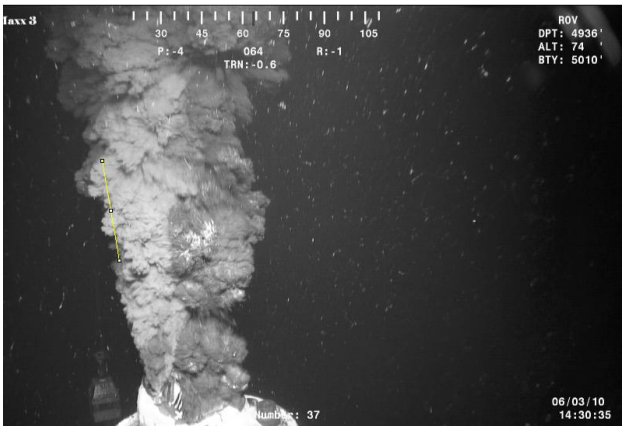

S7 – .233 s, 44.7 cm, 189 cm/s

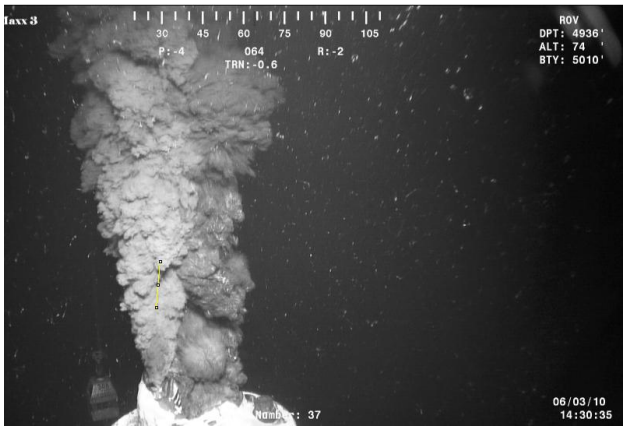

S8 – 0.267 s, 46.23 cm = 173 cm/s

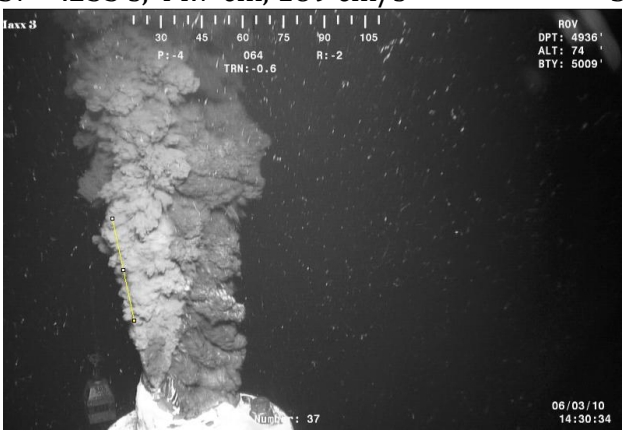

S9 – 0.333 s, 55.84 cm, 166.6 cm/s

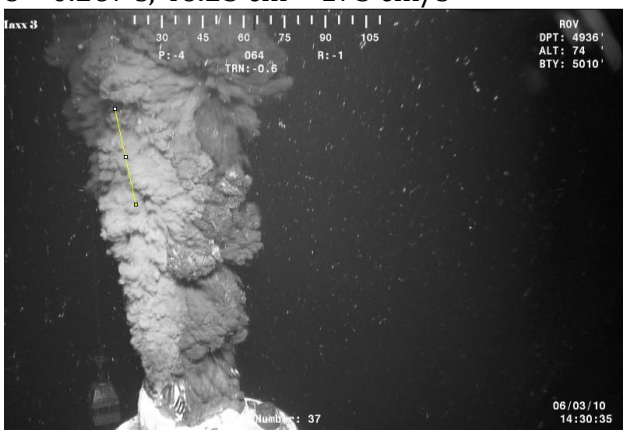

S10 – 0.267 s, 53.5 cm, 200 cm/s

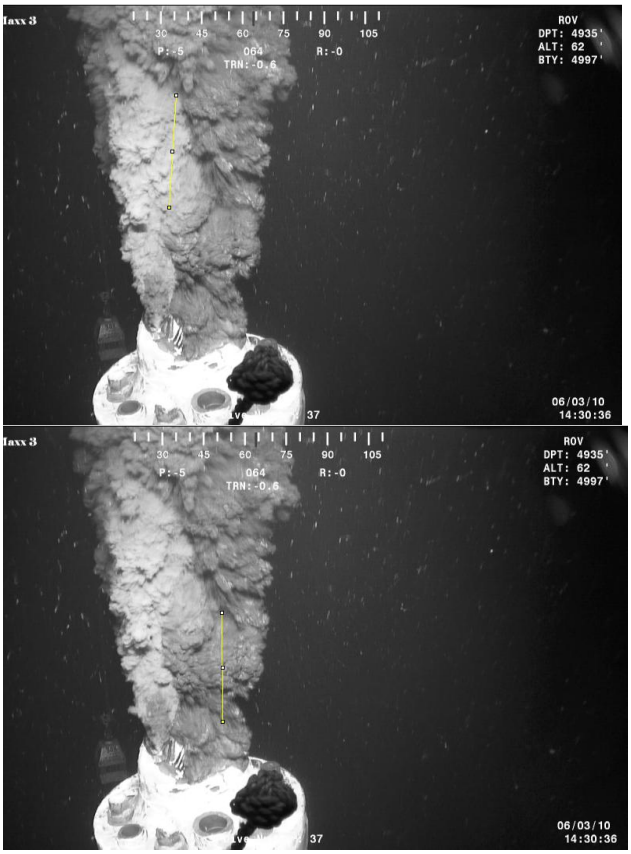

S11- 0.3 s, 37 cm, 123 cm/s

S12- 0.2 s, 44.2 cm, 221 cm/s

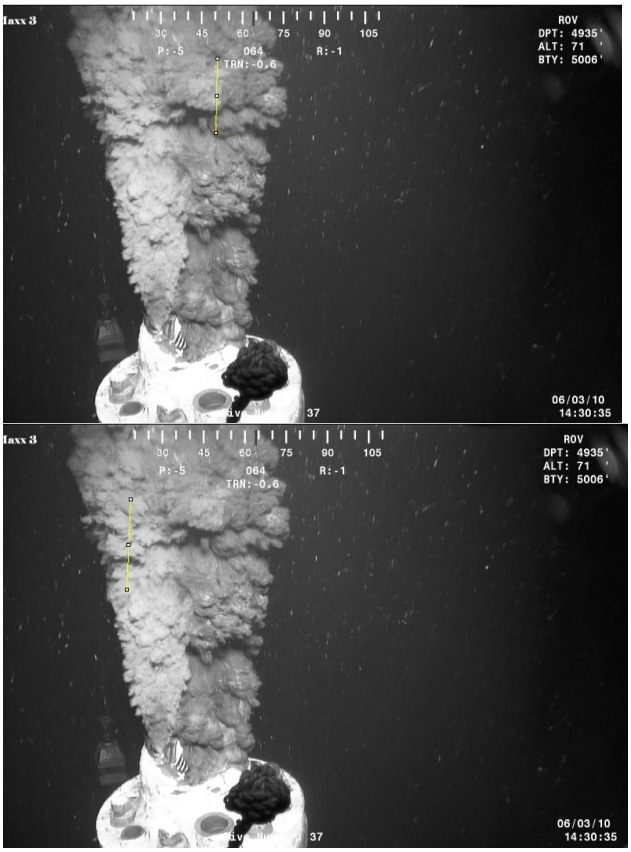

Fig. 13 – Hand analysis. Yellow line shows feature tracked.

HDIV analysis

Because the flows were so fast, a large initial interrogation window, 128 pixels was used with a 75% overlap, and a sensitivity filter of 3 standard deviations. Two subsequent passes at 50% the original window brought final window size to 32 pixels (or ~16 cm).

Analysis shows some of the complexity of the surface flow, with highly divergent flows in some portions, and negative velocities in others (due to rolling vortices). The HDIV analysis generally showed lower velocities in the paler plume, likely due to the lower contrast, higher velocity, and rapid evolution of features rendering them difficult to impossible for the routines to track. Evidence that velocities in the light colored plume are actually higher is provided by velocity data, showing an acceleration of darker colored plume near the interface between the two, which would only occur if the lighter color plume was moving faster, in agreement with the hand analysis.

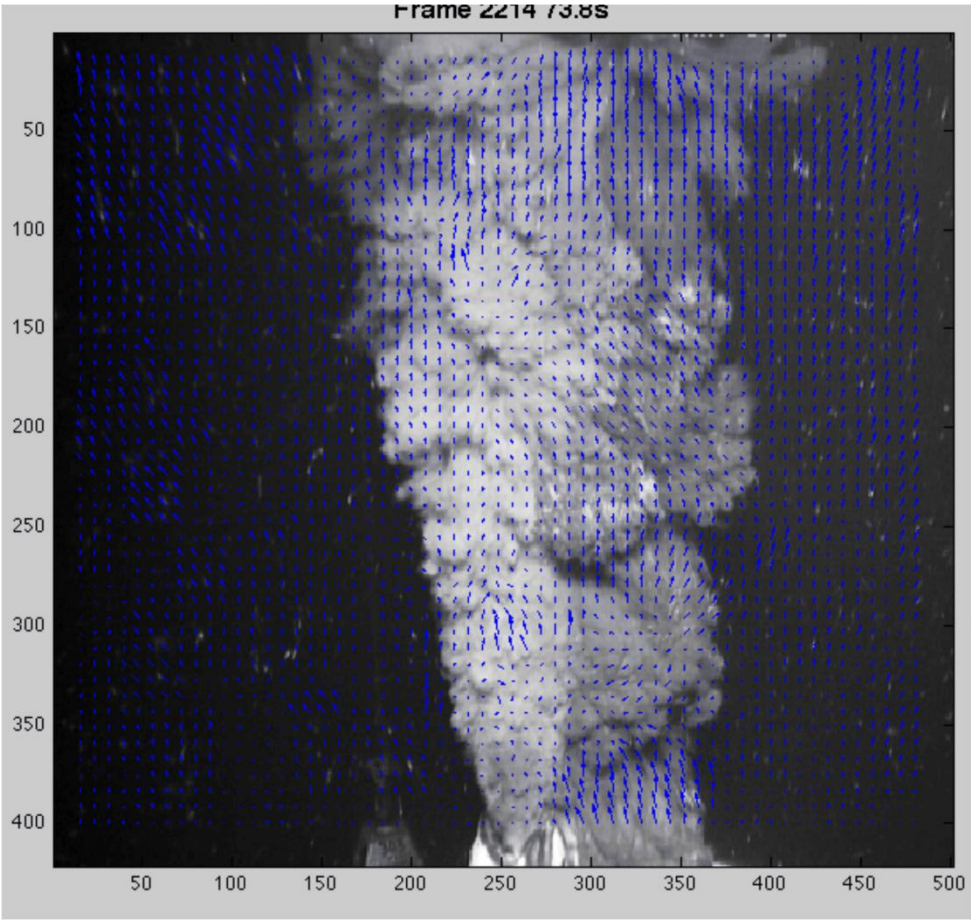

Fig. 14 - HDIV velocity vectors showing areas of highly divergent boils, strong upward flow, and strong entrainment.

Vertical velocities averaged over 0.33 s (over which the size scale changes minimally) show strong velocities near the pipe entryway, and near the upper plume edge. A uniform size scale of 2 cm/pixel was used, leading to errors on the order of approximately 10-20%. This upper higher velocity area, comparable to the tracked velocities in the hand analysis, likely correlates to segments where clear features are being advected. Other areas actually show negative velocity excursions, due to boils rolling, such as the feature at 350 vertical pixels in the darker plume. Visual inspection reveals that although the plume appears to be sinking, the entire vortex is rising. As a result, a mean surface velocity might be in the range of 20 – 30 cm/s, or about a fourth to a fifth of the hand analysis. One interpretation is that the difference is between the momentum plume and the main plume velocity, suggesting a ratio of 4-5, rather than 2.3. Note, however, the velocities are not really in the momentum plume, but are on an undulating surface of the bubble plume itself – which is far more distinctly defined because this plume is in the acceleration phase than a normal plume. Large-scale (50 m depth) studies by Milgram [1983] for bubble flows in fresh, quiescent water suggest a high ratio momentum/core plume velocity ratio. Given the uncertainty in the ratio between momentum and velocity plumes, and the challenge of tracking the light plume, which transports significant mass, HDIV was not used to estimate a flux.

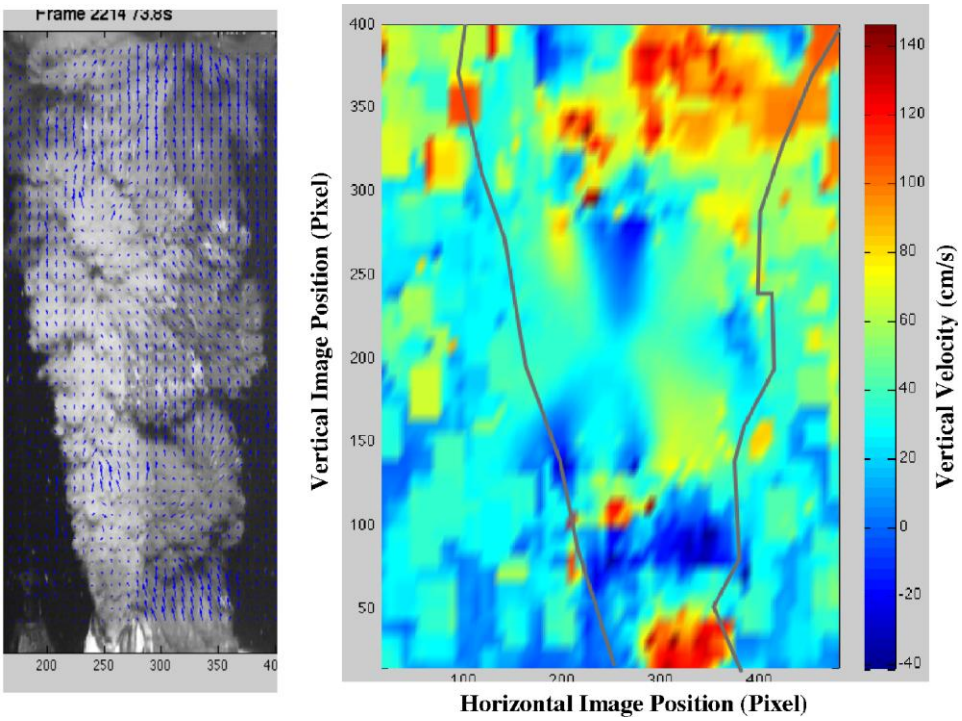

Fig. 15. A) velocity vectors as in Fig. 14. B) mean of 0.33 s of vertical velocity data. Lines highlight approximate edge of the plume.

FINAL WORD

The flows herein have large uncertainties attached, but the dominant uncertainty arises from variability in these kind of systems, as well as unknowns. For example, we have been assured that there is no produced water, yet, if there was no water in the system, then hydrate flakes could not form (the time is too short for hydrate flakes of centimeter size to form after exiting from the nozzle exit). Thus, water must be entering the system, or the absence of produced water is an artifact of the samples used to make this determination, and the density of the fluid exiting the pipe is significantly higher.

However, the biggest unknown arises from temporal variability and that only a few seconds of video (or tens of minutes prior to the riser cut that) have been analyzed. More video was not analyzed due to BP not providing the video suitably fast. Had hard drives been fed-ex-ed overnight, then several additional days would have been available for analysis.

Natural seep systems are examples of hydrocarbon migration systems where faults and fractures serve the analogous role to the well pipe. As a result, similar variability can be anticipated from the leaking well pipe. This variability can be orders of magnitude on a whole range of time scales and can include blowouts (Leifer et al., 2006). As a result, extreme caution must be used in applying these numbers for mitigation strategies, a healthy safety margin, factor of two MUST be engineered in for activities to be conducted safely.

Given the variability in the seep – well system, the importance of the flow rate numbers to response and safety, and the numerous calculation uncertainties due to poor knowledge of processes at these depths and the precise nature of the flow, the call for an experiment to directly measure the flow makes enormous sense to provide confidence in the TFRT's analyses, and to calibrate the HDIV analysis techniques. I provide the study plan below, which was presented to the team.

- - - - - - -

Independent Validation Study of the Flow Rate

My experience on the TFRT strongly highlights the need for independent data for flow rate verification to assure public confidence in our work. This can be done quickly and accurately, using field-demonstrated, published, techniques on a two-track approach:

- **Prioritize collection of independent data**, to make the measurements needed to provide a non-BP value based on solid science.
    - A simple monitoring experiment, as detailed *below*, could be performed on a week time scale of the decision to proceed.
    - Readily repeatable to provide data until well emissions stabilize.
    - Includes monitoring capability
- **Investigate the BP-provided data** to estimate reasonable and scientifically defensible uncertainty bounds on the emission range.

Proposed Experiment:

a. Measure the plume's "work" (physics' sense). Dye injection and fluorometer/video measurement of plume fluid velocity (*hydrates clog paddle-velocimeters, bubbles prevent ADCP usage*), not plume structures (*avoid deriving phase speed from HDIV on "crests"*) to provide the mass flux. The difference between mass and buoyancy fluxes (latter from plume's work) yields oil flux.
b. Multibeam scanning sonar (250 kHz) to measure plume growth and derive net entrainment rate. Also provides long-term monitoring of variability.
c. CTD measurements and hydrocasts downcurrent of the plume to measure plume detrainment rates. Temperature, salinity, and O_2 measured during casts will identify detrainment zones (intrusions). Niskin bottle samples from these zones will be sub-sampled for C_1-C_5 and DOC concentration analyses to trace and quantify mass fluxes from the plume to the water column. This will provide critical data for validating mass balance calculations in (a) and identifying the hydrocarbons' fate.
d. High quality, size-calibrated, plume video above the plume acceleration phase, observations from multiple angles.
e. Several repeats to "calibrate" the monitoring sonar allowing sonar return to be related to flux variability. Note, sonar does not penetrate dense bubble plumes, sonar only shows the plume outlines. However, plume dimensional-growth (*net entrainment*) directly relates to the buoyancy flux.
f. Directly and repeatedly sample the flow to measure the oil to gas ratio. A Niskin bottles on ROV will work fine, followed by video observation and shipboard.
g. Multibeam site survey to confirm that the study leak is the dominant leak.

This study should be coordinated with airborne remote sensing data. Development of a remote sensing approach to spill quantification is a NASA/NOAA/USGS effort under Dr Leifer's leadership. Coordination would leverage the value and accuracy of both efforts.

References on the marine application of the destratification strategy available on request.

Regards,
Ira Leifer, Ph.D.
+1(805)893-4931 **Cell** +1(805)252-3636 **Email** ira.leifer@bubbleology.com

References

Bradley, E. S., I. Leifer, and D. A. Roberts (2009), Atmospheric long-term monitoring of temporal trends in seep field emissions *Atmospheric Environments*, Submitted.
Leifer, I., B. P. Luyendyk, J. Boles, and J. F. Clark (2006), Natural marine seepage blowout: Contribution to atmospheric methane, *Global Biogeochemical Cycles*, *20*(GB3008), doi:10.1029/2005GB002668.
Leifer, I., H. Jeuthe, S. H. Gjøsund, and V. Johansen (2009), Engineered and natural marine seep, bubble-driven buoyancy flows, *J. Phys. Oceanography*, *39*(12), 3071-3090.
Milgram, J. H. (1983), Mean flow in round bubble plumes, *Journal Fluid Mechanics*, *133*, 345–376.
Rehder, G., I. Leifer, P. G. Brewer, G. Friederich, and E. T. Peltzer (2009), Controls on methane bubble dissolution inside and outside the hydrate stability field from open ocean field experiments and numerical modeling, *Mar. Chem.*, *114*(1/2), 19-30.
Vazquez, A., I. Leifer, and R. M. Sanchez (2010), Consideration of the dynamic forces during bubble growth in a capillary tube, *Chemical Engineering Science*, *65*(13), 4046-4054.

Appendix 7: Estimate of the Max Oil Leak Rate from the BP Deepwater Horizon

Estimate of the Maximum Oil Leak Rate from the BP Deepwater Horizon Based on Velocity Measurements, Theoretical Analysis, and CFD Simulations of Oil Leak Jets

by

Franklin Shaffer, Nathan Weiland[5], Mehrdad Shahnam, Madhava Syamlal, George Richards
US DOE National Energy Technology Laboratory

Prepared for the Phase 2 Report of the Plume Analysis Team
of the U.S. Flow Research Technology Group (FRTG)

Submitted on June 15, 2010

Introduction

The mission of the Plume Analysis Team of the U.S. Flow Rate Technical Group (FRTG) is to conduct an independent scientific estimate of the total average flow rate of oil leaking from the oil leak jets at the sea floor under the BP Deepwater Horizon site. The Plume Analysis Team is using videos of oil leak jets for this analysis taken by BP's Remotely Operated Vehicles (ROVs).

In Phase 1, the Plume Analysis Team estimated a minimum potential value for the total average oil leak rate, primarily based on Particle Image Velocimetry (PIV) measurements of jet velocities using BP videos of the oil leak jets. The Phase 1 Analysis was intended to provide a lower limit for the estimate of the total average oil leak rate during the period from the time of the BP Horizon accident until prior to the riser cut procedure (around 27 May 2010). The Plume Analysis Team concluded that the minimum oil leak rate was in the range of 12000 to 25000 barrels per day (bpd).

In Phase 2, the Plume Analysis Team conducted a more detailed analysis to estimate the maximum potential value for the total average flow rate of oil. The Phase 2 estimate is to be an upper bound (i.e., worst case scenario).

This report presents an estimate of the maximum potential value of the oil flow rate discharging from the riser kink and the riser end. The estimates are based on three different analysis approaches conducted by three separate teams of researchers at the USDOE National Energy Technology Laboratory (NETL) as follows:

[5] Also Research Assistant Professor of Mechanical Engineering, West Virginia University

- The first analysis approach was to measure oil jet velocities using Feature Tracking Velocimetry, which is similar to Particle Image Velocimetry (PIV) using NETL's proprietary high speed PIV software (Patent Pending, U.S. Patent Application No. 12765317); this analysis was applied to one jet at the riser kink and to the jet at the riser end.
- The second analysis approach analyzed the trajectory of the buoyant jets and estimated the flow rate based on the established theory of turbulent jets; this analysis was applied to the same plumes as the FTV analysis (namely, one jet at the riser kink and the jet at the riser end).
- The third analysis approach involved computer simulations of the multiphase jet at the riser end using computational fluid dynamics (CFD); the comparison of jet profiles from these simulations with profiles seen in the ROV images of the riser-end jet provided confirmatory observations for the range of the maximum potential flow rate.

In this report, we present an integrated assessment based on these three approaches, including an assessment of assumptions and uncertainties embodied in each approach.

Background

On April 20, 2010, the BP Deepwater Horizon oil well failed catastrophically and the Blowout Preventer (BOP) failed to seal the oil well. The riser pipe bent in a >90 degree kink approximately one meter above the top of the BOP and a section of about 500 feet of riser fell to position horizontally on the sea floor as shown in the schematic below (Fig. 1). The riser pipe was severed about 500 feet from the well with the end of the riser pipe open to the ocean. Pressurized oil and gas produced a turbulent, buoyant jet emitting from the end of the riser (hereafter called the Riser End Jet). The inner diameter of the riser is 19.5", but near the end of the riser, the riser is slightly deformed, reducing the inner diameter of the end of the riser to about 16.5 inches. It is estimated that considerably more than half of the oil is leaking from the Riser End Jet. At the kink in the riser just above the BOP, the riser developed small holes in several places with oil/gas jets emitting from the holes. These are referred to as Riser Kink Jets.

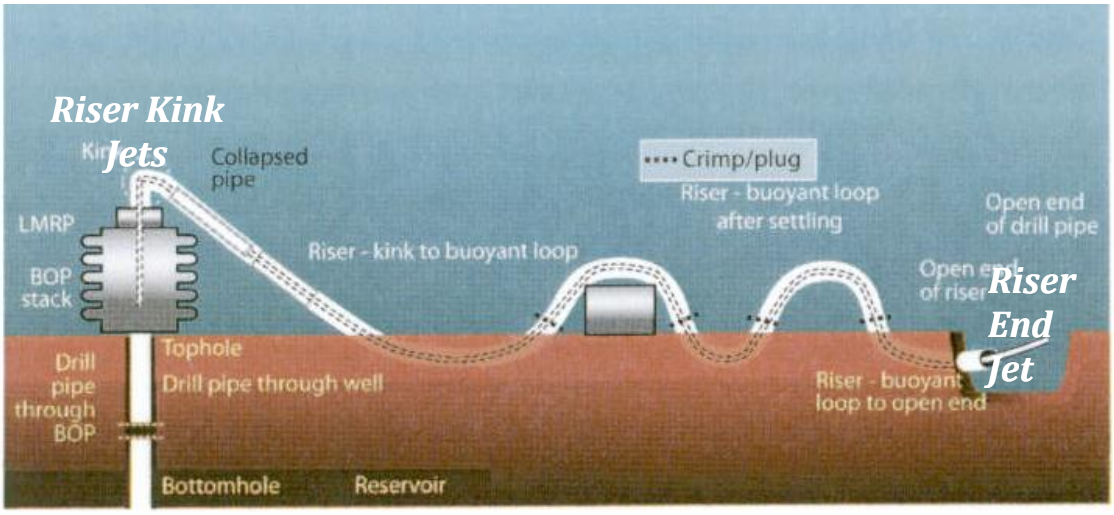

Figure 1: Schematic diagram of the BOP and riser, showing the positions of the jets analyzed in this report.

Example screenshots of jets emitting from many openings on the top side of the riser kink area above the BOP are shown below (Figs. 2 and 3). The main jet in the center of the image (J_1 in Fig. 3) is a classical, momentum driven turbulent jet with a 26 degree total divergence angle. The brown-orange color of the Riser Kink Jets suggests that the fluid is a mixture of oil and water. Entrainment of water into this turbulent jet is discussed in the section of this report on jet theory.

Figure 3 has an analysis of the complex flow patterns drawn onto the jets. This image was provided by one of the Plume Analysis Team experts, Professor Ömer Savas from the University of California at Berkeley. Because of the main jet labeled J_1 is the only jet that has an unobstructed, clear view, velocity measurements were made only for the main jet J1. Several team members made the assumption that the other jets produce (in total) about the same flow rate as the J_1 jet. So we assumed the total oil flow rate from the Riser Kink Jets could be represented by twice the value estimated for the J_1 jet.

Figure 2: Several jets emitting from openings in the Riser Kink area above the BOP.

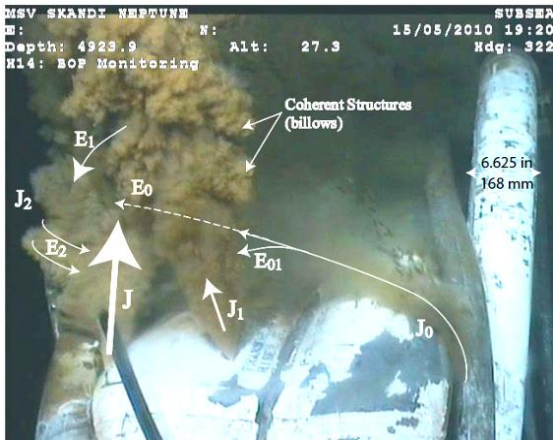

Figure 3: Schematic of complicated flow patterns of several jets emitting from the Riser Kink. Courtesy of Professor Ömer Savas of U.C. Berkeley.

Screenshots of a BP video of the Riser End Jet are shown below (Figs. 4 and 5). The screenshot in Figure 4 was captured when the jet was dominated by oil (dark), whereas the screenshot in Figure 5 was captured when the Riser End Jet was dominated by gas. The goal of this analysis is to estimate total average oil leak rate, so velocity was measured only on images showing oil-dominated jets.

Figure 4: Riser End Jet when oil dominates the flow.

Figure 5: Riser End Jet when gas dominates the flow.

As mentioned above, NETL employed a multiple analysis approach. Three separate analyses by three different teams used different approaches to understand these oil leak jets. The following sections discuss each of three separate analysis approaches.

ANALYSIS APPROACH 1: Measurement of Jet Velocity by Manual Feature Tracking Velocimetry

Several videos taken by BP Remotely Operated Vehicles (ROVs) of the oil leak jets were used in this analysis. The videos were selected by BP and delivered to Bill Lehr of NOAA, the Plume Team Leader. The first major assumption made in this analysis is that the short video clips provided by BP, less than five hours in total, are statistically representative of the total average oil leak flow rate over the period of time from the start of the oil leak until the riser was cut below the kink for the Top Hat procedure. The members of the Plume Analysis Team using PIV were able to analyze less than 30 minutes of the videos to measure jet velocities. Based on experience with other sea-floor oil leaks, one expert on the Plume Analysis Team, Dr. Ira Leifer (University of California at Santa Barbara Marine Science Institute) indicated that oil leaks similar to the BP Horizon leak can vary significantly with time. Hence, Dr. Leifer recommended that estimates of the total average oil leak rate be accompanied by a statement that the actual total average flow rate could be as low as one half of the estimate and as high as twice the estimate because of natural variability in oil leak rates from deep wells below the sea floor..

The file name of the video clip used by NETL to measure jet velocities for the Riser Kink Jets is:

- H14_BOP_Plume_May_15_1920-1945.asf

Two files were used to measure jet velocities for the Riser End Jet:

- 20100514224719234@H14_Ch1-ProRes.mov
- 20100514221717125@H14_Ch1-H264h_ProRes.mov

For the Plume Team's Phase 1 estimate of minimum oil leak rate, NETL used its proprietary PIV software to track jet features in order to measure jet velocity. In this Phase 2 analysis, more time was devoted to studying the image features of the jets in order to test the accuracy of automatic PIV analysis. The video from BP was highly compressed (at a compression level of 75% using Apple Pro Res codec), resulting in compression artifacts (appearing as 8x8 pixel blocks) that hindered automatic PIV analysis. A careful study of the PIV data revealed that there was a significant level of error in the automatic tracking of jet features. The NETL analysis relied instead on manual recognition and tracking of jet features in the compressed video in order to avoid introducing another source of uncertainty. Prior to analysis, the videos were enhanced using the National Institute of Health (NIH) ImageJ software. Following image enhancement, jet features were tracked, recorded, and analyzed using the MTrackJ plugin tool of ImageJ . Although this approach was more time intensive, it was found to give a more reliable evaluation of jet features on both the Riser Kink Jet and the Riser End Jet.

Turbulent jets generate turbulent eddies that propagate along the jet in proportion to jet velocity. However, the turbulent eddies sometimes slow and flow radially outward tangential to the jet's streamwise centerline. Large structures in turbulent jets can also exhibit reverse spin due to the motion of vortices. It was noticed that turbulent eddies and flow structures propagating with jet velocity exhibited image blur because of the 1/25 second exposure time of the video camera in the ROV. It was also found that the front and back edges of some turbulent structures were distinct and had high contrast with the video background. Therefore, preference was given to tracking turbulent structures that exhibited image motion blur and had distinct upstream or downstream boundaries as being most representative to true jet velocity. Methane hydrates appearing as bright white dots on the dark surface of the oil-dominated jets provided another feature with which to track and measure jet velocity.

Manual feature tracking produced the jet velocity measurements at the jet periphery for both the Riser Kink Jet and the Riser End Jet. The Riser Kink has several jets, but only one of the jets has a clear, unobstructed view. Figure 6 shows the feature tracks manually identified in the main jet of the Riser Kink Jet. In Figure 6, color is used only to make the tracks easier to see. Color does not indicate magnitude of velocity. Velocities were measured only for the unobstructed main jet. An average velocity of 1.7 m/s was measured at a distance of 0.6 meters downstream from the jet exit. The jet exit diameter was measured to be 0.75 inches.

Figure 6: Feature tracks manually identified in the main jet of the Riser Kink Jet. (The trajectories of features shown in this image were pseudocolored randomly so they are easier to see. The colors do not represent velocity magnitude)

For the Riser End Jet, velocities were measured at two locations on the bottom edge of the jet (Fig. 8). One location was 0.8 meters downstream from the jet exit and the other location was further downstream at 1.5 meters from the jet exit. Jet velocity was measured only when the jet was dark in color and assumed to be all oil. Gas velocities were not measured in this analysis.

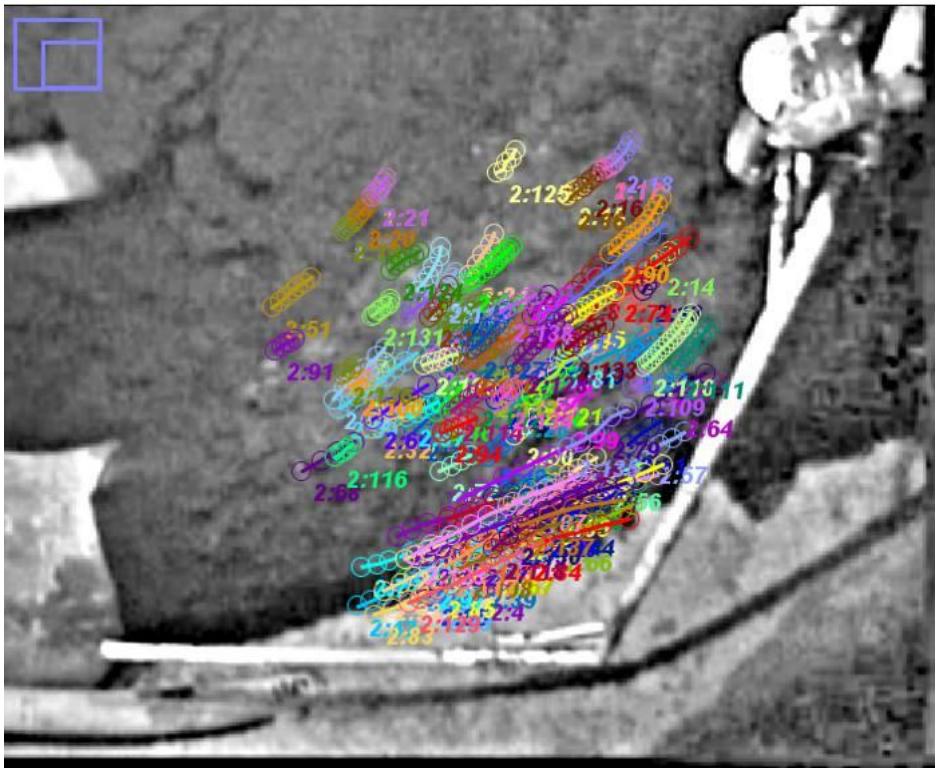

Figure 7: Feature tracks manually identified in the main jet of the Riser End Jet.

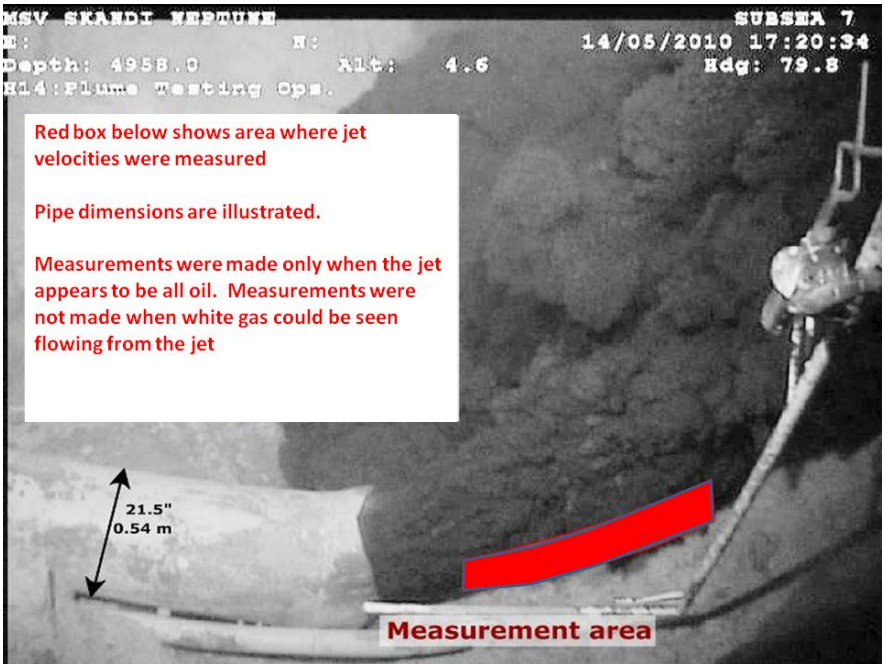

Figure 8: An enhanced view of the bottom edge of the Riser End Jet.

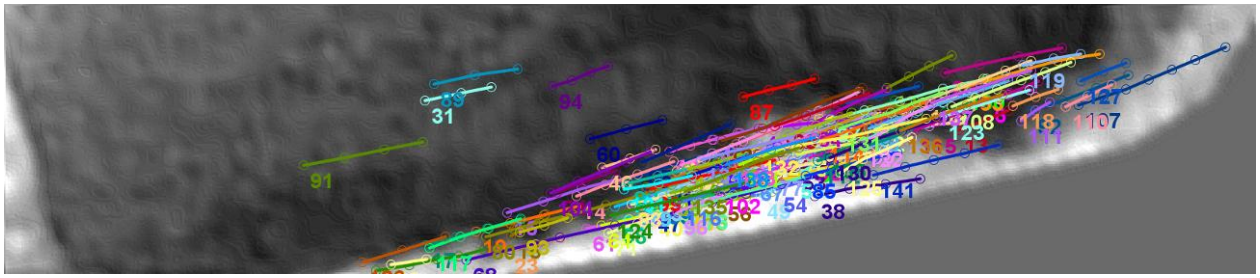

Figure 9: An enhanced view of the bottom edge of the Riser End Jet showing tracked features.

Figure 9 shows a magnified and enhanced view of the bottom edge of the jet. The light area on the far left of the image is the end of the riser. It was found that the shadow of the jet on the bright sea floor just below the jet provided a very high contrast image of the jet boundary. This allowed more accurate recognition and tracking of jet features. More than 500 velocity measurements were extracted from this video over a period of 250 seconds.

A total average velocity of 0.8 m/s was measured at the location 0.8 meters downstream of the Riser End Jet along the bottom edge of the jet. A total average velocity of 0.7 m/s was measured at the location centered at 1.5 meters downstream of the Riser End Jet exit.

Calculation of Total Oil Leak Rate using FTV Velocity Measurements

Total average oil leak rate from the Riser End Jet: As discussed above, manual FTV measured a total average velocity of 0.8 m/s at an average distance of 0.8 meters downstream of the exit of the Riser End Jet. Following the same analysis and nomenclature for determining total average oil leak rate as defined by Plume Team member Professor Ömer of U.C. Berkeley, the total average oil leak rate from the Riser End Jet can be calculated as:

$$\dot{Q}_{oil} = \overline{V_{PIV} A_{PIV}} X_{oil} \varepsilon_{oil} \pm U_{\dot{Q}_{oil}}$$

where $\overline{V}_{PIV}$ is the total average velocity of the oil jet, $\overline{A}_{FTV}$ is the average cross-sectional area of the jet at the location where the PIV/FTV measurement was made, $\overline{X}_{oil}$ is the fraction of gas dissolved in the oil, $\bar{\varepsilon}_{oil}$ is the intermittency factor (fraction of time oil is flowing out the Riser End Jet), and $U_{\dot{Q}_{oil}}$ is the measurement uncertainty of the FTV technique.

It is assumed that the effect of the ROV being at a small angle to the orthogonal of the jet is negligible. The assumption of the Plume Team that all gas has separated out of the oil during transit between the BOP and Riser End Jet is adopted here so that so $\overline{X}_{oil}$ =1. Other Plume Team members have measured the intermittency factor to be $\bar{\varepsilon}_{oil}$ = 0.5 indicating that all oil was flowing out of the Riser End Jet for 50% of the time. The rest of the time gas was flowing out the Riser End Jet.

Other Plume Team members doing PIV analysis have estimated the measurement uncertainty of PIV to be ±5%. However, because of the poor resolution and quality of the video samples provided to the Plume Team, this analysis here assumes measurement uncertainty is

higher, in the range of ±10%. Applying this assumed uncertainty and the values of $\bar{X}_{oil}$ =1 and $\bar{\varepsilon}_{oil}$ =0.5, the equation for average oil flow rate out of the Riser End Jet becomes

$$\dot{Q}_{oil} = \overline{V_{PIV} A_{PIV}} 0.5 \pm 0.1 \dot{Q}_{oil}$$

The cross sectional area of the jet is given by

$$A_{PIV} = \pi d_{jet}^2 / 4$$

The jet diameter at the center location of the FTV measurements was measured directly from the BP video to be approximately 0.6 meters, yielding a cross sectional area of 0.28 m^2. With a value of $\bar{V}_{PIV}$ = 0.8 meters/second from FTV and assuming that the velocity is the same across the diameter of the jet at this location, the total oil flow rate is

$$\dot{Q}_{oil} = \overline{0.8 * 0.28} * 0.5 = 0.11 \text{ m}^3/\text{s} \pm 0.011 \text{ m}^3/\text{s}$$

To convert to barrels per day, conversion factors of 264.2 gallons/sec per m^3/s and 42 gallons per barrel of crude oil are applied. Therefore, the total average oil leak rate is calculated to be **60,000 barrels per day ± 6,000 barrel per day of oil for the Riser End Jet using Feature Tracking Velocimetry.**

Total average oil leak rate from the Riser Kink Jets: Using a similar analysis for the Riser Kink Jets and assuming that the jet is well mixed, steady and is 29% oil (of $\bar{X}_{oil}$ = 0.29 and $\bar{\varepsilon}_{oil}$ =1.0), the equation for total average oil flow rate becomes:

$$\dot{Q}_{oil} = \overline{V_{PIV} A_{PIV}} 0.29 \pm 0.1 \dot{Q}_{oil}$$

The diameter of the Riser Kink Jet at a distance of 0.6 meters downstream of the jet exit is measured to be approximately 0.25 meters. This gives a cross sectional area of

$$A_{PIV} = \frac{\pi}{4} d_{jet}^2 = 3.1415/4 * (0.25\text{m})^2 = 0.05 \text{ m}^2$$

The total average oil leak rate from jet J_1 of the Riser Kink Jets is then calculated as:

$$\dot{Q}_{oil} = \overline{1.7 * 0.053} * 0.29 \pm 0.1 \dot{Q}_{oil} = 0.023 \text{ m}^3/\text{s} \pm 0.0023 \text{ m}^3/\text{s}$$

Adopting the assumption of Professor Savas and other Plume Team members that the combined flow rate of other jets of the Riser Kink Jets is twice that of jet J_1, **the total average oil flow rate is 25,000 barrels per day ± 2,500 barrel per day of oil for the Riser Kink Jet using Feature Tracking Velocimetry**.

Combined total average oil leak rate:

Combining the flow rates of the Riser Kink Jets and the Riser End Jet, this analysis produces a total average oil leak rate of 85,000 barrels per day ± 8,500 barrel per day of oil from Riser End Jet and Riser Kink Jet using Feature Tracking Velocimetry .

Additional Assumptions:

It should be noted that this analysis does not include the effect of natural variability of the discharge rate from oil wells. According to one Plume Team members with expertise and experience with similar oil wells on the ocean floor, natural variability is significant and could change the estimate by a factor of 0.5 to 2.0.

Rather than guess the radial velocity profile in this FTV analysis, a better approach is to use established theory of turbulent jets to determine radial velocity profile. This is the subject of the next section.

ANALYSIS APPROACH 2: Application of Turbulent Jet Theory

This analysis of the oil leak rates is analytical in nature. The vertical Riser Kink Jets and the horizontal Riser End Jet are analyzed by different methods. The Riser End Jet analysis is meant to be coupled to the feature tracking measurements described in the previous section of this report. The analysis of the main J_1 Riser Kink Jet was done as a stand-alone analysis.

General values used throughout the analyses are:

- Density of seawater, ρ_{water} = 1028 kg/m^3 (from: Bullard, Physical properties of sea water, http://www.kayelaby.npl.co.uk/general_physics/2_7/2_7_9.html)
- Density of oil at discharge, ρ_{oil} = 689 kg/m^3
- Density of gas at discharge, ρ_{gas} = 136 kg/m^3

It is emphasized that the jet exit diameter is a critical part of this analysis because the *square* of the diameter will control the volume flow for a given pressure drop. This is further confounded by the recognition that the physical hole is likely to be distorted since it was formed during the pipe bending. The effective diameter used above is consistent with image analysis. As seen later, a range of jet diameters is considered to bound this flow.

Theoretical Analysis of Riser Kink Jet J1

This jet is assumed to behave as a classical axisymmetric momentum-dominated turbulent jet. These types of jets generally behave very predictably with regard to mass entrainment, jet spreading, velocity profiles, and the like. For a given measurement of velocity at a location on the periphery of the jet, two things need to be known in order to make a reasonable estimate of the total oil flow rate: the amount of oil in the combined oil + gas + water jet at that location, and the jet velocity profile. These are addressed separately below.

For both of these analyses, the geometry and conditions assumed at the exit of the jet are:

- The jet exit is a circular hole, d_0 = 0.75" ± 0.25" in diameter, based on image analysis.
- The ratio of the volume of oil to the volume of oil + gas at the jet exit, $X_{o,exit}$ = 0.5 ± 0.1, based on intermittency analyses from FRTG team members in the initial report. This gives a nominal density of combined oil + gas exiting the jet, $\underline{\rho_{exit}}$ = 412.5 ± 55.3 kg/m^3

Water Entrainment Scaling: The spreading of the oil/gas jet as it exits the hole in the riser kink is due in large part to entrainment of water into the jet. The theory used here does not account for the immiscible nature of the fluids; this would need to be included in a more detailed analysis. For momentum-dominated jets, this entrainment follows well-studied scaling laws that depend on the fluid density difference and distance downstream from the jet exit. Near to the exit of the jet, entrainment is nonlinear until the flow achieves self-similar scaling, after which mass entrainment is linear with downstream distance. The near-field region for an orifice can be characterized as the region less than 15 jet exit diameters downstream (x/d_0 < 15), while for other, better studied geometries such as the long pipe, this region can extend to 30 or more exit diameters from the jet

exit (Nathan et al, 2006). Since velocity measurements were not made in this region, we will assume a constant mass entrainment, $C_{e,15}$, up to this location, x/d_0 = 15. The mass flow rate of entrained water, m_{water}, as a function of the mass flow rate of the jet exit fluid, m_{exit}, is expressed as:

$$m_{water} / m_{exit} = C_{e,15}(\rho_{water}/\rho_{exit})^{1/2}$$

Values for $C_{e,15}$ are taken from the literature. The ideal situation of a jet issuing from a sharp-edged orifice in a flat plate cannot be found in the literature, however, Hill (1972) found $C_{e,15}$ = 4 for a contoured nozzle in a flat plate, while Mi et al (2007) found $C_{e,15}$ = 3.4 for a sharp-edged orifice in a small plate (d_0/d_{plate} = 0.38). Using the best available data, we will assume an average value of $C_{e,15}$ = 3.7 ± 0.3. Based on these numbers, the mass of jet fluid (oil + gas) 15 jet diameters downstream of the jet exit is only 14.5% of the total jet mass, the rest is water.

In the far-field, beyond x/d_0 = 15, the local mass entrainment rate is proportional to distance per:

$$dm_{water}/dx = C_{el}*m_{exit}/d_0*(\rho_{water}/\rho_{exit})^{1/2}$$

where C_{el} is the local entrainment rate, chosen to be C_{el} = 0.32 after Ricou and Spalding (1961) and Hill (1972), who both measured entrainment in a contoured nozzle from a flat plate. This value is consistent with the results of Mi et al (2007) and several others as well, and carries little uncertainty. Integrating this equation from x/d_0 = 15 on downstream and adding the effect of near field entrainment yields:

$$\frac{m_{water}}{m_{exit}} = \left(\frac{\rho_{water}}{\rho_{exit}}\right)^{1/2}\left[C_{e,15} + C_{el}\left(\frac{x}{d_0} - 15\right)\right]$$

Converting this to a volumetric basis and accounting for the ratio of oil to gas in the jet exit yields the following equation for the volume fraction of oil in the jet at a downstream location x/d_0 > 15 of:

$$X_{oil,jet}(x) = \frac{V_{oil}}{V_{oil} + V_{gas} + V_{water}} = \frac{X_{oil,exit}}{1 + \left(\frac{\rho_{exit}}{\rho_{water}}\right)^{1/2}\left[C_{e,15} + C_{el}\left(\frac{x}{d_0} - 15\right)\right]}$$

Using this equation, the oil volume fraction at the location of the FTV measurements above (x = 0.6 m) is just 7.5%, the gas volume fraction is also 7.5%, and the remaining 85% is entrained water. As this analysis shows, lack of proper accounting for water entrainment can lead to an order of magnitude error in the estimate of the oil leak rate based on PIV measurements at a particular downstream location.

<u>*Velocity Profile Scaling*</u>: In momentum-dominated jets, the far-field (x/d_0 > 15, for our purposes) axial jet velocity profile, $U(r)$, is known to follow a Gaussian profile:

$$U(r) = U_{cl}e^{-(r/\delta)^2 ln(2)}$$

where U_{cl} is the centerline velocity, r is the radial distance from the centerline, and δ is the half-width of the jet, defined to be the location where the centerline velocity falls to half its value. The jet half width increases linearly with x in the far-field, so the jet spreading rate is typically

measured as δ/x as a constant. Incorporating this jet spreading rate, the jet centerline velocity can be estimated from a velocity measurement, U_{PIV}, at a radial location, R, and a downstream axial location, X, as:

$$U_{cl} = U_{PIV} e^{(R/X)^2 (x/\delta)^2 ln(2)}$$

The velocity measurement occurs at the outer edge of the jet. The velocity profile in the interior of the jet can be accounted for with the expression for $U(r)$ above, and the total volumetric flow in the interior of the jet, Q_{jet}, can be determined by integrating that expression from the centerline to the radial point of measurement, R. Utilizing the expression for U_{cl} above, this integration yields:

$$Q_{jet} = \frac{\pi X^2}{ln(2)} \left(\frac{\delta}{x}\right)^2 U_{PIV} \left[e^{(R/X)^2 (x/\delta)^2 ln(2)} - 1\right]$$

This value is very sensitive to uncertainties in the values for R and X, as determined from the feature tracking measurements described in the previous section, and in particular to δ/x, which must be determined from the literature. Most values for δ/x in the literature are for jets from long pipes or contracting nozzles, though jet spreading rates from these configurations can vary significantly from those in sharp-edges orifices (Mi et al., 2001). Common values of jet spreading rate for contracting nozzles range from $\delta/x \approx 0.096$ (Quinn, 2006) to 0.113 (Richards and Pitts, 1993). For sharp-edged orifices, this rate ranges from $\delta/x \approx 0.098$ (Quinn, 2006) to 0.182 (Mi et al, 2001). Most of these values are for jets that do not issue from a flat wall, but rather the open atmosphere, where spreading rates can be 20% higher than for jets issuing from a wall (Abdel-Rahman et al, 1997). These values are independent of the density differences across the jet. As a conservative estimate, the value of 0.182 is chosen for these analyses, though from the above references it should be noted that very significant uncertainty is attached to this number. In particular, lower spreading rates can yield large and often unphysical jet centerline velocities, depending on the values used for X and R. Further investigation into the proper jet spreading rate is warranted in continued analysis of this problem, and may also turn out to be affected by the immiscibility of the two fluids.

The volume flow rate of oil out of the kink jet, based on a measurement of total average velocity at a particular jet location, can be made by multiplying the above expressions for Q_{jet} and $X_{oil,jet}$ together. In this manner, multiple estimates of the jet leak rate can be made from the plethora of averaged velocity measurements and locations attained, and statistics of probable maximum and minimum flow rates can be made. Uncertainties in d_o, $X_{o,exit}$, and the above constants from the literature should also be taken into account while calculating these estimated leak rates from the kink jet.

FTV measurements yield an average jet velocity of U_{PIV} = 1.7 m/s with an uncertainty of 10% at the jet periphery, a distance of X = 0.6 meters downstream of the jet exit. The average jet spread half-angle is measured to be 12.5° on the video, though this is roughly the location of the center of the turbulent vortices as they propagate downstream. The FTV measurements track the outer surfaces of these structures, which appear at a maximum spread angle of 15.5° for the

largest structures. An appropriate average spread angle for these structures is taken to be 14° ± 1.5°, to account for the tracking of the outer surfaces of the largest to the smallest structures in the shear layer. The peripheral FTV measurement location at an axial location of 0.6 m is therefore estimated to be at a radius of R = 0.15 ± 0.02 m. Applying these numbers to the theoretical analysis of the Riser Kink Jet J_1 yields a best estimate for the total average oil flow rate of 10,000 barrels per day of oil for the Riser Kink Jet using Turbulent Jet Theory.

The largest sources of uncertainty in this analysis come from the estimation of the jet exit diameter at 0.75" ± 0.25", the volume ratio of oil to (oil + gas) at the jet exit of 0.5 ± 0.1, the FTV measurement uncertainty of 10%, and the measurement uncertainty of the radius, R, at about 12%. Since this last uncertainty appears in the exponential in the above equation for Q_{jet}, the impact on this measurement on the jet velocity measurement is very large – this uncertainty alone yields a range of 6700 to 15,000 bbl/day total oil flow rate from the jet. The remaining uncertainties combined using the sum of squares method roughly yield a 40% uncertainty, independent of the uncertainty of the R measurement location, yielding a range of 6000 to 14,000 bbl/day leak rate. If the other jets are assumed to have a flow rate of the same amount as the main jet, J_1, (as discussed above), then the **total average oil flow rate from all Riser Kink Jets doubles to 12,000 to 28,000 bpd, for Turbulent Jet Theory, independent of the uncertainty in *R***. Clearly this technique will require substantial refinement and reduction of uncertainties if another estimate of the kink jet flow rates is required. However, having accounted for water entrainment and the jet velocity profile, uncertainties in this measurement technique should be smaller than those that do not include these effects.

These estimates are very sensitive to the assumptions used in the analysis approach as well as the precision of evaluating the edge-velocity from the FTV measurement. As an independent check on the analysis, a much simpler calculation was made based on a knowledge of the pressure in the riser kink versus the ambient sea pressure. This approach uses the orifice equation that is found in handbooks such as Marks Standard Handbook for Mechanical Engineering, Eighth Ed. (1978) McGraw Hill, pp 61-64:

$$\text{Volume flow} = K^*\text{Area}^* (2^*\Delta P/\rho)^{1/2}$$

The flow coefficient K is estimated here as 0.6, which is typical of an orifice. The pressure drop is taken from information provided to the analysis team and is 400 psi between the interior of the riser and the sea environment. Assuming the same properties for density as used above, the calculated flow for the range of jet diameters (0.75+/- 0.25 inches) is:

0.5 inch	0.75 inch	1 inch
1940 bbl/day	4360 bbl/day	7760 bbl/day

This analysis suggests the estimates from the FTV and jet profile are substantially larger than an orifice flow prediction. This discrepancy may arise from the range of uncertain parameters that exist in the jet analysis and FTV measurement. Notably, the FTV measures come from a range of observed velocities that are statistically averaged, to provide an edge velocity. This process can lead to an *overestimation* of the flow. This is because the actual velocity profile may take on a shape that is not Gaussian, resulting in a lower flow rate than predicted from the FTV measurement and jet analysis. Thus, the FTV and jet analysis should be viewed as a *maximum*

flow estimate from the J1 Riser Kinks, subject to the assumptions already presented. Likewise, the flows from the other jets in the kink area have not been analyzed due to their position, but appear to have similar orders of magnitude.

Theoretical Analysis of the Riser End Jet

Analysis of this jet involves buoyant jet flow from an inclined pipe similar to Peters and Gottgens (1991). They attained a set of differential equations for the jet trajectory in the presence of no ambient flow, which was analytically solved by Gore and Jian (1993) to yield an explicit jet trajectory. An attempt was made to match these theoretical studies to experimental observations of hydrogen and helium leaks into air by Kim et al (2009), with reasonable success. The basic geometry and nomenclature for the situation under study is shown in Fig. 10, taken from Kim et al (2009):

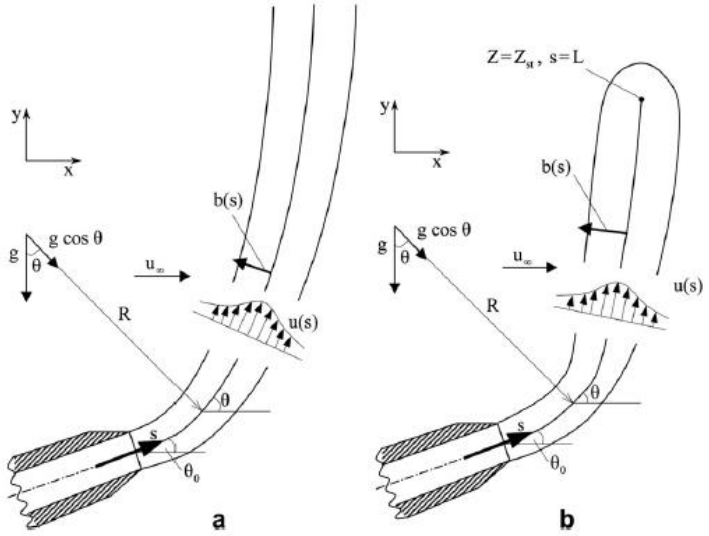

Figure 10: Schematic geometry and nomenclature used in the analysis of the Riser End Jet (from Kim et al, 2009).

In this analysis, s is the curvilinear coordinate of the jet centerline, b is roughly the jet half-width, and θ is the jet angle relative to the horizontal. The jet angle can be expressed as:

$$\tan\theta = \tan\theta_0 + \frac{1}{\sqrt{\rho_0/\rho_\infty}\cos\theta_0 Fr^*}\left[\left(\frac{s}{d}\right) + 2\beta\left(\frac{s}{d}\right)^2 + \frac{4}{3}\beta^2\left(\frac{s}{d}\right)^3\right]$$

where θ_0 is the initial jet angle relative to the horizontal, ρ_0 is the jet exit density, here assumed to be entirely oil ($\rho_0 = \rho_{oil}$), ρ_∞ is the ambient density, here equal to water ($\rho_\infty = \rho_{water}$), and d is the jet exit diameter, assumed here to be 0.42 m. The term Fr^* is a modified Froude number:

$$Fr^* = \frac{u_0^2}{gd}\sqrt{\rho_0/\rho_\infty}\,\frac{\rho_\infty}{\alpha(\rho_\infty - \rho_{st})}$$

where u_0 is the bulk jet exit velocity, g is the gravitational constant, α is a fitting parameter, assumed by Peters and Gottgens to be equal to unity (α = 1), and ρ_{st} is a mixed density

downstream from the jet exit at a location where the jet fluid and ambient fluid have mixed in stoichiometric proportions. One of the difficulties with this analysis is the fact that ρ_{st} has no meaning in an unreacting flow problem such as ours. In our analyses, we have chosen $\rho_{st} = \rho_{oil}$ as a reasonable approximation. Also, in the above equation, β is a jet spreading parameter such that $b = \beta s + d/2$ (Gore and Jian, 1993). This was determined in the original analyses to be $\beta = C_\beta(\rho_{st}/\rho_\infty)^{1/2}$, with a calculated value for the constant $C_\beta = 0.23$. Substitution of ρ_{st} for ρ_{oil} in this expression yields very good agreement with the observed jet spreading rate, however, the half-width b is roughly half of the centerline velocity, and not necessarily that at the edge of the jet as seen in the videos. Peters and Gottgens note that a more accepted value for the half-width of a constant-density jet is $\beta = 0.085$, though other appropriate values for the half-width could be used as well. We will conservatively choose $C_\beta = 0.104$ to yield $\beta = 0.085$ in this analysis, though larger values of C_β will certainly result in higher oil leak flow rates. This value of C_β is comparable to jet spreading rates of other studies (Richards and Pitts, 1993), and should be better representative of low velocity mixing in immiscible fluids, compared to the value $C_\beta = 0.23$. Given more time, a detailed analysis of experimental and CFD velocity profiles can be performed to significantly reduce the uncertainty attached to this value. A change in the value of C_β by 20% alters the estimation of the leak rate by only about 5% however, which is the conservative estimate of the flow rate uncertainty we'll attach to the uncertainty in C_β.

Another uncertainty in this analysis lies in the value of $\alpha = 1$, where α is used to approximate the following integral (Peters and Gottgens, 1991):

$$2\int_0^\infty (\rho_\infty - \bar{\rho}) r \, dr = b^2 \alpha \, (\rho_\infty - \rho_{st})$$

where $\bar{\rho}$ is the time averaged density. Replacing ρ_{st} with ρ_{oil} in this equation yields $\alpha = 1$ if the integral is evaluated at the jet exit, however, as $\bar{\rho}$ increases towards ρ_∞ with increasing downstream distance s and jet width b, it is expected that α would decrease under the substitution of ρ_{st} for ρ_{oil}. As a result, the jet scaling above is expected to deteriorate at appreciable distances downstream from the jet exit. The current analysis is undertaken with a value of $\alpha = 1$, however, comparison with the riser jet profile and trajectory is weighted towards the near-field region closer to the jet exit, where this relationship is still valid. Improvement in the model could be made with more accurate fits for α to experimental or CFD modeling data, however, time constraints have excluded the possibility of this analysis at this time.

Application of the above analysis to the Riser End Jet involves making an estimate of the jet exit velocity, u_0, computing the modified Froude number using the above equation, and then computing the angle θ as a function of the curvilinear coordinate, s. This relationship can then be mapped to standard horizontal and vertical coordinates, and the resulting centerline trajectory can be compared against the actual jet trajectory from the BP videos. Additionally, the upper and lower jet boundaries can be calculated from the relationship $b = \beta s + d/2$ above, using $C_\beta = 0.23$, which can also be compared to the videos. Adjustments to the initial jet angle and jet velocity are performed iteratively to attain a good match to the observed jet profile.

Figure 11a below shows the result for an initial jet angle of $\theta_0 = 12°$ and a bulk jet exit velocity of 3.1 m/s, where, as noted above, the best fit is made to the initial portion of the jet, up to

roughly 5 jet diameters downstream of the exit. The computed jet boundaries match the observed boundaries very well, and the resulting exit velocity yields a total flow rate of 232,000 barrels of oil per day with only oil flowing out of the riser. Multiplied by the intermittency factor of 0.5 to account for periodic gas flow, the estimated oil flow rate is 116,000 barrels of oil per day. Also shown in Figure 11b is a result using the image employed in the CFD analysis below.

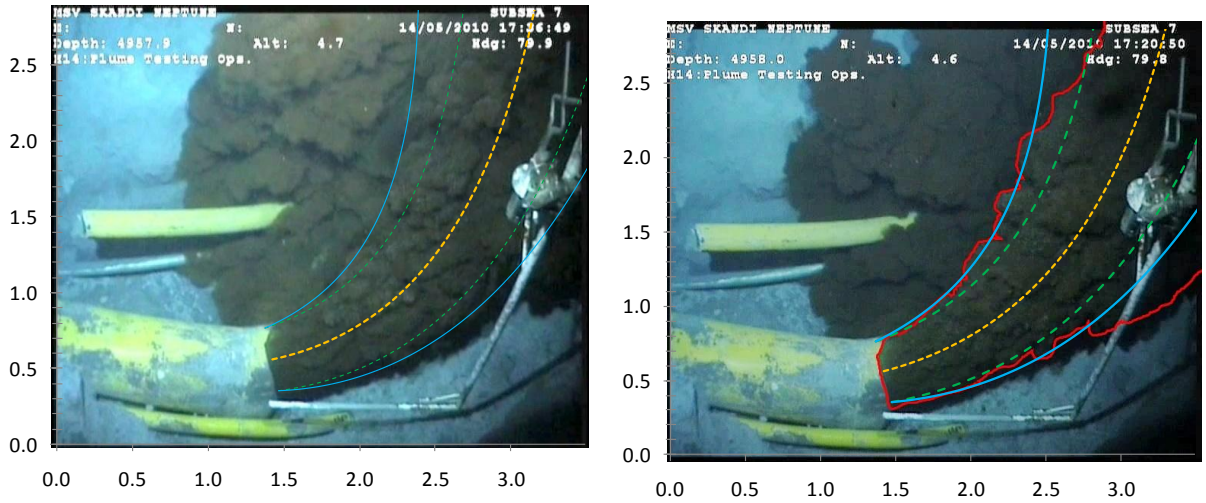

Figure 11. Jet centerline, half width, and edge profiles predicted by theoretical analysis are shown as yellow, green, and blue lines, respectively. Notice that the jet is casting a shadow on the ocean floor, so the bottom edge of the jet is slightly above the bottom edge of the dark area.

The primary assumptions made in this analysis are:

- Only oil is flowing out of the riser in the analyzed videos,
- The pipe exit is a circular hole of 16.5" diameter,
- There is no ambient flow of water in the immediate vicinity of the jet,
- The jet is unaffected by its proximity to the walls or floor of the trench in which it lies,
- The camera angle of the videos with respect to the horizontal is small,
- The analysis applies to immiscible fluids.
- The videos analyzed are representative of the average "oil-only" flow conditions exiting the pipe.
- And, as above, the fitting relationship $\alpha = 1$ applies in the near-field region of the jet.

As such, the fitting of the analytical relationships for the jet trajectory and boundaries is still somewhat subjective. Analysis of a range of u_0 and θ_0 that could be considered to produce an acceptable fit on a particular image yield an uncertainty estimate of ±25%. Further, it should be noted that "oil-only" riser flows can be observed to vary in flow rate in the videos. An accurate estimate of the true average flow rate can only be done by analyzing many jet plume images spanning several days and averaging their results, which is currently prohibitive given the time intensive nature of the task. In addition a true estimate of oil flow rates will require analysis of *all* of the video footage that has been recorded, beyond what limited footage has been supplied to date by BP. That said, we have averaged the estimated flow rates from the 6 video images we have analyzed to yield a best estimate oil leak rate of 116,00 bbl/day, and applied the standard deviation of 12% as the uncertainty on this average representing the true temporal average of the

flow rates. Combined uncertainties were determined by the sum of the squares of the individual component uncertainties, including those for C_β (5%), the trajectory matching methodology (25%), the "time" averaging of the image results (12%), and 20% uncertainty on the intermittency flow rate. As such, the analysis conducted with the approach outlined above suggests that **the total time averaged oil flow rate is in the range of 76,000 to 156,000 bbl/day of oil for the Riser End Jet using Turbulent Jet Theory**.

Combined total average oil leak rate

Combining the Approach 2 estimates for the Riser Kink Jet and the Riser End Jet yields a **best estimate total oil flow rate of 126,000 bbl/day, with a range of 82,000 to 170,000 bbl/day of oil using Turbulent Jet Theory.**

ANALYSIS APPROACH 3: Computational Fluid Dynamics Simulations of the Riser End Leak Jet

The objective of the third analysis approach was to use Computational Fluid Dynamics (CFD) to estimate the total flow rate of oil being discharged from the Riser End Jet. The approach taken is to estimate an oil flow rate from the Riser End Jet, then compare the size, shape and trajectory of the simulated oil plume with the size, shape and trajectory of the oil jets seen in videos provided by BP of the Riser End Jet.

For this study, the Volume of Fluid (VOF) multiphase model, available in the commercial CFD software ANSYS FLUENT was selected. For this analysis, it is assumed that the jet fluid is entirely oil with no dissolved natural gas. Therefore, the two phases under consideration are oil and sea water. Figure 12 shows the computational domain. Oil flows through the last 8.382 m of the riser and discharges into a 16.76 m by 8.98 m by 17.77 m volume filled with sea water.

Given the time frame available to perform the simulations, it was not possible to optimize the computational grid. A reasonable 'first case' course mesh was employed that insured that the computations could be performed in the allotted time.

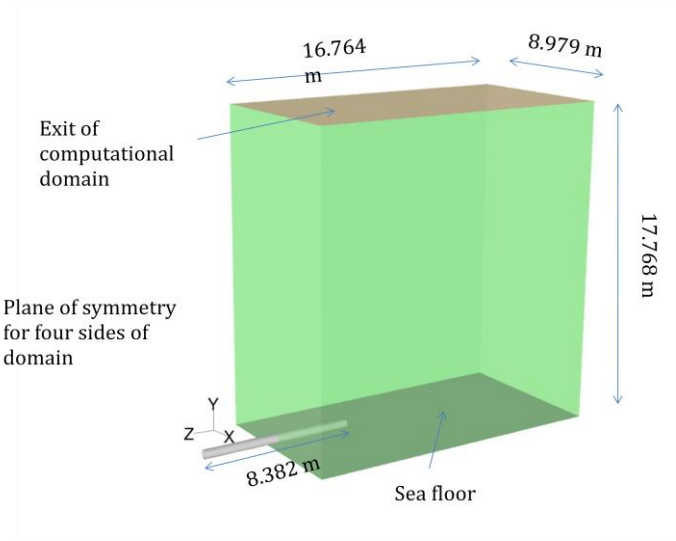

Figure 12. Dimensions of the computational domain.

The entire domain is at the temperature and pressure measured at a depth of 5000 ft in sea water. The input conditions to the model are:

Riser inner diameter = 19.5 in Riser diameter constricted (at exit) = 16.5 in Ambient pressure = 2248 psi Sea water density = 1028 kg/m^3 Sea water temperature = 4 ^{o}C Sea water viscosity = 1.88E-03 Pa	Oil temperature = 110 ^{o}F Oil density = 688.8 kg/m^3 Oil viscosity = 0.00053 Pa-s Oil surface tension = 0.0167 N/m

The oil viscosity used in the simulations was that estimated at the well bottom hole, based on BP measurements. Due to the large pressure drop from there to the Riser End exit, a significant

fraction of the dissolved methane is released resulting in the observed slugging phenomena. As a result, the viscosity of the liquid oil increases by about a factor of two. This should not significantly affect these preliminary CFD calculations.

Since the orientation of the broken riser with respect to the sea floor is not easily measured from the videos provided by BP (because the ROV's are floating at an unmeasured orientation), in the simulation, it is assumed that the broken riser lies parallel to the sea floor at a distance of 18 inches above the sea floor. In the CFD model, the entrance to the computational domain (8.382m within the pipe) was assumed to be a mass flow rate inlet (oil flow rate specified). At the exit of the computational domain is assumed to be a pressure outlet with an absolute pressure of 2248 psi (ambient pressure). A symmetry boundary condition is selected for the four planes surrounding the computational domain. A close up view of the exit of the broken riser can be seen in Figure 13.

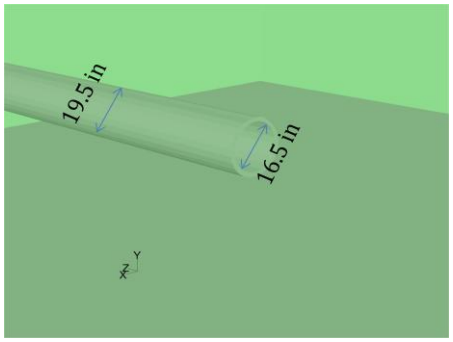

Figure 13. A close-up view of the exit plane of the broken riser.

A series of simulations were conducted at oil flow rates of 19,000 bpd, 35,000 bpd, 75,000 bpd and 85,000 bpd. Figure 14141414 shows the flow composition inside the broken riser at various oil flow rates simulated. It's clear that there is considerable amount of sea water in the riser at flow rates of 19,000 bpd and 35,000 bpd. A close inspection of the videos of the spill indicates there is no flow of sea water upstream into the broken riser, although this visual observation does not rule out a small amount of seawater flowing upstream. No attempt was made to assess the minimum level of upstream sea water that could be observed from the videos. Based on this observation, it was concluded that flow rates of 19,000 bpd and 35,000 bpd of oil are not sufficient to prevent the sea water from moving upstream into the riser.

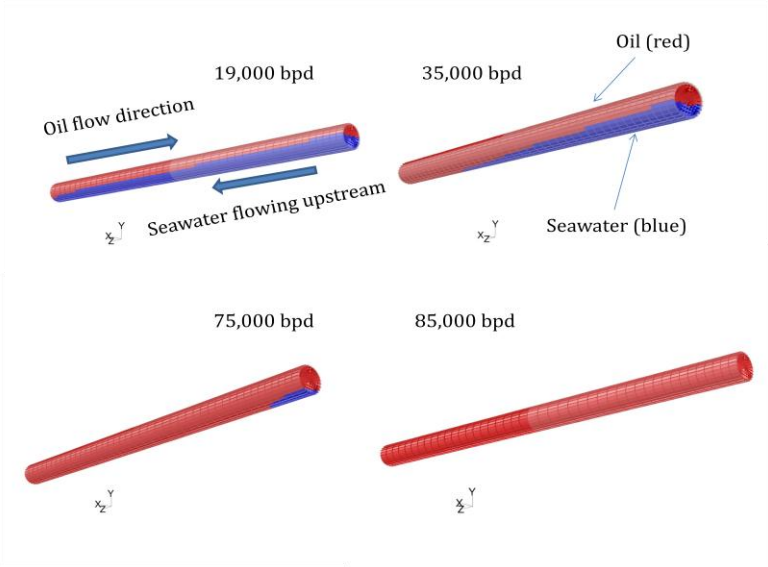

Figure 14 . Oil and seawater flow inside the broken riser at an oil flow rate of 19,000 bpd, 35,000 bpd, 75,000 bpd and 85,000 bpd.

As seen in Figure 14, there is small amount of sea water upstream in the riser at 75,000 bpd and no sea water is present upstream in the riser at 85,000 bpd. At a flow rate of about 75,000 bpd of oil,, the amount of sea water flowing into the riser is assumed to be negligible. Additional two phase simulations with the VOF model were conducted to determine how much more the oil flow rate has to increase in order to produce a jet simulation that is similar to the Riser End Jet seen in videos provided by BP.

Figure 15 shows the simulated plume shape and penetration (simulation shown in green) compared to actual plume shape and penetration (image data shown in red) at four different oil flow rate: 19,000 bpd, 35,000 bpd, 75,000 bpd and 100,000 bpd. The red outline from image data was created by visual observation of plume color intensity. The green outline from the simulation denotes a contour of oil volume fraction of 0.01 (i.e. 1% oil by volume). Since the riser was assumed to lay parallel to the ocean floor in the CFD simulations, the simulated plume at oil flow rate of 100,000 bpd was overlaid on top of the actual plume, such that the simulated jet centerline and the actual jet centerline were visually on top of each other. The same riser orientation, as in the case of 100,000 bpd, was used for oil flow rates of 19,000, 35,000 and 75,000 bpd in Figure 15. As seen in Figure 15, streamwise (normal to the jet exit) oil jet penetration into sea water and the size of the oil plume for flow rate of 100,000 bpd agrees more favorably to the actual plume streamwise penetration and size, than the simulated plume at oil flow rate of 75,000 bpd.

19,000 bpd 35,000 bpd

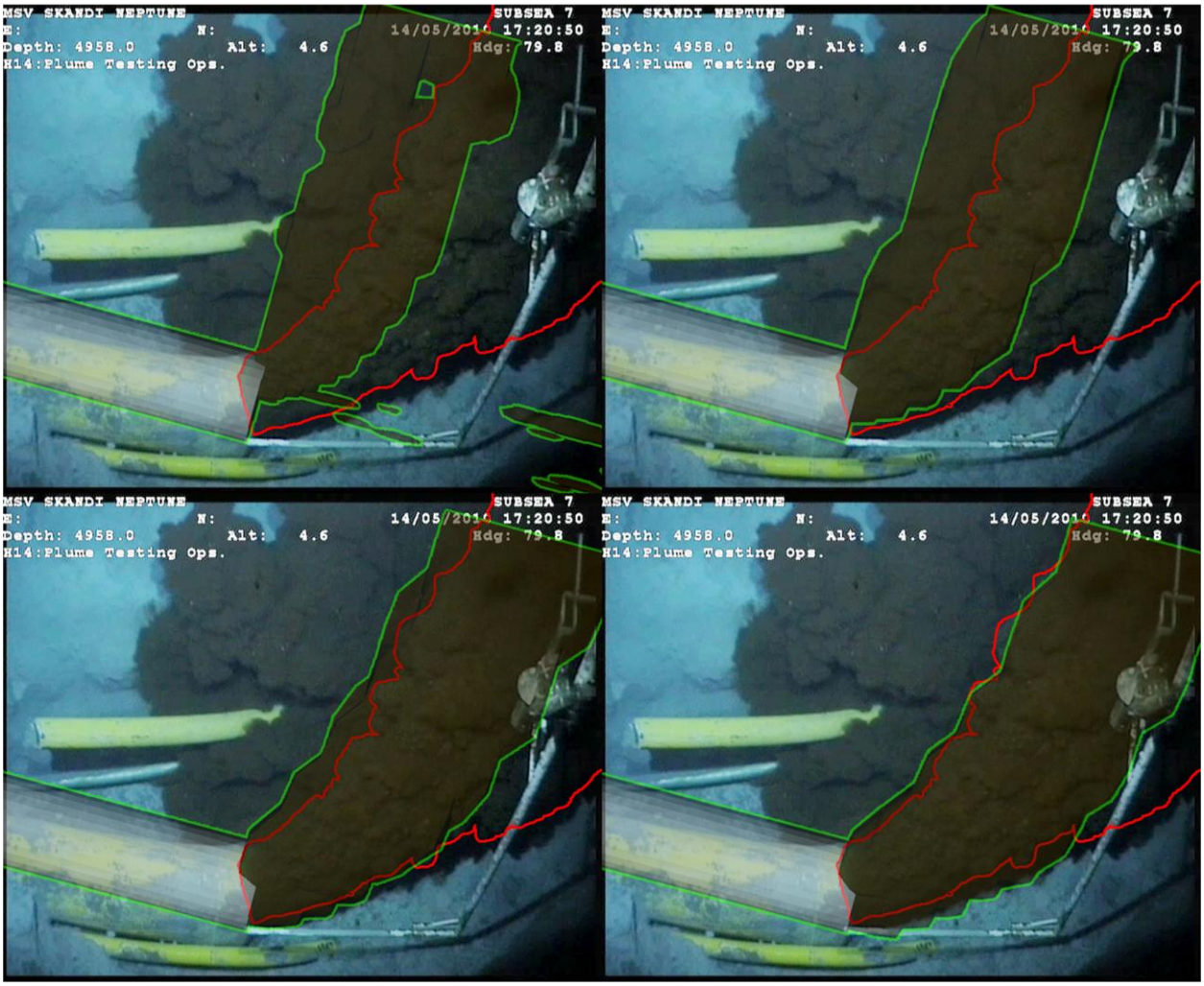

75,000 bpd 100,000 bpd

Figure 15. Comparisons of simulated oil plume size (green) with the actual plume size (red), at different oil flow rates.

As pointed out earlier, this simulation considers oil flow only. The intermittent change between total gas flow and total oil flow caused by the slugging behavior in the riser section was not modeled.

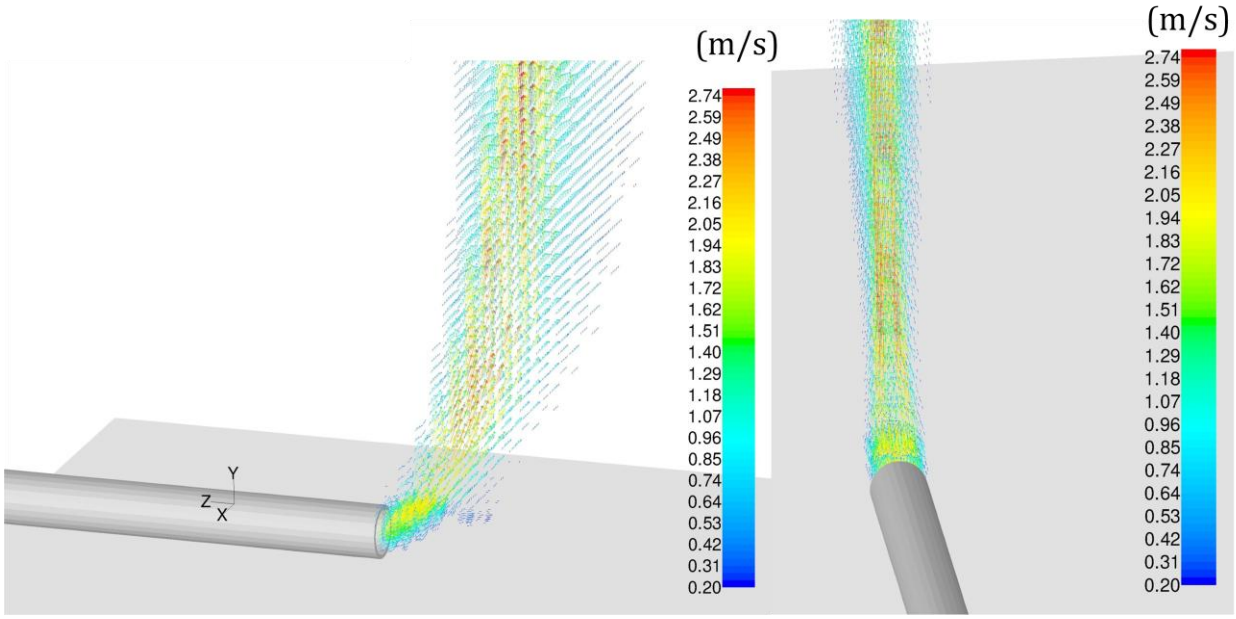

Figure 16. Contours of oil plume velocity downstream of the exit of broken riser at oil flow rate of 100,000 bpd.

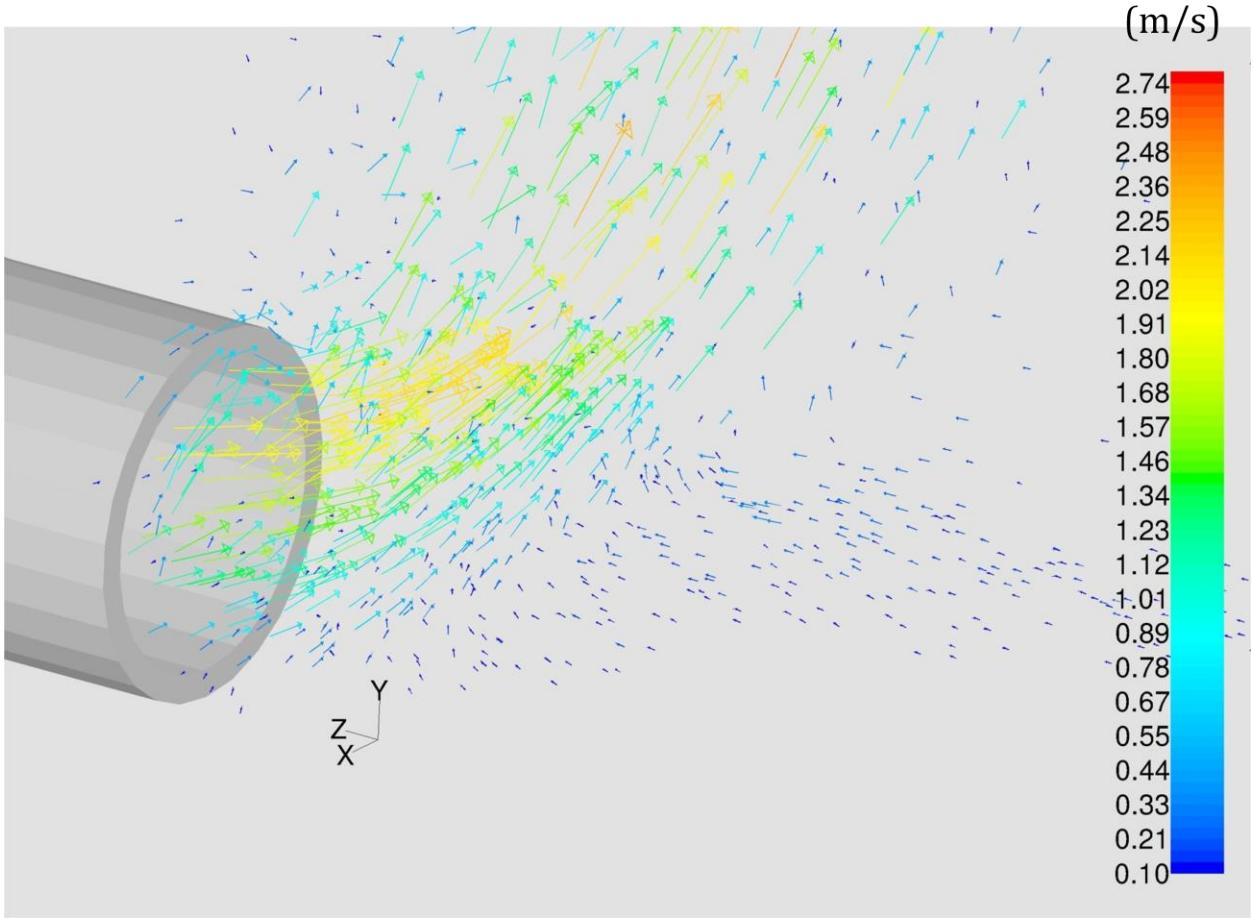

Figure 17. A close-up views of oil plume velocity vectors near the exit plane of riser at oil flow rate of 100,000 bpd.

Applying an intermittency factor of 0.5 for the ratio of the time oil is flowing to the total time, estimated total average oil flow rate at the Riser End Jet is 50,000 barrels per day of oil using Computational Fluid Dynamics.

Summary and Conclusions

The NETL has used three different analysis approaches by three different groups of researchers to produce estimates of total average oil flow rate from the BP Deepwater Horizon site. In addition to the assumptions denoted in the analysis descriptions above, the following assumptions apply to these three analyses:

- We have been provided video clips showing all oil leaks present in the system;
- The video clips provided by BP were representative of the average flow behavior of the jets;
- The total period of video for which jet velocity was measured using Approach 1 was representative of the entire period covered by this analysis, which is from April 20, 2010, to end of May 2010;
- There is no variability in oil leak rate over the period of analysis;

The results of these three analyses are summarized as follows:

Approach 1: Feature Tracking Velocimetry
Riser Kink Jets Leak Rate- total average oil flow rate is 25,000 barrels per day ± 2,500 barrels per day
Riser End Jet Leak Rate – total average oil flow rate is 60,000 barrels per day ± 6,000 barrel per day
Combined Total Leak Rate – total average oil flow rate is 85,000 barrels per day ± 8,500 barrel per day.

Approach 2: Turbulent Jet Theory
Riser Kink Jets Leak Rate - total average oil flow rate is 12,000 – 28,000 barrels per day
Riser End Jet Leak Rate - total average oil flow rate is 76,000 - 156,000 barrels per day
Combined Total Leak Rate- total average oil flow rate of 126,000 barrels per day, with a range of 82,000 -170,000 barrel per day.

Approach 3: Multiphase Computational Fluid Dynamics
Riser Kink Jets Leak Rate – not calculated
Riser End Jet Leak Rate - total average oil flow rate is 50,000 barrels per day
Combined Total Leak – not calculated

It is recognized that the range of uncertainty for these analyses is large. The measurement uncertainty alone has been estimated by members of the Plume Team from NIST to be in the range of +/- 40%. Estimates for uncertainty were made for Approach 1 and Approach 2 and are reflected in the values above. Uncertainty estimates were not made for the CFD result of Approach 3.

References

Abdel-Rahman, A. A., Chakroun, W., and Al-Fahed, S. F., 1997. "LDA measurements in the turbulent round jet," *Mechanics Research Communications*, **24**:277-288.

Gore, J. P., and Jian, C. Q., 1993. "Analytical solution to the flame trajectory based on the analysis of "Scaling of buoyant turbulent jet diffusion flames" by N. Peters and J. Gottgens," *Combust. Flame*, **93**:336-337.

Hill, B. J., 1972. "Measurement of local entrainment rate in the initial region of axisymmetric turbulent air jets," *J. Fluid Mech.*, 51:773-779.

Kim, J. S., Yang, W, Kim, Y., and Won, S. H., 2009. "Behavior of buoyancy and momentum controlled hydrogen jets and flames emitted into the quiescent atmosphere," *Journal of Loss Prevention in the Process Industries*, **22**:943-949.

Mi, J., Kalt, P., Nathan, G. J., and Wong, C. Y., 2007. "PIV measurements of a turbulent jet issuing from round sharp-edged plate," *Exp. Fluids*, **42**:625-637.

Mi, J., Nathan, G. J., and Nobes, D. S., 2001. "Mixing characteristics of axisymmetric free jets from a contoured nozzle, and orifice plate and a pipe," *J. Fluids Eng.*, **123**:878-883.

Nathan, G. J., Mi., J., Alwahabi, Z. T., Newbold, G. J. R., and Nobes, D. S., 2006. "Impacts of a jet's exit flow pattern on mixing and combustion performance," *Prog. Energy Combust. Sci.*, **32**:496-538.

Peters, N., and Gottgens, J., 1991. "Scaling of buoyant turbulent jet diffusion flames," *Combust. Flame*, **85**:206-214.

Quinn, W. R., 2006. "Upstream nozzle shaping effects on near field flow in round turbulent free jets," *European Journal of Mechanics B/Fluids*, **25**:279-301.

Richards, C. D., and Pitts, W. M., 1993. "Global density effects on the self-preservation behavior of turbulent free jets," *J. Fluid Mech.*, **254**:417-435.

Ricou, F. P., and Spalding, D. B., 1961. "Measurements of entrainment by axisymmetrical turbulent jets," *J. Fluid Mech.*, 11:21-32.

Appendix 8: Flow Rate Estimation from Feature Tracking

Flow Rate Estimation from Feature Tracking on the Video of the Spill Sites based on Statistical Correlation Algorithms

Juan C. Lasheras and Juan C. del Álamo
University of California San Diego
Alberto Aliseda, Oscar Flores and James Riley
University of Washington

Working as part of the Plume Team within the Flow Rate Technical Group

Preamble

This report is the result of the work of a team of researchers from the Universities of Washington and California, San Diego, named above. This work was performed to address the need to assess the flow rate of oil into the Gulf of Mexico from the site of the Deepwater Horizon Incident. It is based on the analysis of several hours of video that was made available to the Plume Team within the FRTG through a NOAA ftp server.

The authors got involved in this problem at the request from NOAA to attempt to estimate the flow rate of oil discharging from the broken riser of the oil well from video images taken by Remotely Operated Vehicles (ROVs). The UW-UCSD team was part of the Flow Rate Technical Group that was created under the direction of Dr. Marcia McNutt to address this critical need. The sole purpose of our study is to provide information to the National Incident Command , as requested by Dr. McNutt. This report is not intended to be used for any purpose other than that.

The circumstances that gave rise to the leak (Deepwater Horizon explosion and sinking), the depth at which the oil was leaking (5000 feet underwater at the bottom of the Gulf of Mexico, 25 miles off the coast of Louisiana) and the urgency under which this project developed made this study an incredibly difficult engineering endeavor, with no time or opportunity for the careful analysis that the authors always employ in their normal research activities. The measurement of the flow rate of a turbulent two-phase flow jet from video sequences taken at 30 frames per second presents enormous challenges. Owing the gravity of the situation, and the pressing need to have an estimated range to aid the response of the National Incident Command, the authors accepted the request from the Federal Government while recognizing the severe limitations imposed by this technique. The use of underwater video images from moving ROVs to measure velocities and estimate flow rates had never been tried before (to the best of our knowledge). This difficulty was coupled with the complex nature of the crude oil flowing through the broken riser, with a mixture of oil and gas of unknown compositions, and under constant phase changes. The urgent national need for an estimate to inform and guide the response effort needs to be taken into account to understand the conditions under which this group operated. All the work described in this report was carried out between May 13 and June 13, 2010.

The problem of estimating the flow rate of oil coming out of the riser pipe after the explosion and sinking of the Deepwater Horizon is broken into two parts. First we analyze the flow rate of crude

oil discharged from two main sites before the riser pipe was cut on June 2nd. The primary discharge site was located at the open end of the riser pipe where oil and gas are coming out of a 21.5 in OD, 19.5in nominal ID pipe lying horizontally for several thousand feet on the bottom of the Gulf of Mexico (see Figure 1). The second site was located on top of the blow out preventer (BOP) were the riser pipe was bent as it fell from its vertical position, crimpled and formed several cracks through which an oil/gas mixture was observed escaping. A sketch of the overall setting, with the two areas of interest marked, is given in Figure 1. A trench was excavated around the open end of the riser area and video cameras on the ROVs conducted surveillance of the spill site. The ROVs also injected oil dispersant at the site from the time the trench was excavated to the time the riser was cut just above the Blow Out Preventer (BOP) on June 2nd. The second part of the report focuses on the estimation of the flow rate discharging after the riser pipe was cut. At that time, and until the LMRP was placed, the flow of crude oil was coming out only from a single site and the uncertainties associated with the presence of multiple leaks of unknown geometries was removed.

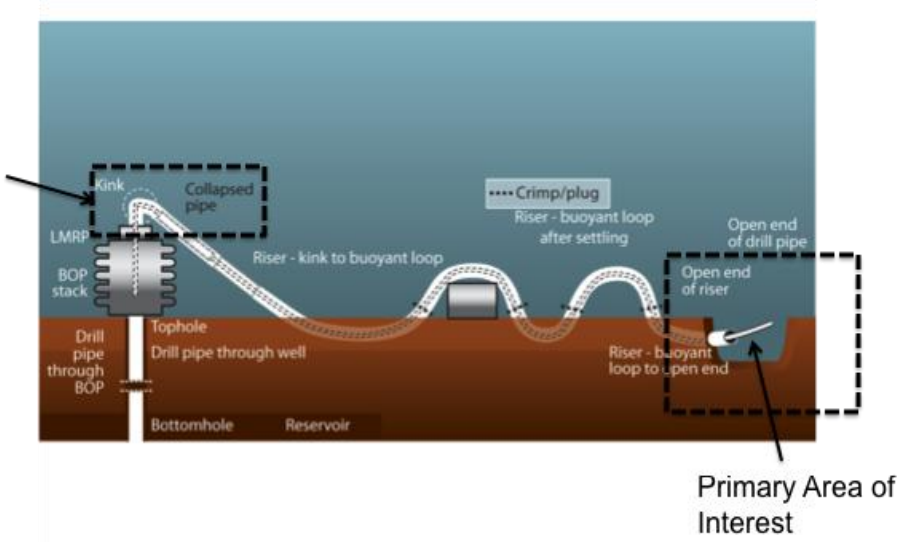

Figure 1: Sketch of the BOP and riser lying on the sea bed.

This second analysis is believe to be provide a more accurate estimate of the current flow rate after the installation of the Top Hat Cap. If one assumes that the presence of the Top Hat cap on the cut riser installed later does not induce a significant change in the flow rate from the oil well (the back pressure produced by the cap is negligible compared to the hydrostatic pressure differences and the viscous losses associated with the flow from the reservoir to the cap), then the estimate of flow after the riser was cut and before the cap was installed is representative of the total flow once the cap was installed and operated (the sum of the flow going up the LMRP and the flow going out of the cap through vents and leaks between the cap and the flange it sits on).

Section I: Estimate of the Oil Flow Rate before the riser pipe was cut on June 2nd.

Before the riser pipe was cut on June 2nd, there were two leak sites: 1) a primary leak site was located at the open end of the riser pipe, and 2) second leak site was at the top of the Blow Out Preventer (BOP) where the riser pipe bent as it fell from its vertical position to the horizontal one resting on the bottom, crimpled and formed several cracks. The two subsections below estimate the oil flow rate coming out from each of these sites.

Section I.A. Estimate of the Oil Flow Rate at the Open End of Riser. Analysis of the Temporal Evolution of the Velocity and Composition.

This section analyzes the temporal evolution of the velocity and composition discharging from the open end of the riser. The results of this section are based on the analysis of three different videos:

- 5 minutes 051720101304crater.mpg, of May 17th
- 30 minutes 20100514235708344@H14Ch1H264h.mov of May 14th
- 16 minutes 20100514220052312@H14Ch1H264h.mov of May 14

These videos were found to be the more appropriate for the analysis, since they showed the end of the riser from the side, with the position of the ROV and the focus of the camera varying little in time.

I.A.i General observations:

After the accident, the riser pipe sunk to the ocean floor and crude oil flowing through the riser pipe began to be discharge at its open end. Due to progressive cooling and condensation of heavy hydrocarbon fractions, the crude oil flow in the long riser pipe (> 1000 feet) resting on the sea floor segregates and formed a two-phase flow composed of a mixture of condensed hydrocarbons (oil) and gas flowing in the "slug flow" regime as shown in Figure 2.

At the open end of the riser the gas-oil flow is highly intermittent with

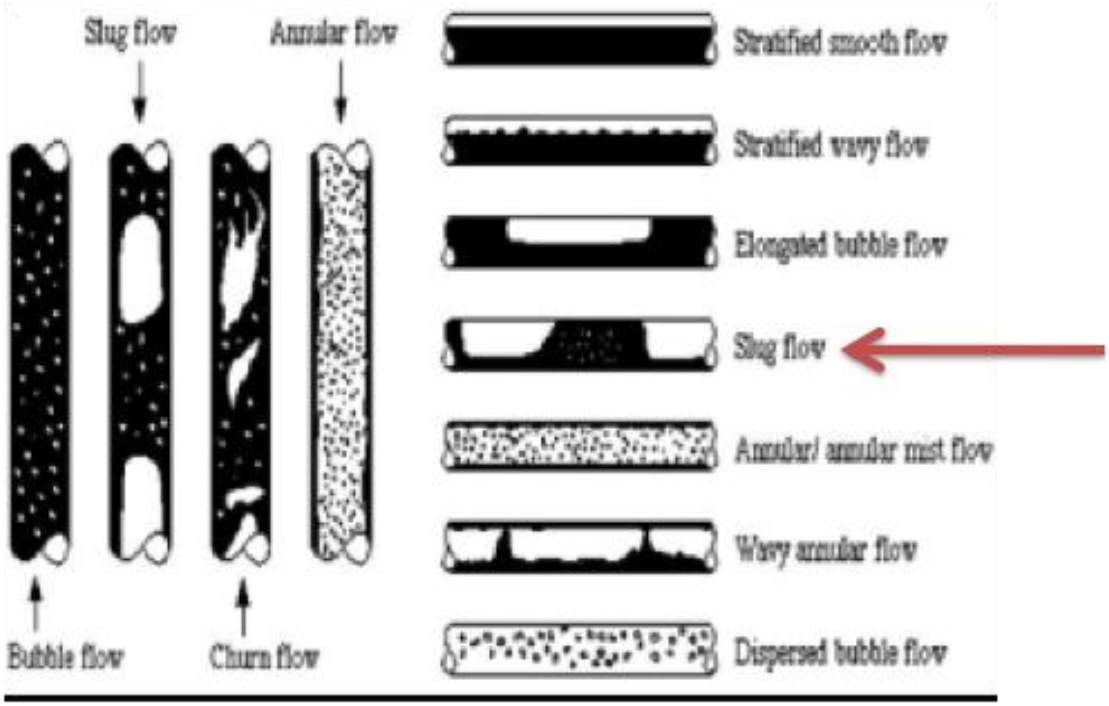

Figure 2: Different regimes for gas/oil flowing in a pipe.

As shown in figure 3, the "slug flow regime" is characterized by the high intermittency of the flow, which shows different events including

- Events dominated by the discharge of almost pure gas. This regime is made evident not only by the sharp change in brightness, but more importantly, because the jet becomes "buoyancy-driven", showing a parabolic shape near the outlet and becoming completely vertical 3 to 4 diameters downstream (see Figure 3a).
- Events dominated by what appears to be the discharge of almost pure condensed oil. This regime is evident by the change to a mostly uniform dark color, and more importantly, because the jet is then mainly "momentum-driven" and discharges almost horizontally and has a very small parabolic curvature, consistent wit smaller buoyancy effects (see Figure 3b).
- Events where a mixture of gas and oil is discharged simultaneously (see Figure 3c).

To be able to measure the oil discharged from the open end of the riser by digital image processing of these videos, it is essential to estimate with sufficient confidence the period of these events and the fraction of oil being discharged during each event.

a)

b)

c)

Figure 3: Frames from 20100514220052312@H14Ch1H264h.mov, showing the intermittency in the flow of gas and oil in the horizontal riser pipe.

I.A.ii Image Brightness Analysis

To characterize the temporal variability in the flow of oil and gas, a Region of Interest (ROI) that includes the pipe exit and the gas and oil plumes was chosen and digital image processing was applied on it to calculate the average image brightness for each frame of the movies that were

Figure 4. Definition of the Region of Interest in the images from the riser pipe's exit

studied. The ROI used for this analysis is shown in figure 4. The average image brightness of each frame in a movie was normalized between 0 (minimal average intensity recorded in the movie) and 1 (maximal average intensity recorded in the movie). The normalized average image brightness is used as a surrogate for the relative concentration of gas and oil at the pipe's exit. Measuring the time variation of the normalized average brightness shows the intermittency of the gas/oil flow rate. Results from this analysis are shown in figure 5.

In the movies we analyzed, we observed a cyclic repetition of a brightness pattern consisting of a gradual increase in the brightness level, followed by a sharp decrease. Visual observations of the frames

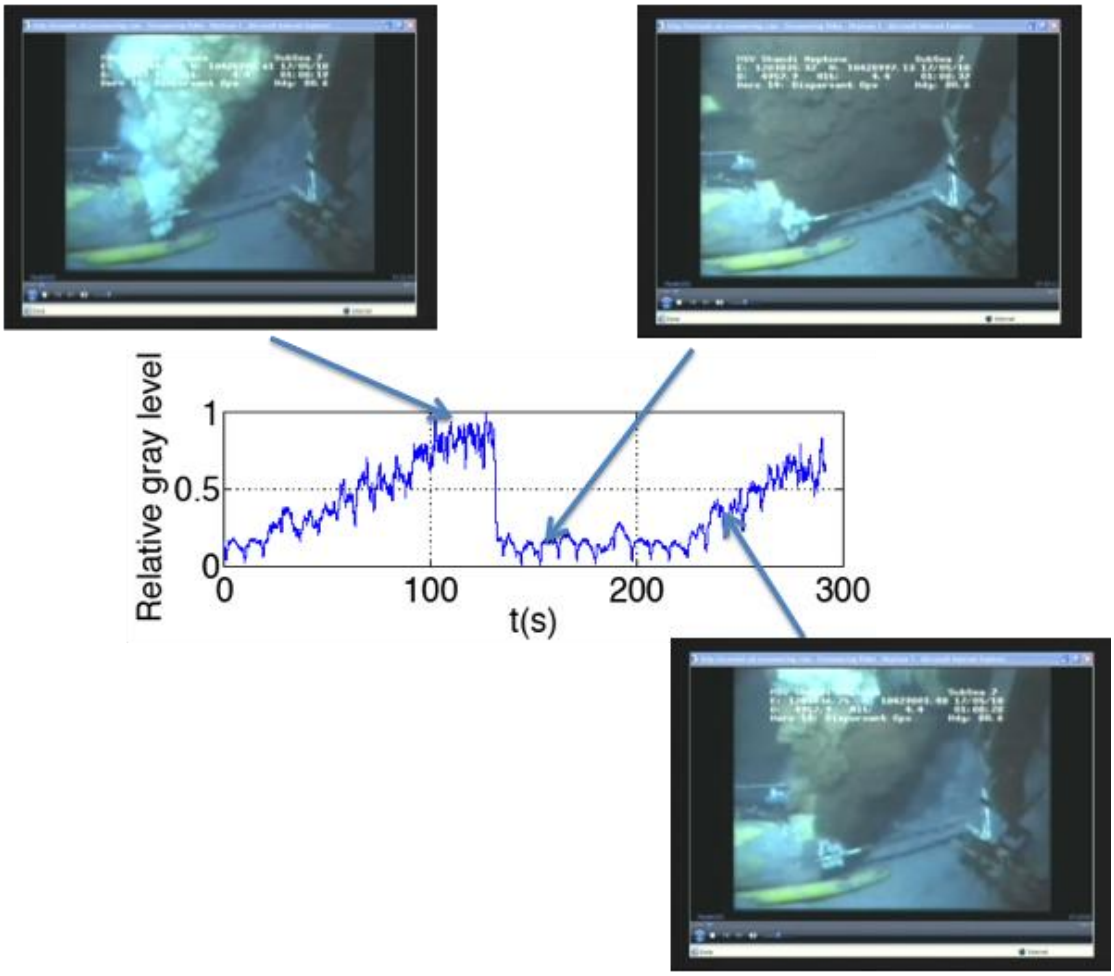

Figure 5. Time trace from 051720101304crater.mpg (5 minute clip from May 17th)

indicate that at the peak of brightness level, the riser appears to be discharging mostly gas, while the lowest values correspond to the riser discharging what appears to be mostly oil. The time between successive ramps is approximately 3 min (see figure 5). The standard deviation of the average brightness in the ROI shows the same 3 minute period (see figure 6).

The analysis of the grey levels of two longer image sequences from May 14th (see Figure 7) confirms the "slug flow" regime found in the short 5 minute clip from May 17th. In both movies the gas slugs appear to come in pairs (uniformly spaced an average time T' approximately 70 s) and with a very well-defined time periodicity between the pairs of T ≈ 200 s

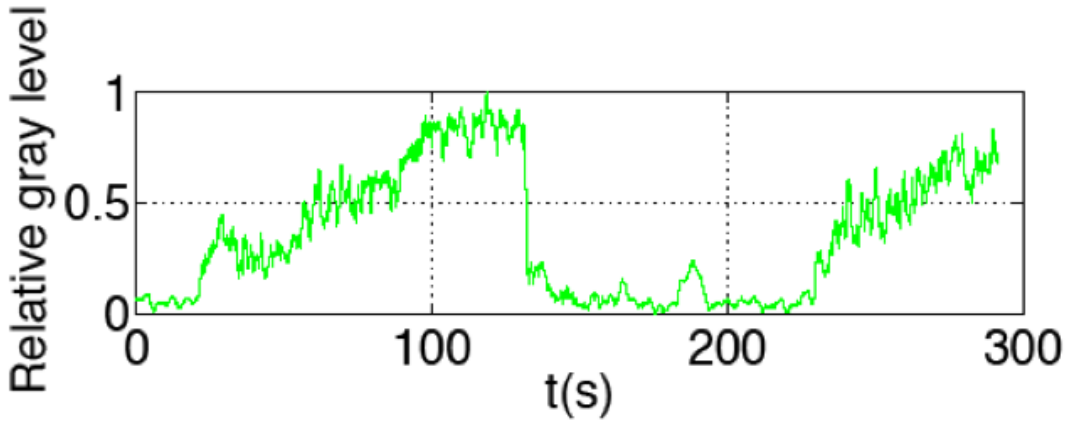

Figure 6. Standard deviation of image brightness (grey level) inside the ROI defined in image Time trace from 051720101304crater.mpg (5 minute clip from May 17th)

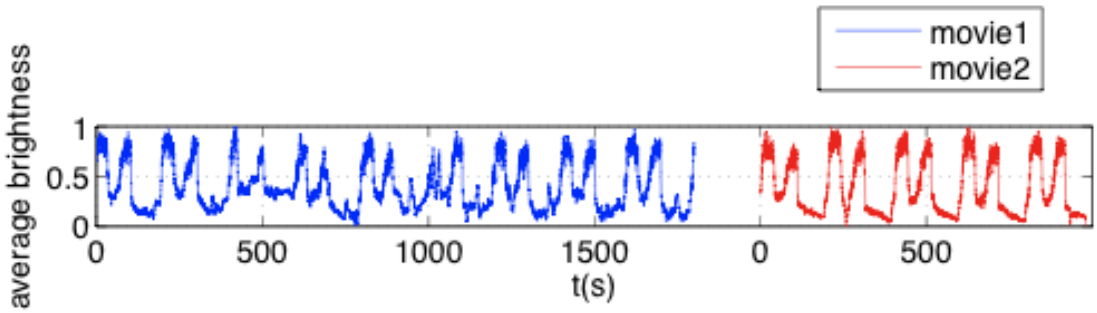

Figure 7. Temporal evolution of the average brightness in an ROI at the riser exit.
30 minutes 20100514235708344@H14_Ch1-H264h.mov of May 14th
16 minutes 20100514220052312@H14_Ch1-H264h.mov on May 14th

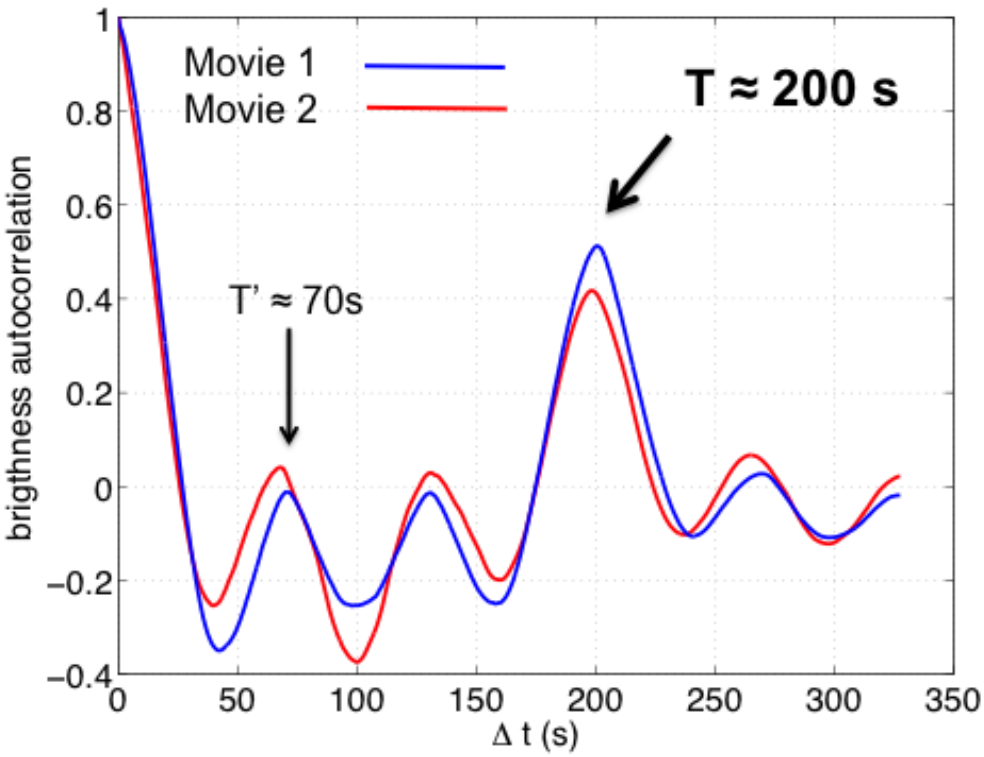

Figure 8. Temporal autocorrelation of the average brightness in an ROI at the riser exit. 30 minutes 20100514235708344@H14_Ch1-H264h.mov on May 14th 16 minutes 20100514220052312@H14_Ch1-H264h.mov on May 14th

with a very well-defined time periodicity between the pairs of T ≈ 200 s ≈ 3.3 minutes. Autocorrelation analysis of the time variation of the average brightness intensity (see Figure 8) confirms the periodic behavior of the oil/gas composition with two distinct peaks at 70s and 200s observed in figure 7.

Assuming that the concentration is directly proportional to the normalized average brightness, one can estimate the fraction of time that is occupied by gas and oil, by integration in time of the above signal:

20100514235708344@H14_Ch1-H264h.mov
GAS/OIL time fraction = 38/62

20100514220052312@H14_Ch1-H264h.mov
GAS/OIL time fraction = 40/60

Note that the above estimated gas to oil ratio from the integration of the average brightness represents an upper bound since we have assumed that there is only condensed oil being discharged when the normalized average pixel intensity in the ROI is minimum and pure gas when is maximum. This assumption is rather restrictive since one can observe in the videos that there is always a small fraction of oil flowing at the bottom of the riser pipe when the brightness is at a maximum and a similarly small amount of gas flowing at the top of the pipe when the intensity is at a minimum.

I.A.iii Cross Correlation Image Velocimetry (PIV)

Three independent measurements have been carried out using two different PIV correlation algorithms. UCSD used segments from 20100514224719234@H14_Ch1-H264h.mov (17:47:17 -> 17:56:59).

UW used 2 consecutive image sequences totaling 44:50 minutes, 20100514220052312@H14_Ch1-H264h.mov and 20100514221717125@H14_Ch1-H264h.mov (17:00:49->17:45:39).

Figure 9 shows the geometry of the riser pipe end with the different lengths used for spatial calibration of the images and areas used to compute the flow rate.

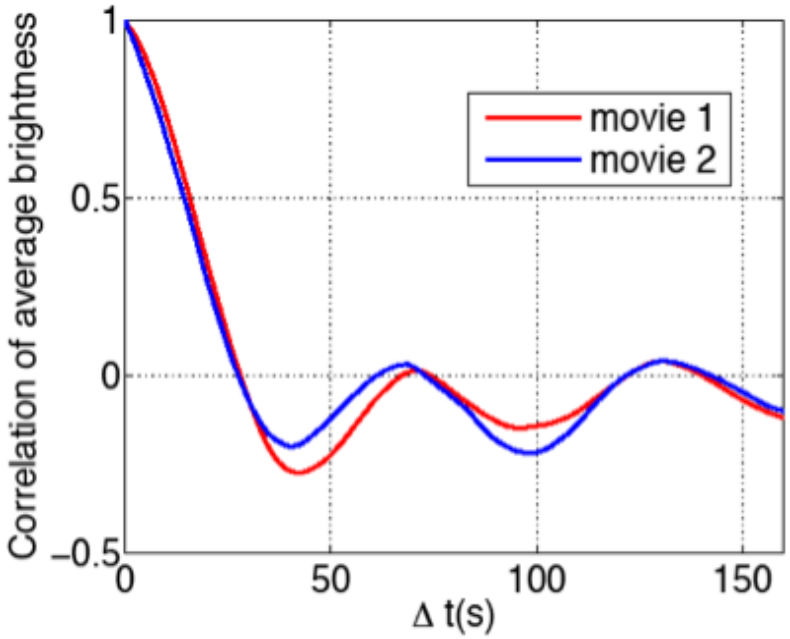

Figure 9.

The result of analyzing, with an Ensemble PIV algorithm, 100 consecutive frames over 4 seconds in sequence 20100514224719234@H14_Ch1-H264h.mov is shown in figure 10. This 4 second segment was chosen as representative of the time when the image brightness is very low associated with an outflow composed mostly of oil. Prior to processing, image brightness was inverted in all frames so that dark features in the movie were tracked as bright features by the image correlation in the PIV algorithm. In order to estimate the flow rate, it is important to measure as close as possible to the pipe exit, so that we are in the potential cone, and the horizontal velocities of the surface features can be related to the velocities at the pipe exit. However, the surface features are still not clearly visible and that prevented us from measuring immediately downstream of the exit. Thus, we masked out the first quarter diameter of the jet from the PIV algorithm. The PIV results show that one diameter downstream of the exit, the maximum horizontal velocities are of the order of 0.2 m/s. To remove operator bias, the same sequence were analyzed, using a different PIV software and operator and a different mask, yielding the same result (see Figure 11).

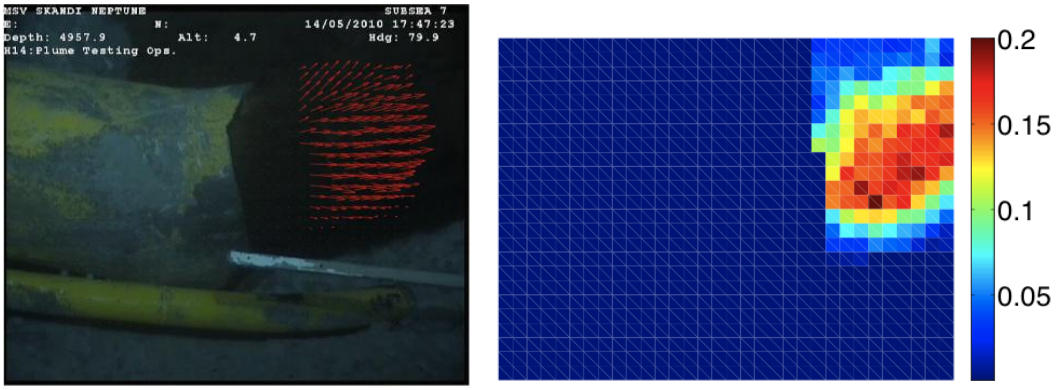

Figure 10. Velocity vectors (left panel) and color map of the horizontal velocity component in m/s (right panel) obtained by applying a PIV algorithm to the images of the jet outflow from the riser pipe.

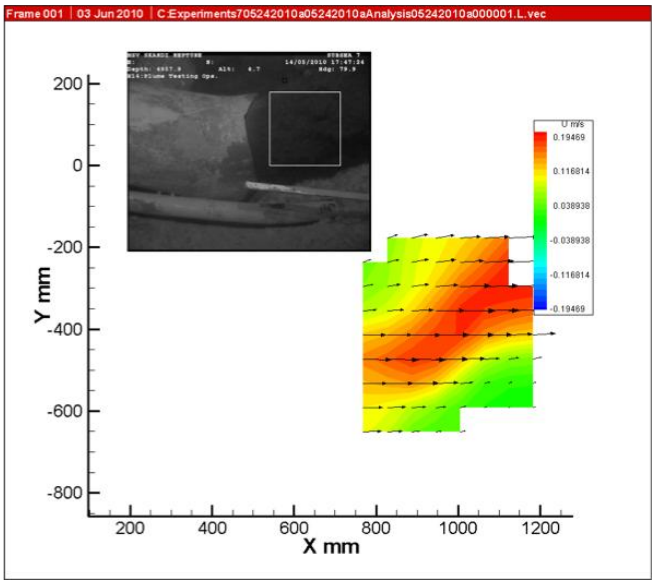

Figure 11. Alternative PIV analysis of the same time segment shown in figure 10.

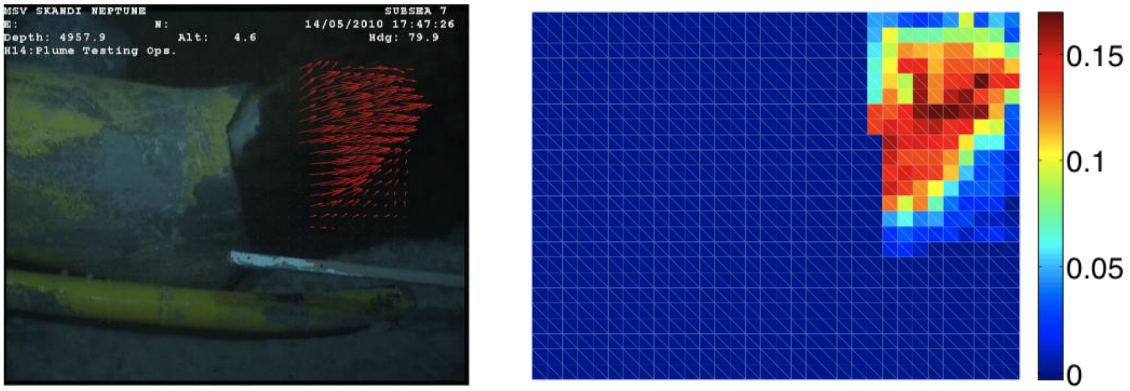

Figure 12. Velocity vectors (left panel) and color map of the horizontal velocity component (right panel) from image correlation with a PIV algorithm at a time when the flow is transitioning from mostly oil to mostly gas.

Figure 12 shows the result of applying the ensemble PIV algorithm to 100 consecutive images over 4 seconds at the initial stages of the formation of a gas slug (20100514224719234@H14_Ch1-H264h.mov). Note that the jet becomes more buoyant, but the horizontal component of velocity remains almost the same as in the previous case.

I.A.iv Estimate of the Oil Discharging from the Open End of Riser

ESTIMATES 1 (UCSD)

We know that

- the peak magnitude of the velocity of the surface features measured in the ensemble records is 0.2 m/s (figures 10 to 12);
- the mean velocity of the surface features measured in the ensemble records is 0.12 m/s (figures 10 to 12);
- the cross sectional area of the pipe is 214 in^2;

and consider that

- the average Gas/Oil temporal fraction is 40/60, as measured from the analysis of the time variation of the average brightness intensity.

Using these data, different assumptions of the relation between the measured convection velocities of the surface features (V_{conv}) and the average bulk velocity of the potential core of the jet ($V_{bulkjet}$) lead to the following estimates for the flow rate:

- If we assume that $V_{bulkjet}$ is approximately 3/2 of the maximum V_{conv} measured, we estimate ≈ **14000 bbl/day** of condensed oil.
- If we assume that $V_{bulkjet}$ is approximately twice the maximum V_{conv} measured, we estimate an oil flow rate ≈ **18000 bbl/day**.
- If we assume that $V_{bulkjet}$ is approximately 3/2 the average V_{conv} measured, we estimate an oil flow rate ≈ **8000 bbl/day**.
- If we assume that $V_{bulkjet}$ is approximately twice the average V_{conv} measured, we estimate an oil flow rate ≈ **11000 bbl/day**.

The resulting range of estimates is **8000-18000 bbl/day flowing at the open end of the riser.**

ESTIMATES 2 (UW)

Combined Grey Level – Feature Tracking Velocimetry

We measure the relative oil/gas concentration from the grey level along the blue line shown in figure 13. Unlike the UCSD technique described above, this is a pointwise estimate of the local concentration, no averaging is performed inside an area or along the measurement line.

We apply the PIV algorithm on the whole image. Measurements from 100 image pairs are averaged, weighted by the signal to noise ratio at each measurement window. Time dependent flow rate integrated along the cross section of the jet in 2 different ways:

- Q = Area * 2 max(V_x) * mean(c) (black line in lower panel of figure 14)
- Q = Area * 2 max (V_x * c) (red line in lower panel of figure 14)

As observed in figure 14, the differences between both expressions are minimal.

The factor of 2 in the expressions for the flow rate is obtained by assuming that the convective velocity of the features measured by the PIV algorithm is around ½ of the maximum velocity of the jet. Figure 14 shows the flow rates computed with that factor, giving an averaged flow rate of **12600 bbl/day**. When the factor of 1.5 proposed by UCSD is used in the calculations, the averaged flow rate is reduced to **9450** bbl/day.

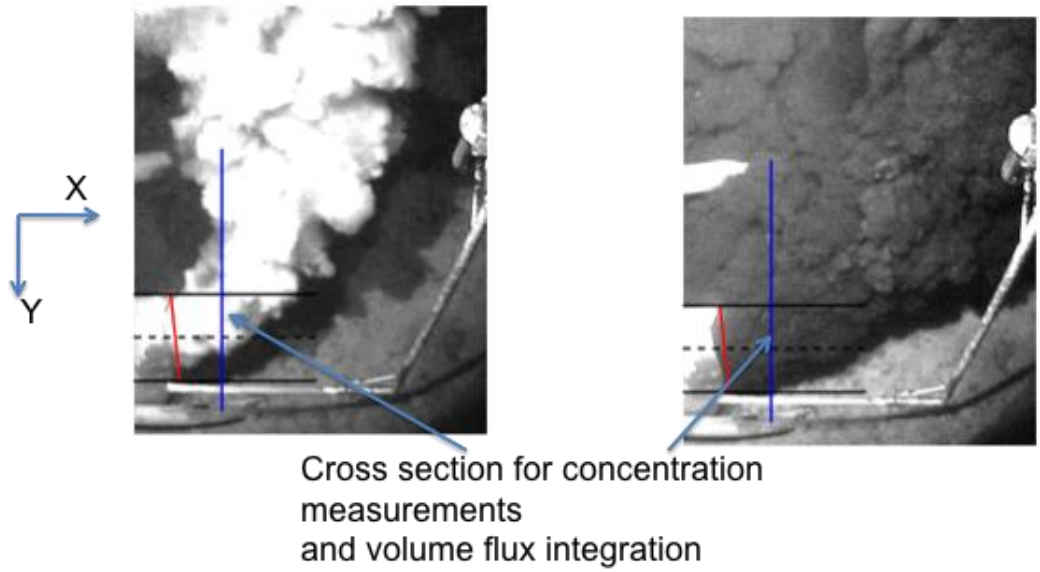

Figure 13. Sketch of the geometry used for the velocity and concentration measurements for estimate 3.

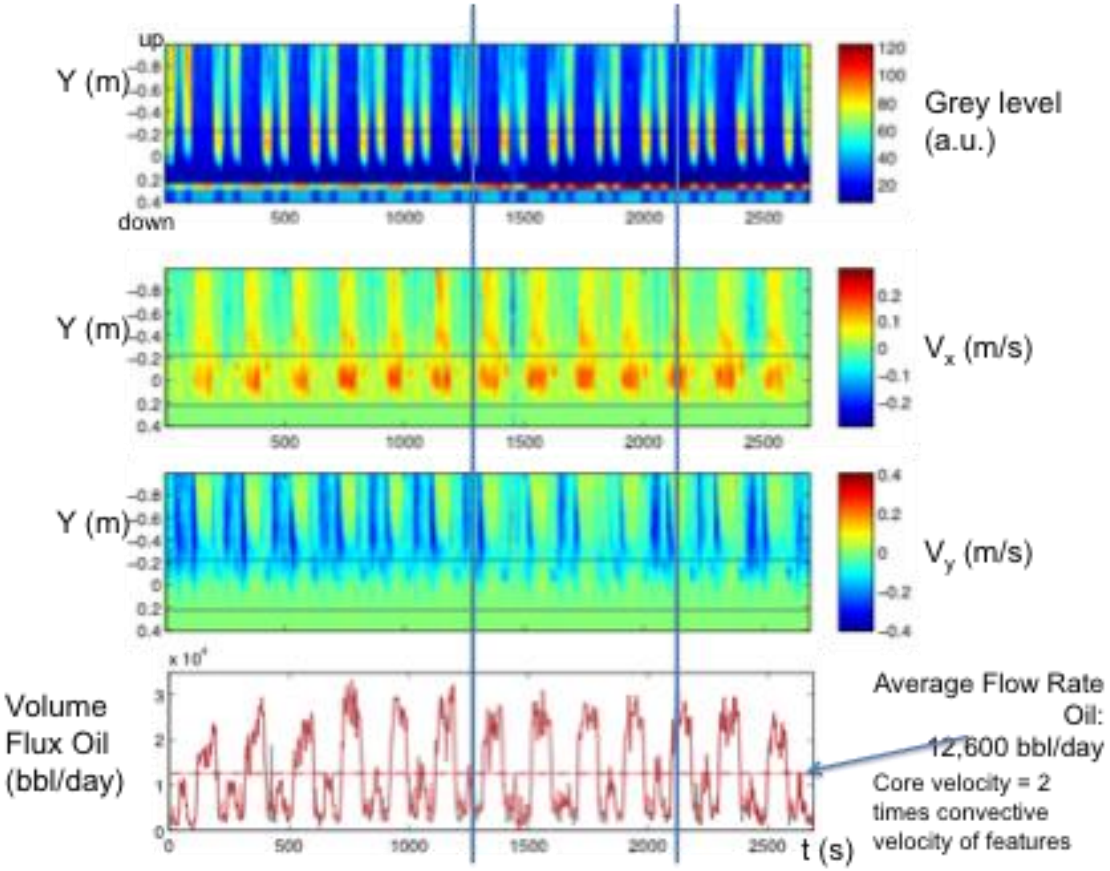

Figure 14. Results from image analysis showing the relative gas/oil concentration, horizontal and vertical velocities and the integrated oil flow rate.

CONCLUSIONS FROM SECTION I.A

- **The gas/oil mixture discharging from the open end of the riser is a highly intermittent slug flow.**
- **There are two well defined periods (70, 200 s) over which the flow oscillates between mostly gas to apparently (annular flow of oil around a gas core) mostly oil. However, there may be even longer periods of gas-oil flow fluctuation in the range of hours or even as long as days that must be characterized.**
- **Analysis of time histories of the grey level signal from the fluid leaving the exit of the pipe flow was done assuming this quantity to be directly proportional to the gas/oil fraction. The average gas/oil fraction measured in this way was ≈ 40/60. UCSD used this value to correct the average flow rates obtained from velocity measurements. UW integrated the instantaneous product of the velocity and estimated gas/oil fraction, obtaining similar results.**
- **Based on Feature Tracking Velocimetry and concentrations measurements, and using the assumptions indicated above, we estimate the condensed oil flow rate from the open end of the riser to be between 8,000 bbl/day and 18,000 bbl/day.**

Section I.B: Estimate of the Oil Flow Rate Discharging from the Leaks at the Kink on the Top of the Blow Out Preventer.

The jets emanating from the various holes in the kink of the riser pipe located on top of the BOP is momentum-dominated. We have measured the spreading half-angle and is ≈ 13.5 degrees (Figure 15), which is the spreading angle of high Re number turbulent jets in the absence of buoyancy forces. Therefore we are confident that buoyancy does not play a dominant role in the development of the jet at the relative short distances where the measurements are performed. Estimating the total flow from the several leaks in the kink at the top of the BOP is more challenging than the flow of the riser pipe because we have been able to measure only the larger jet located at the center of the kink. It is very difficult to measure the flow rate of the other additional two smaller jets, one which impinges directly on an auxiliary line (see Figure 15), which makes it necessary to extrapolate the flow rate of those leaks from the main leak that is the only one where measurements can be performed. Furthermore, it is impossible to perform measurements at or near the leak orifices. This is due to their small size and the high speed of the jets coming out of them, combined to the limited temporal and spatial resolution of the images, which causes the image of that near field region to be blurry.

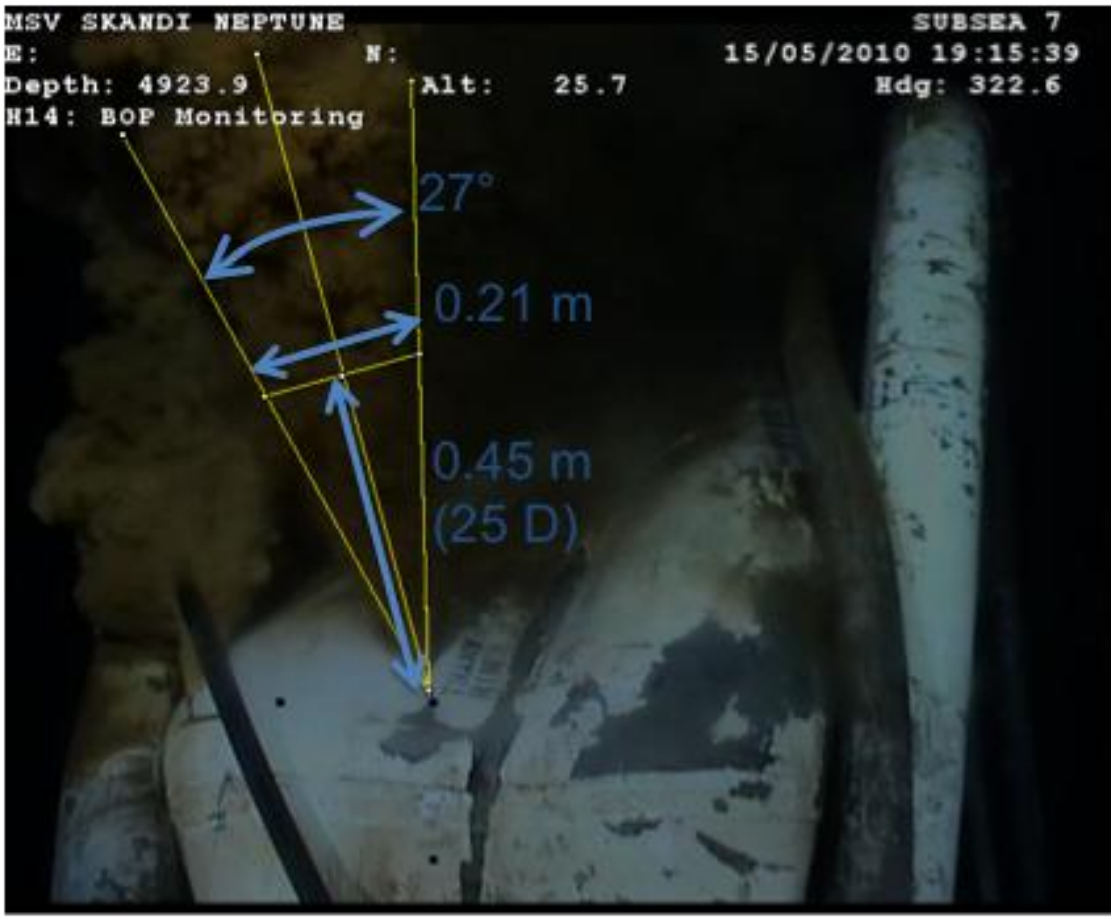

Figure 15. Sketch of the location of PIV measurements in the main leak on the kink at the top of the BOP. The jet is still momentum dominated (buoyancy effects not considered).

We analyzed images from sequential movies: H14 BOP Plume May 15 1915-1920.asf (5 minutes) and H14 BOP Plume May 15 1920-1945.asf (25 minutes). Velocity measurements were made at a cross section about 25 Diameters downstream of the exit (the leak orifice is estimated to be about 1.2 cm in width). At this point the diameter of the jet is 0.21 m (100 pixels). According to a recent study on the dynamics of light jets (Foisy et al. 2010. IJHFF 31, 307–314) the entrainment at that point makes up about half the volume flux in the jet. Using these measurements and estimates about entrainment from the literature on light jets, we can evaluate the flow rate from the leak with several simple assumptions, namely that the jet velocity is axisymmetric and has a Gaussian radial profile, and the ratio of maximum velocity to measured velocity is equal to 2 (see Figure 16). We avoid the need to accurately assess the orifice diameter and the virtual origin of the jet. These two quantities are very difficult to evaluate and they have an enormous influence on the outcome of a possible flow rate calculation that depends on them (the flow rate goes like the ratio of diameters squared and approximately like the inverse of the ratio of virtual origins).

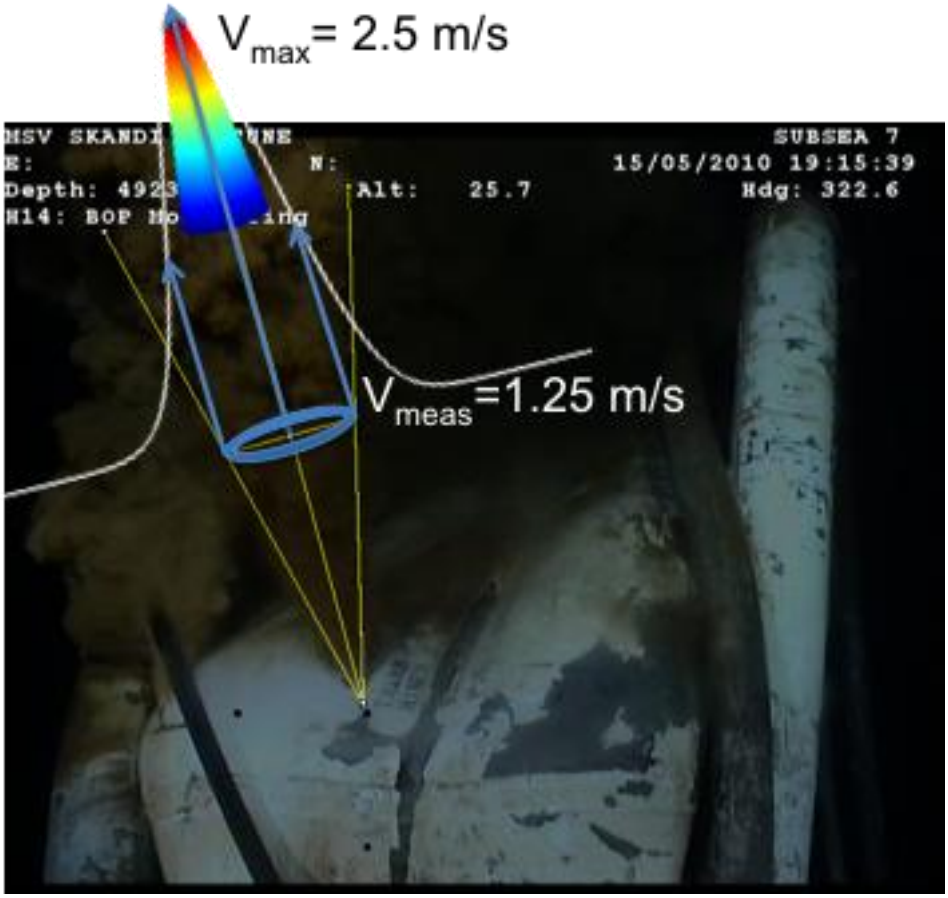

Figure 16. Sketch of the model used to relate the velocity measurements to the oil flow rate at the kink jet.

Considering the entrainment and assuming a 75/25 gas to oil ratio, we get **6,000 bbl/day**. If we assume a 59/41 gas to oil ratio, based on the latest data on the collection from the LMRP system that started on June 3rd, we get **10,000 bbl/day.** Considering the other two jets, we will assume that they discharge half of the amount measured in the stronger central jet. Therefore the total flow rate from the kink is estimated to be between **9,000 bb/day** and **15,000 bbl/day**.

CONCLUSIONS FROM SECTION I.B

- **The analysis of the leaks at the kink on top of the BOP has significantly higher uncertainty than the estimates of the riser's end, due to**
  - **The existence of several leaks, some of which cannot be measured**
  - **The small size of the orifices and fast speed of the jets coming out of them, combined to insufficient temporal and spatial resolution of the movies analyzed.**
- **The jet emanating from the kink is momentum-dominated.**
- **Velocity measurements made 25 Diameters downstream one orifice, together with**
  - **an estimated entrainment of half the volume flux in the jet taken from the literature of compressible jets,**
  - **assumed 75/25 or 59/41 gas/oil ratios,**
  - **axisymmetric Gaussian velocity profile in the jet,**
  - **maximum to measured velocity equal to 2,**
  - **assumed that the total flow from all the leaks is equal to 1.5 times the flow estimated from the main leak,**

lead to a total flow rate from the kink between 9,000 bb/day and 15,000 bbl/day.

bill

CONCLUSIONS FROM SECTION I

Analysis of the measured time histories of the grey level signal from the fluid at the open end of the riser reveals gas/oil temporal fraction of 40/60. However, there may be even longer periods of gas-oil flow fluctuation in the range of hours or even as long as days that must be characterized.

Based on Feature Tracking Velocimetry and concentrations measurements, and using the assumptions indicated above, we estimate the condensed oil flow rate

- **from the open end of the riser = 8,000 bbl/day to 18,000 bbl/day**
- **from the kink on top of BOP = 9,000 bbl/day to 15,0000 bbl/day**

TOTAL ESTIMATE = 17,000 to 33,000 bbl/day

Section II: Estimate of the Oil Flow Rate After the Cut of the Riser

The geometry of the riser pipe after the cut just above the Blow Out Preventer is shown in figure 17. We use 19.5 inches as the interior diameter of the pipe and assume that the exit is round and neglect the effect of the drilling pipe inside the riser and the metal flap across the section resulting from the uneven cut. The resulting cross sectional area used in the calculations is 0.1927 m^2.

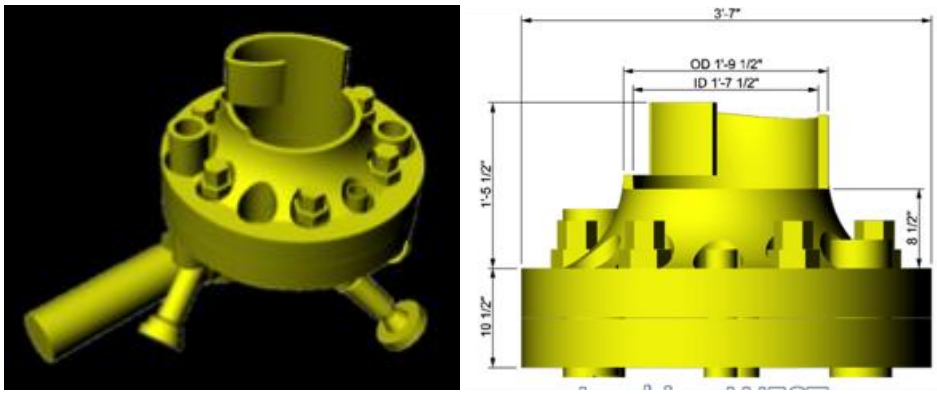

Figure 17. Sketch of the geometry of the riser pipe after the cut just above the flange on top of the BOP.

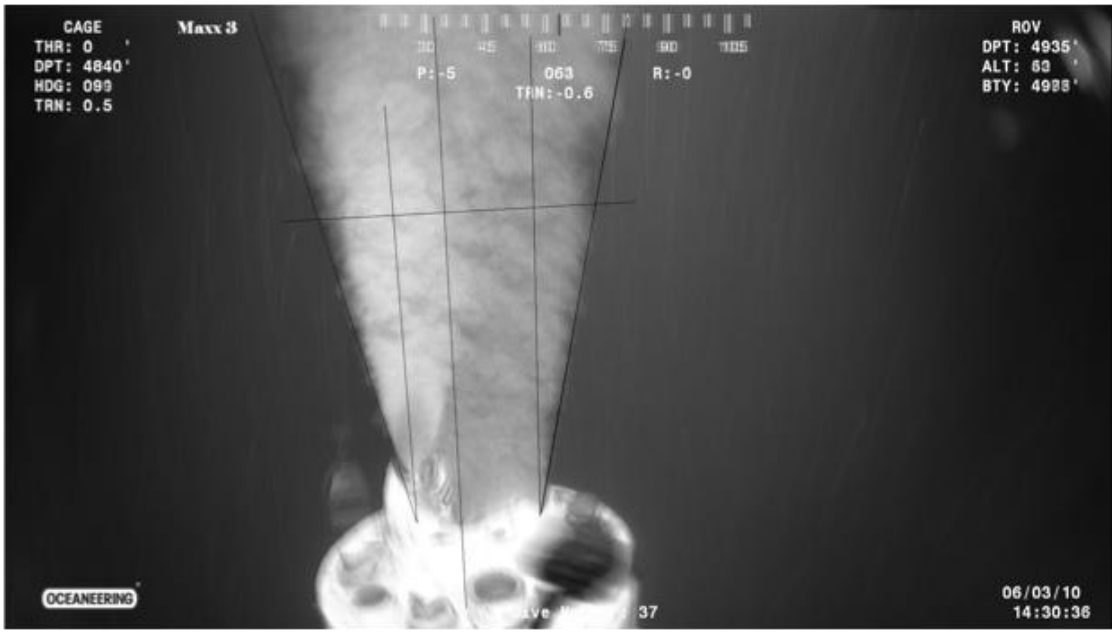

Figure 18. Time averaged black and white image intensity

Observation of the flow coming out of the cut riser shows that the jet discharging from the riser is "momentum-driven" up to at least 3 jet diameters downstream, after which it starts to be strongly influenced by buoyancy. The regime is that of a continuous bubbly gas/oil uniformly mixed as opposed to the intermittent slug flow observed at the open end of the riser discussed in section 1. Figure 18 is obtained by superposition of a sequence of 50 images averaging the grey level at each pixel. The instantaneous features are washed out, but the average shape of the jet is brought to the forefront, showing the 13.5° half angle for the spreading characteristic of momentum driven jets.

II.A Results from UCSD Analysis

We performed ensemble PIV measurements of two sequences of the movie TOPHAT_06-03-10_14-29-22.avi. The first sequence was from 14:30:46 to 14:30:48 (50 frames, 49 pairs, Figure 19 left panel), while the second sequence was from 14:30:35 to 14:30:36 (30 frames, 29 pairs, Figure 19 right panel). These measurements showed that the maximum velocity of the coherent structures of the jet immediately downstream of the outlet is ≈ 0.5 m/s and that this velocity decreases to ≈ 0.4 m/s approximately one diameter downstream of the outlet.

Using these measurements of the convection velocity of the coherent structures, the only step necessary to estimate the flow rate is to relate the measured velocity to the jet exit velocity. Because we are taking our measurements next the jet's exit, we are within the potential cone and therefore the centerline velocity of the jet is still equal to the jet exit velocity. Analysis of the literature from uniform density mixing layers suggest a value for that ratio of 1.6. This value was estimated by considering that the coherent turbulent structures in a shear flow propagate with an advection velocity equal to the mean of the streamwise velocity that they sample in their interior (Townsend 1976), which has been tested successfully for wall turbulence (del Álamo and Jiménez, 2009). We apply this idea to the shear layers surrounding the potential cone of the jet (see Figure 20), which were characterized by Wygnanski and Fiedler (1970). The level of intermittency in the shear layer, γ, is used as a fiduciary indicator of the presence of turbulent coherent structures, so that the average of the mean streamwise velocity weighted with γ provides an estimate of the convection velocity of the jet turbulent structures, which yields a ratio of 1/0.62 ≈ 1.6 between the velocity of the jet coherent structures measured by PIV and the bulk flow velocity at the potential cone of the jet.

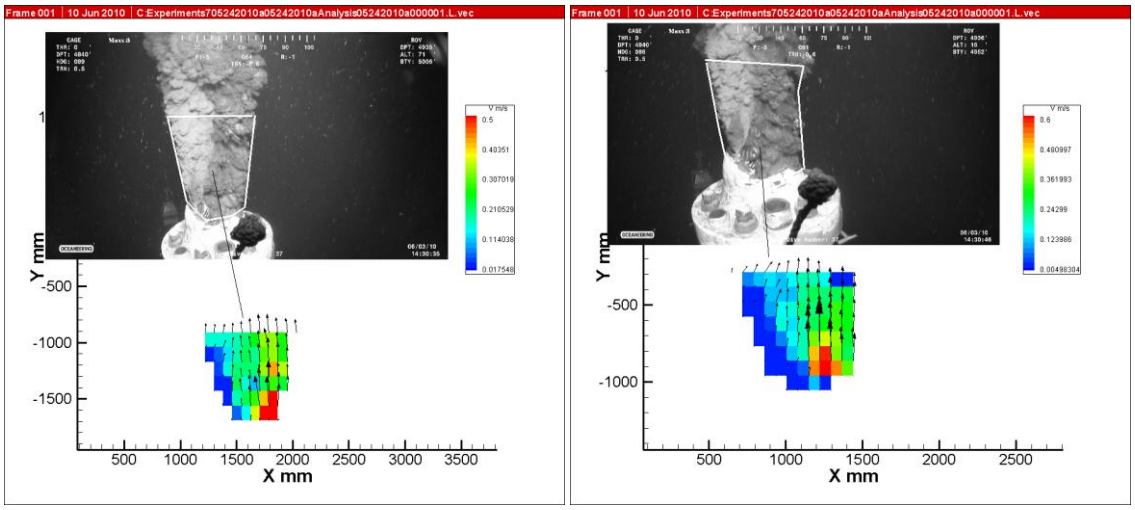

Figure 19. Velocity measurements from the correlation of image pairs through the PIV algorithm. The images come from two sequences of the movie TOPHAT_06-03-10_14-29-22.avi. The first sequence was from 14:30:46 to 14:30:48 (50 frames, 49 pairs, Figure 19 left panel), while the second sequence was from 14:30:35 to 14:30:36 (30 frames, 29 pairs, Figure 19 right panel).

We use the factor estimated above to convert the velocities measured with PIV next to the pipe exit (≈ 0.5 m/s) into estimated bulk velocities at the potential cone of the jet A conservative factor of 2.5 by multiplying 1.6 times the square root of the density ratio between the surrounding fluid and the jet ($\approx 1.6 \times \sqrt{1030/415}$) is applied as we move downstream of the exit, where the velocities measured by PIV are ≈ 0.4 m/s. We use an Oil / Gas ratio of 0.41 as reported by BP from the LMRP collection data and the cross-sectional area the jet exit deduced from the geometry of the pipe after the riser cut (see Figure 17). The range of possible values for the estimated oil volume flow rate that comes out of the riser is shown in Table 1. The most plausible value of the flow rate, **Q ≈ 35000 bbl/day**, is outlined in the table.

Correction Factor	PIV Velocity (m/s)	Area (m^2)	OIL/GAS	FLOW RATE (bbl/day)
1.6	0.4	0.1927	0.41	28000
2.5	0.4	0.1927	0.41	43000
1.6	**0.5**	**0.1927**	**0.41**	**35000**
2.5	0.5	0.1927	0.41	54000

Table 1. Flow rate estimates from the movie TOPHAT_06-03-10_14-29-22.avi after the riser pipe was cut above the BOP.

Results from UW Analysis

1. Video segment: TOP_HAT_060310_14:30:35_37.

Ensemble averaged over 54 image pairs (Frames 2203 to 2258).

This is the original sequence that we compared in the first group discussion of the FRTG on Thursday, June 10, 2010. We have resolved the inconsistency in the PIV measurements by focusing on the same very near region of the jet development, closer than 1 diameter to the riser pipe's end. The results are shown in figures 20 and 21. We all measure a maximum velocity of V_max ≈ 0.58 m/s (UCSD, UW and Purdue). The maximum velocity is always found very close to the rim, less than 0.25 D downstream.

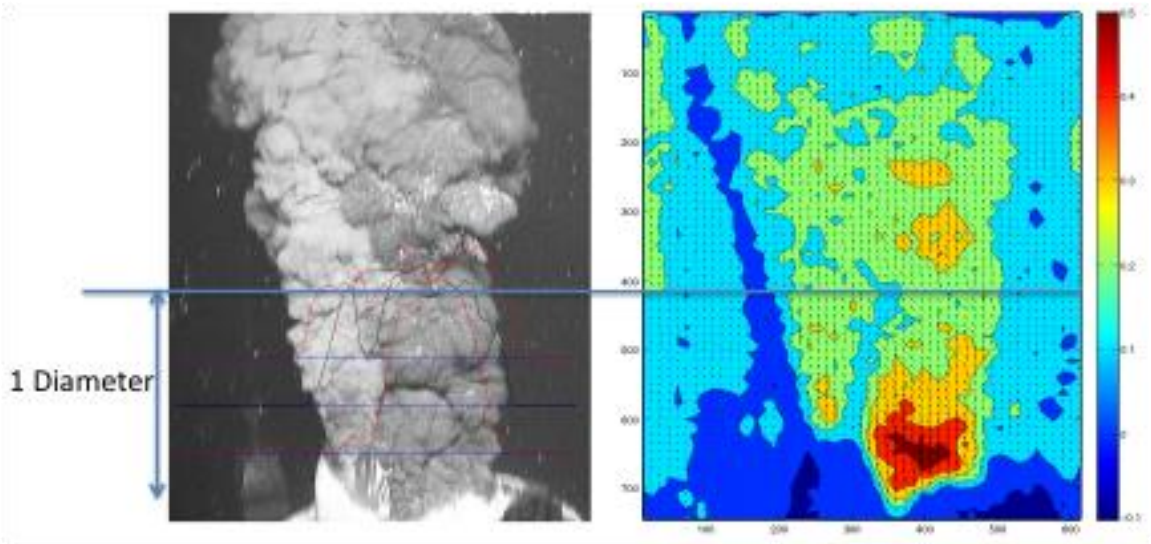

Figure 20. Image of the riser pipe outflow (left) and correlation velocity measurements (right) with the locations at which the flow rate is evaluated marked.

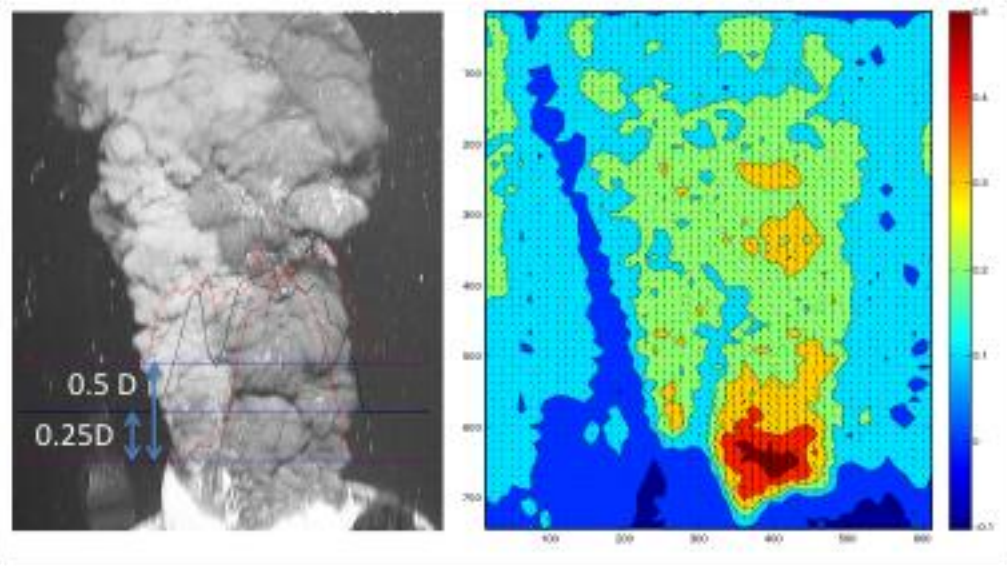

Figure 21. Side by side presentation of the riser outflow and the velocity measurements with the three cross sections used to calculate the flow rate (right at the nozzle, 0.25 D and 0.5D downstream).

Because the highest velocity is found near the jet exit, we apply a factor of 1.6 to calculate the core velocity and the flow rate. Conservative factors of 2 and 3.15 ($\approx 2 \times \sqrt{1030/415}$) are applied as we move downstream. Note that further downstream the coherent structures have more time to develop and the density ratio between the density of the jet and the entrained fluid can play a role. With these assumptions, we obtained the following results from this image sequence:

- At section z=0.5D, V_max=0.3498 m/s with a factor of 3.15 we get **Q=46,688 bbl/day**.
- At section z=0.25D, V_max=0.4157 m/s with a factor of 2 we get **Q=35,746, bbl/day**.
- At section z=0, V_max=0.5773 m/s and with a factor of 1.6 we get **Q=39,710 bbl/day.**

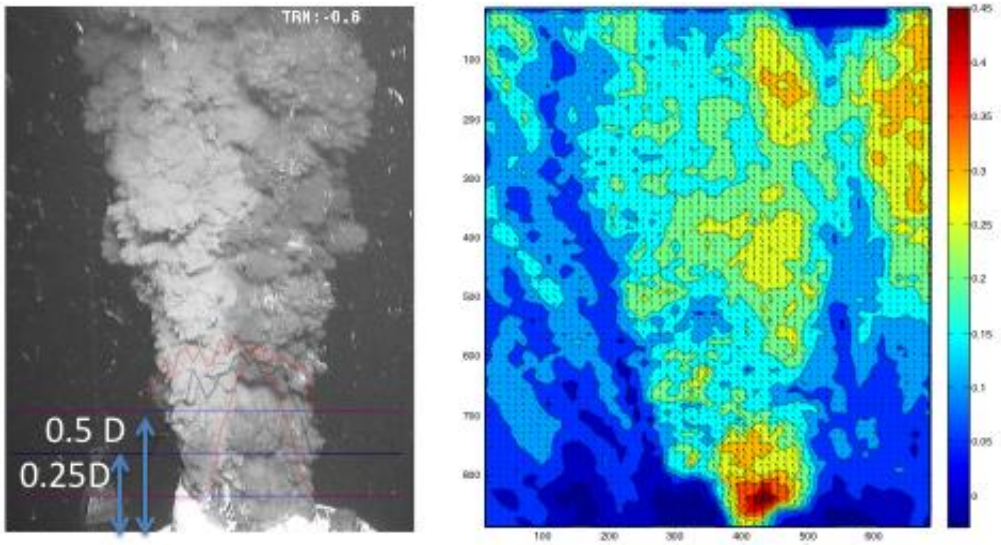

Figure 22. Image and velocity measurements from image sequence 14:30:33 to 35.

2. Video Segment: TOP_HAT_060310_14:30:33_35.

Ensemble averaged over 50 frames.

In this sequence the maximum velocity is V_max ≈ 0.50 m/s. The maximum velocity is always found right on the rim, away from the pipe flap that wrap around the light jet. With these assumptions, we obtained the following results from this image sequence:

- At section z=0.5D, V_max=0.2579 m/s with a factor of 3.15 we get **Q=34,422 bbl/day**.
- At section z=0.25D, V_max=0.3385 m/s with a factor of 2 we get **Q=29,105 bbl/day**.
- At section z=0, V_max=0.4913 m/s and with a factor of 1.6 we get **Q=33,794 bbl/day**.

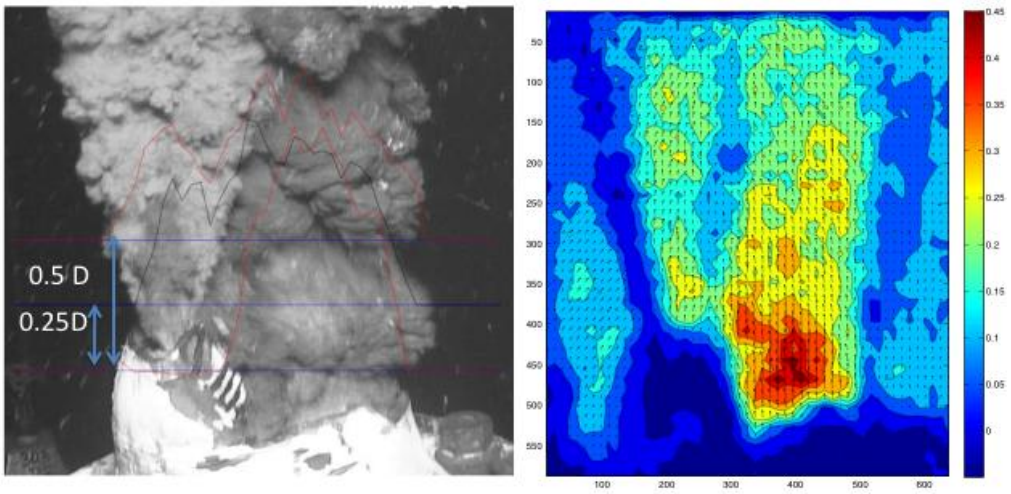

Figure 23. Sketch of the measurement region on the flow image and the velocity measurements at the third video sequenced analyzed.

3. Video Segment: TOP_HAT_060310_14:30:47_49

Ensemble averaged over 76 frames.

In this sequence the maximum velocity is V_max ≈ 0.50 m/s. The maximum velocity is always found right on the rim, away from the pipe flap that wrap around the light jet (see Figure 23). With these assumptions, we obtained the following results from this image sequence:

- At section z=0.5D, V_max=0.3451 m/s with a factor of 3.15 we get **Q=46,601bbl/day**.
- At section z=0.25D, V_max=0.3385 m/s with a factor of 2 we get **Q=31,934bbl/day**.
- At section z=0, V_max=0.4913 m/s and with a factor of 1.6 we get **Q=33,602 bbl/day**.

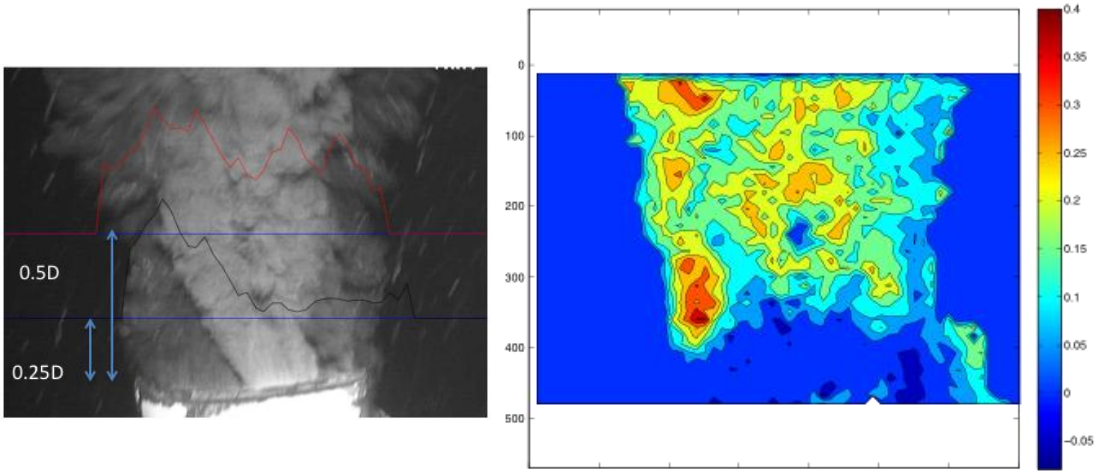

Figure 24. Zoomed in image of the outflow from the riser pipe's end, with the lighter jet in the front of the image. Velocity measurements show a very low velocity of the lighter jet, but maximum velocities close to the rim and away from the lighter jet.

4. Video Sequence: TOP_HAT_060310_14:31:35_41

Ensemble averaged over 180 frames

This sequence is focused on the jet carrying lighter fluid which dominates the image in Figures 24 and 25. The velocity of the light grey jet is always smaller than the main, dark jet. In this sequence the maximum velocity is V_max ≈ 0.40 m/s. The maximum velocity is always found right on the rim, away from the pipe flap that wraps around the light jet. With these assumptions, we obtained the following results from this image sequence:

- At section z=0.5D, V_max=0. 2729 m/s with a factor of 3.15 we get **Q=36424bbl/day.**
- At section z=0.25D, V_max=0. 2546 m/s with a factor of 2 we get **Q=21891bbl/day.**
- At section z=0, V_max=0. 4137m/s and with a factor of 1.6 we get **Q=28,457 bbl/day.**

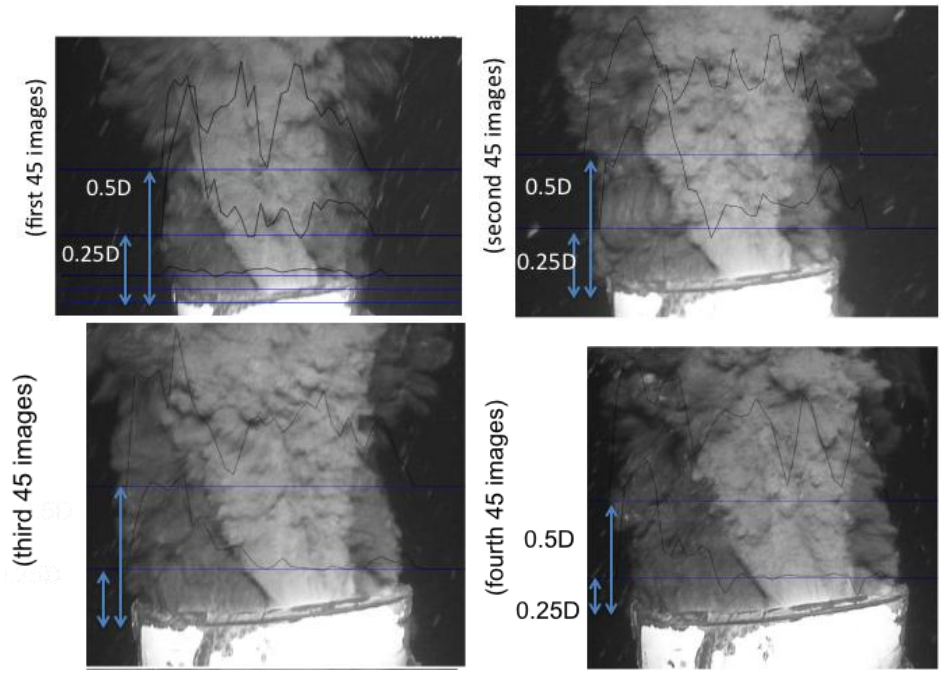

Figure 25. Four images from the 180 frame sequence showed in figure 24, with the superimposed velocity profiles from ensemble averages in four subsequences of 45 frames each.

The range of flow rate estimations obtained from the four videos is summarized in Table 2 below.

Correction Factor	Velocity (m/s)	OIL/GAS	FLOW RATE (STB/day)
1.6	0.41	0.41	28000
2	**0.25**	**0.41**	**22000**
3.15	0.26	0.41	35000
1.6	**0.49**	**0.41**	**34000**
2	0.35	0.41	30000
3.15	0.31	0.41	41000
1.6	0.58	0.41	40000
2	0.42	0.41	36000
3.15	**0.35**	**0.41**	**47000**

Table 2. Flow rate estimates from the videos taken on 06032010 after the riser pipe was cut above the BOP. The lighter cells at the top represent the minimum flow rate calculations, the intermediate part of the table represents the averages and the bottom part (darker) has the maximum values. The absolute minimum, best estimate and absolute maximum are marked in bold.

CONCLUSIONS FROM SECTION 2

- **Image correlation techniques (PIV) provides consistent velocity measurements across different sequences, algorithms and users.**
- **The main source of uncertainty lies in the relationship between measured velocity of turbulent coherent structures in the outer interface of the jet and the velocity at the potential cone of the jet (developed vs. developing flow, coherent structures, entrainment with different density, etc.). This introduces a variability in the estimations of up to 300%.**
- **Secondary sources of uncertainty are:**
  - **temporal fluctuations**
  - **use of mean or averaged velocity,**
  - **cross sectional area of the pipe at exit,**
  - **constant vs. inhomogeneous oil volume fraction (0.41),**
  - **ROV velocity,**

FINAL ESTIMATE = Best estimate of 34,000 bbl/day with a range of between 22,000 to 54,000 bbl/day.

Appendix 9: Plume Team Biographies

Dr. Alberto Aliseda is an Assistant Professor of Mechanical Engineering at the University of Washington. His research and teaching focuses on fluid mechanics with applications to Energy, Enviromental and Biomedical Flows.

Dr. Paul Bommer is a Senior Lecturer in Petroleum Engineering at the University of Texas at Austin. He teaches courses in drilling, production, artificial lift, and facilities. He also spent twenty-five years in private practice, specializing in drilling and production operations and oil and gas appraisals.

Dr. Pedro I. Espina serves as Program Analyst at the Office of the Director of NIST. Dr. Espina served as the International Liaison of the International Bureau of Weights and Measures. Dr. Espina also served a Scientific Advisor at the Chemical Science and Technology Laboratory of NIST, and is the former Leader of the NIST Flow Metrology Group.

Dr. Oscar Flores is a Research Associate in the Department of Mechanical Engineering at University of Washington. His primary area of research is fluid mechanics, with emphasis on wall-bounded turbulent flows and on density-stratified turbulent flows.

Dr. Juan C. Lasheras is Stanford S. and Beverly P. Penner Professor of Engineering and Applied Sciences Distinguished Professor of Mechanical and Aerospace Engineering and Bioengineering at University of California at San Diego. He is Chairman of the American Physical Society/Division of Fluid Dynamics. His research interests include turbulent flows, two-phase flows, and bio-medical fluid mechanics, and biomechanics.

Dr. William (Bill) J. Lehr is Senior Scientist at the Office of Response and Restoration of the National Oceanic and Atmospheric Administration (NOAA). He was previously Spill Response Group Leader for the same organization, technical analyst with NASA Jet Propulsion Laboratory and held a joint appointment with the Research Institute and Mathematical Science Department at the University of Petroleum and Minerals. Dr. Lehr is an expert in the field of hazardous chemical spill modeling and remote sensing of oil spills.

Dr. Ira Leifer is an Associate Researcher at the University of California at Santa Barbara. His research projects include a simulation of a subsurface oil spill by a hydrocarbon seep, and an estimate of the release points of oil slicks in the ocean using the natural laboratory of the Santa Barbara Channel.

Dr. James J. Riley is Paccar Professor of Engineering at the University of Washington and former Chairman of the American Physical Society/Division of Fluid Dynamics. He is a pioneer in the development and application of direct numerical simulation to transitioning and turbulent flows. His current research emphasizes turbulent, chemically-reacting flows, as well as waves and turbulence in density-stratified flows and rotating flows.

Dr. Omer Savas is a Professor with the Department of Mechanical Engineering at the University of California at Berkeley. His research interests include fluid mechanics, aircraft wake vortices, biofluid mechanics, boundary layers, instrumentation, rotating flows, transient aerodynamics, turbulent flows, and vortex dynamics. His a fellow of the American Physical Society, an Associate Fellow of American Institute of Aeronautics and Astronautics, and A.D. Welliver Fellow of The Boeing Company

Franklin Shaffer is a Senior Research Engineer with USDOE National Energy Technology Laboratory. For 25 years he has led the development of new high speed particle image velocimetry (PIV) tools to study particle flow dynamics of energy processes. He has received numerous national and international awards for development of new high speed imaging tools, including the R&D 100 Award and the Federal Laboratory Award for Excellence in Technology Transfer.

Dr. Steven Wereley is an Associate Professor of Mechanical Engineering at Purdue University. His research interests include biological flows at the cellular level, and electrical and optical manipulation of particles and fluids. He is on the editorial board of Microfluidics and Nanofluidics Journal and Experiments in Fluids and is an Associate Editor of ASME's Journal of Fluids Engineering.

Dr. Poojitha D. Yapa is a Professor of Civil and Environmental Engineering at Clarkson University. His research interests include modeling of deep-water oil and gas jets and plumes, modeling of the fate of oil spills and related oil spill processes, and oil shoreline interaction. He is past associate editor of hydraulic journals of American Society of Civil Engineers (ASCE) as well as the International Association of Hydraulic Research (IAHR).

Appendix 10: Expedited Peer Review Report

While there was not sufficient time to conduct a complete and formal peer review of this report, the following scholars agreed to undertake an expedited review.

Dr. Ronald Adrian	Arizona State University
Dr. Edward Cokelet	Pacific Marine Environmental Laboratory
Dr. Yasuo Onishi	Pacific Northwest National Laboratory
Dr. Peter Cornillon	University of Rhode Island

Their unedited comments are provided below plus any responses from the Team. In certain cases (indicated) their suggested revisions were included in the report.